DOCTORAL THESIS

UNIVERSITAT POLITÈCNICA DE CATALUNYA
BARCELONATECH

Direct current insulator based dielectrophoresis (DC-iDEP) microfluidic chip for blood plasma separation

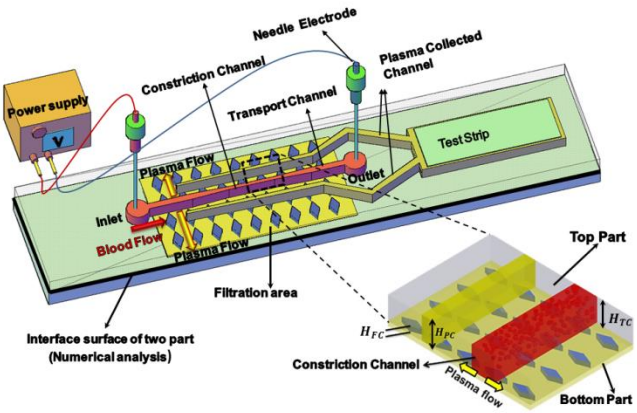

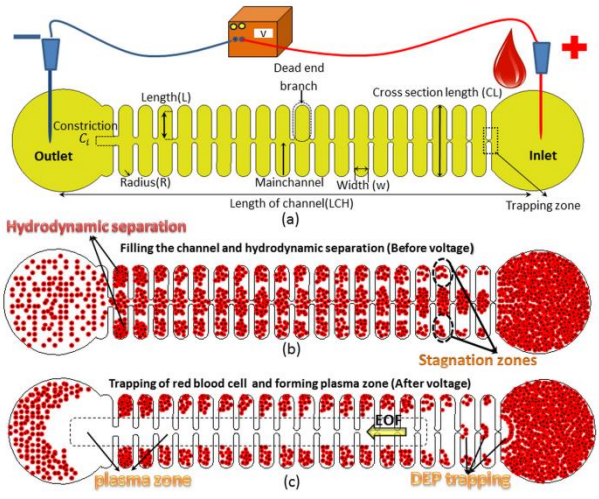

Mahdi Mohammadi

Direct current insulator based dielectrophoresis (DC-iDEP) microfluidic chip for blood plasma separation

Mahdi Mohammadi

Mechanical Engineering Department

Technical University of Catalonia

SUPERVISORS:

Jasmina Casals-Terré and Jordi Sellarès

Printed by the Technical University of Catalonia, Barcelona 2015

Barcelona 2015
www.upc.edu

To all my family.

ABSTRACT

Lab-on-a-Chip (LOC) integrated microfluidics has been a powerful tool for new developments in analytical chemistry. These microfluidic systems enable the miniaturization, integration and automation of complex biochemical assays through the reduction of reagent use and enabling portability.Cell and particle separation in microfluidic systems has recently gained significant attention in many sample preparations for clinical procedures. Direct-current insulator-based dielectrophoresis (DC-iDEP) is a well-known technique that benefits from the electric field gradients generated by an array of posts for separating, moving and trapping biological particle samples. In this thesis a parametric optimization is used to determine the optimum radius of the post for particle separation. Results that are used to design a microfluidic device that with a novel combination of hydrodynamic and di-electrophoretic techniques can achieve plasma separation in a microfluidic channel from fresh blood and for the first time allows optical real-time monitoring of the components of plasma without pre or post processing. Finally, all the results are integrated to create a novel microfluidic chip for blood plasma separation, which combines microfluidics with conventional lateral flow immune chromatography to extract enough plasma to perform a blood panel. The microfluidic chip design is a combination of cross-flow filtration with a reversible electroosmotic flow that prevents clogging at the filter entrance and maximizes the amount of separated plasma. The main advantage of this design is its efficiency, since with a small amount of sample (a single droplet ~10µL) a considerable amount of plasma (more than 1µL) is extracted and collected with high purity (more than 99%) in a reasonable time (5 to 8 minutes). To validate the quality and quantity of the separated plasma and to show its potential as clinical tool, the microfluidic chip has been combined with lateral flow immune chromatography technology to perform a qualitative detection of the TSH (thyroid-stimulating hormone) and a blood panel for measuring cardiac Troponin and Creatine Kinase MB. The results obtained from the microfluidic system are comparable to previous commercial lateral flow assays that required more sample for implementing less tests.

CONTENTS

ACKNOWLEDGMENTS

First and foremost, I would like to thank God Almighty for giving me the strength, ability, knowledge and opportunity to undertake this research study and to persevere and complete it satisfactorily. Without his blessings, this achievement would not have been possible. I also would like to ask him that this research would be a useful tool to help humanity health.

I would like to convey my heartfelt gratitude and sincere appreciation to all people who have helped and inspired me during my doctoral study. This thesis would not have been possible without the guidance of my committee members, help from friends, and support from my family and wife.

I would like to express my sincere appreciation and heartfelt gratitude to, my supervisor Professor Jasmina Casals-Terré. I am so deeply grateful for her help, professionalism, motivation, enthusiasm, and immense knowledge valuable guidance, continuous support through my Ph.D. study and research. Her guidance and support have brought me to a new place in my professional life. My words will never be adequate to express my gratitude towards her. I would like to express my deepest gratitude to my Co-supervisor, Dr. Jordi Sellarès, for his endless guidance, support, caring, patience during my research and study.

I would also like to acknowledge Dr. Roberto Castilla López for his scientific advice and knowledge and many insightful discussions and suggestions.

I would like to express my sincere appreciation to Professor Jens Ducrée for offering me the post-doc position in Ireland. I thank all the present members of our research group: Dr. Michel Sureda, Dr. Hojjat Madadi and Josep Farre for their helpful suggestions and comments during our weekly meetings. I would also like to warm thanks to my friends: Hojjat Madadi, Fateme Shiravand, Ramin Salehi, Mohammad zarei, Hamid Ghorbani, Milad Alidadiani, Reza atashkhoei, who make wonderful, joyful and unforgettable moments of my life during this time.

I must express my very profound gratitude to my first teachers, my mother “Ajab naz Shariati” and my father “Ahmad Mohammadi” who provided me with unfailing support and continuous encouragement in all aspects of my life. Through them never ending love and devotion they have instilled in me the desire to be a life-long learner and specially thanks my brothers”Mohammad and Reza Mohammadi. In addition, I am also extremely indebted to parents of my wife “Akbar Naseh& Mahboobe Ronnasian” for providing me continuous encouragement with throughout my years of study and through the process of researching and writing this thesis.

Finally, I would like to convey my heartfelt gratitude and sincere appreciation to my wife” Mozhgan Naseh”. There are no words to convey how much I love her. She has been a true and great supporter and has unconditionally loved me during my good and bad times. I feel

that we both learned a lot about life and strengthened our commitment during this time for making a wonderful future.

Abbreviations

σ, Conductivity.

ζ, Zeta potential.

ε, Fluid permittivity.

η , Fluid viscosity.

E, Electric field.

V, Voltage.

V_{EOF}, Electro-osmotic flow velocity.

V_{EP}, Electro-phoretic flow velocity.

r, Radius of the particle.

ρ_p , Density of the particle.

ρ , Density of the solution.

λ_D , Debye length.

μ_{EOF} , Electro-osmotic mobility

μ_{DEP} , Dielectrophoretic mobility.

F_{DEP} , Dielectrophoretic force.

DEP, Dielectrophoresis

DC, Direct current

EK, Electronkinetic

eDEP, Electrode based DEP

iDEP, Insulator based DEP

EP, Electrophoresis

RBC, Red blood cell

HCT, Hematocrit

EOF, Electro-osmotic flow

POC, Point-of-care

POCT, Point-of-care test

LOC, Lab on chip

1. Introduction

Due to the increase in the efficiency standards of the health care industry, Point of care (POC) products based on lab on a chip devices are growing in the market. Characteristics present in these products such as smartness, speed, cost-effectiveness and portability have motivated many companies and researchers to developed novel instruments based on this technology, see the POC roadmap and lab on a chip (LOC) technology shown in Figure 1 [1].

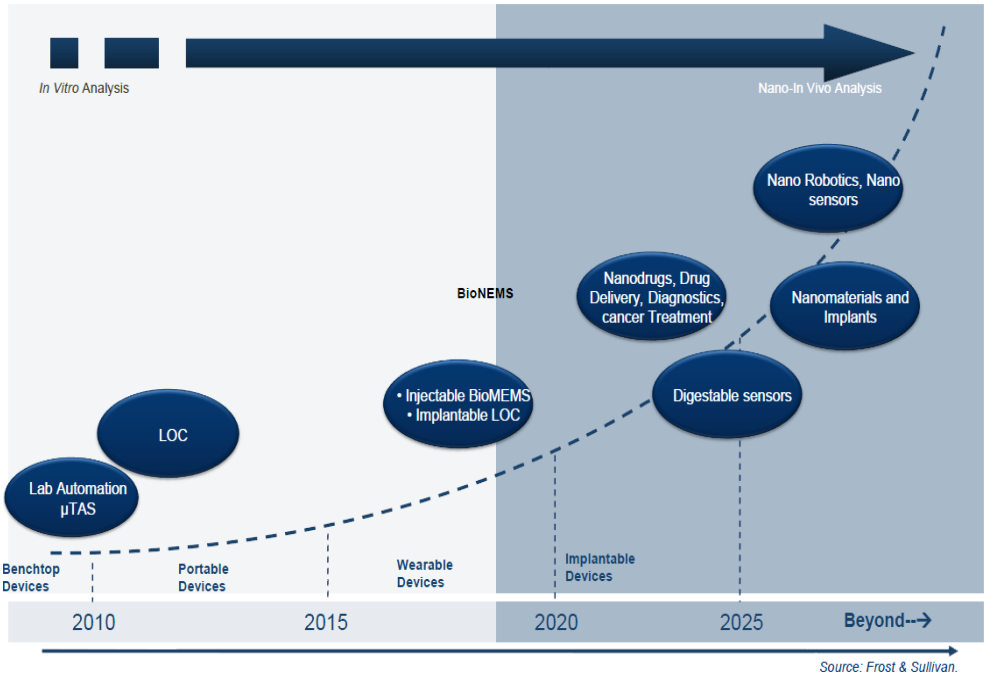

Figure 1. Micro & nano technology applications roadmap [1].

Figure 2 shows the summary of LOC devices and how each company has made its specific design choice to address the common challenges, grouped by the type of diagnostic marker [2].

The purpose of this research is developing a blood plasma separation POC device via DC-Insulator Based Dielectrophoresis (iDEP), which using only a single drop of blood, can separate enough plasma to implement different types of blood tests. DC-iDEP technique is a novel, noninvasive and nondestructive method based on electrokinetic effect that has been applied to different applications such as trapping and separation of bacteria (E coli, B.Subitilis) [3], virus [4], cancer cells [5], protein [6], polystyrene particle [7], latex particles [8] with high efficiency and reasonable time (minutes at most).

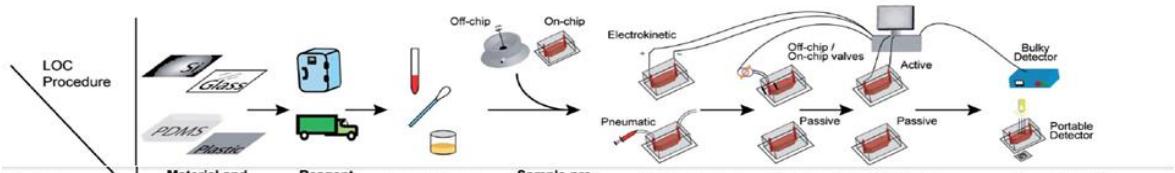

Company	Material and manufacturing	Reagent storage	Sample types	Sample pre-treatment	Fluid actuation	Fluid control	Fluid mixing	Signal detection
Abaxis	Plastic disc	Dry reagents on disc	Whole blood	On disc	Centrifugal and capillary	Passive	Passive	Absorbance
Advanced Liquid Logic	Glass, insulated electrodes	On- and off-chip reservoirs	Whole blood	On chip	Electrokinetic (electrowetting)	Electrokinetic	Electrokinetic	Fluorescence, chemiluminescence
Alere (formerly Inverness Medical)	Plastic and elastically deformable materials	On cartridge	Whole blood (capillary)	On cartridge	Mechanical (peristaltic), capillary	Passive	Passive	Fluorescence
Biosite (Alere)	Strip with textured microstructures	On test strip	Whole blood (venous), plasma	Centrifugation	Capillary	Passive	Passive	Fluroescence
Cepheid	Disposable plastic cartridge	On test cartridge	Whole blood, sputum	Sample dilution buffer, shaking	Pneumatic (syringe plunger)	Rotary valves	Passive, manual	Fluorescence (with molecular beacons)
Claros Diagnostics (Opko)	Plastic cassette	On cassette	Whole blood, urine	On cassette	Pneumatic	Passive	Passive	Absorbance
Daktari Diagnostics	Plastic cartridge	On cartridge blister packs	Whole blood	On cartridge	Pneumatic	Passive	Passive	Electrochemical (impedance spectroscopy)
Diagnostics For All	Paper	Dry reagents on paper	Whole blood, urine	On stamp	Capillary	Passive	Passive	Colorimetric
Epocal (Alere)	Film, epoxy laminates	Dry reagents	Whole blood	On chip	Capillary, pneumatic, electrokinetic	Electrokinetic	Electrokinetic	Electrochemical, chemiluminescence
Focus Dx (Quest)	Plastic (polypropylene)	PCR reagent prep needed	Nasal & pharyngeal swabs	Nucleic acid extraction	Centrifugal	Passive	Passive	Fluroescence
HandyLab (BD)	Disposable cartridges	Dry reagents	Vaginal, rectal, nasal swabs	Broth enrichment, cell lysis (MRSA)	Electrokinetic, thermal pneumatics	Valves	Passive	Fluorescence (with molecular beacons)
i-STAT Corp (Abbott)	Plastic cartridge with silicon microchip	On cartridge	Whole blood, urine	On cartridge	Pneumatic (air bladder), capillary	Passive	Passive	Electrochemical (potentiometry, amperometry, conductivity)
Micronics (Sony)	Plastic, laminates, paper	On cartridge	Whole blood, stool	On cartridge	Pneumatic, capillary	Passive, valves	Passive	Absorbance, colorimetry
MBio Diagnostics, Inc.	Plastic, transparent planar components	On chip	Whole blood	On chip	Pneumatic	Passive	Passive	Fluorescence (with planar waveguides)
Philips	Plastic cartridge	Dry reagents on cartridge	Whole blood, saliva	On cartridge	Pneumatic	Passive	Passive	Optical (frustrated total internal reflectance)
TearLab	Polycarbonate	None	Tear	On chip	Capillary	Passive	Passive	Electrochemical
Zyomyx	Glass, plastic	Dry reagents	Whole blood	Bead-conjugated Ab incubation	Gravitational	Passive	Passive	Colorimetric (cell stacking)

Figure 2.Technology map of design choices made by selected microfluidics companies for a set of common LOC procedures integrated POC diagnostics device [2].

2. Background

Many pathologies and physiological conditions can be diagnosed through the analysis of blood plasma, which provides crucial information of various internal organs. First step, in most blood tests, is plasma extraction from whole blood. In order to fulfill these analyses most researchers, scientists and doctors use centrifugation to separate plasma from whole blood. But this technique requires a laboratory. In order to minimize error, reduce the time from blood collection to the test and provide faster and yet less expensive and comprehensive results, ”lab-on-a-chip” type of devices are an attractive tool for blood plasma separation and analysis. Although many researchers have developed plasma separation from whole blood utilizing different techniques in micro technologies, the volume of extracted plasma to implement the test is still one barrier to achieve a reliable lab on a chip (LOC) blood test.

Currently, microfluidic blood plasma separation techniques can be classified in three main formats: paper-based microfluidics, the CD format and the microfluidic chip format [9]. Although paper-based microfluidics has been widely used in lateral-flow assays, recently the use of paper to build microfluidic circuits shows a great potential to miniaturize blood analysis devices [10, 11, 12]. But, the fact of being relatively new means that issues such as the control over flow rates, mixing, and interaction times between sample and reagents have not yet been perfected, also limiting its application to the analysis of highly concentrated analysts, abundant proteins [12] or glucose [11]. The CD based format, even though it is a miniaturization of the conventional centrifugation method, it has the limitation of requiring specific equipment [13, 14].

The proposed designs to achieve plasma separation can be divided in two main categories: passive and active methods. Active methods need an external force such as such as magnetic [15], electric [16, 17], acoustic [18, 19] to achieve separation. In the category of passive separation methods, researchers exploit several techniques such as dead-end filtration [20], cross flow filtration [21, 22], hydrodynamic separation [23, 24], sedimentation [25, 26], deterministic lateral displacement [27], pinched flow fractionation [28] or biomimetic separation methods [29].

An example of passive methods is the cross-flow micro-device, shown in Figure 3.

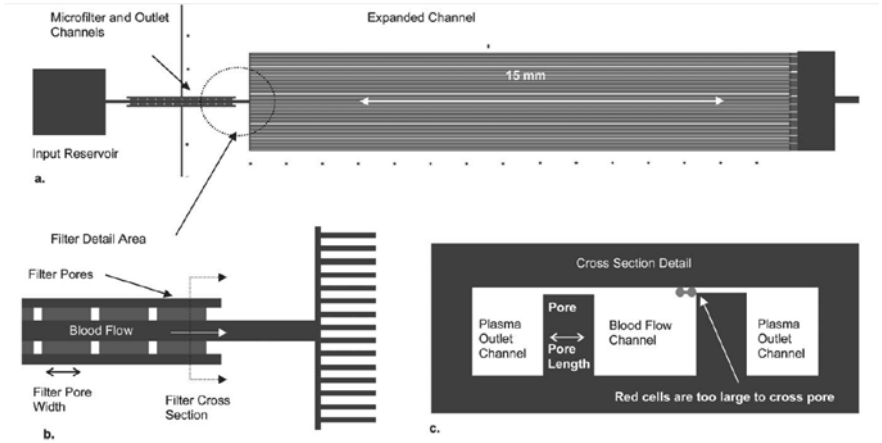

Figure 3. Blood plasma microfilter: (a) top view (b) filter detail area showing filter pores and expanded channel layout, (c) microfilter cross section [30]

Another passive method uses the bifurcation effect to achieve the separation. In this case, the higher-pressure gradient causes the cells to be drawn into the higher flow rate channel, see Figure 4 [31].

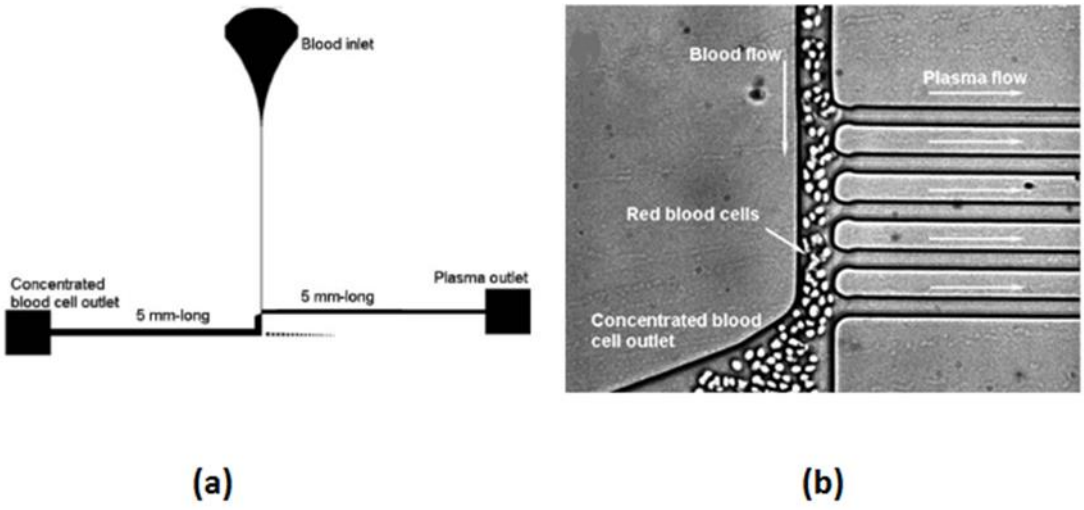

Figure 4. (a) Schematic diagram of a microfluidic blood plasma separation device (b) Photograph of the blood plasma separation region after infusing defibrinated sheep blood [31]

Initially, most of these design principles required a syringe pump to control the required flow rate of the microdevice, which is not always available when thinking in a POC device for blood testing near the patient and in general only few nanoliters of plasma could be separated.

Therefore, some researchers have focused on the use of dielectrophoeresis (DEP) technique that could generate the flow without an external pump. Accordingly, the dielectrophoresis (DEP) method presented good capability to manipulate particles, which has been applied extensively in lab-on-a-chip and biochip for such small volume of sample [32]. Dielectrophoresis is the movement of particles caused by polarization effect when the particles are in the nonuniform electric field applied inside the channel. This electric field can be created either with direct current (DC), and/or alternative current (AC) particles. The nonuniform electric field can be generated using two methods:

1. Electrode-based DEP (eDEP) that employs arrays of electrodes.

2. Insulator based DEP (iDEP) which employs an array of insulating structure.

The electrode-based (eDEP) is a traditional method. Significant development of this method has been presented based on novel electrode structure [16] in many applications for instance: separation of red blood cell (RBC) [33, 34], cancer cell separation [35] or bacteria or virus trapping [36].

Nakashima et al. [33] presented a capillary and dielectrophoresis device. The image shows the top and cross-sectional views of plasma extraction principle from diluted blood (1:9), see Figure 5.

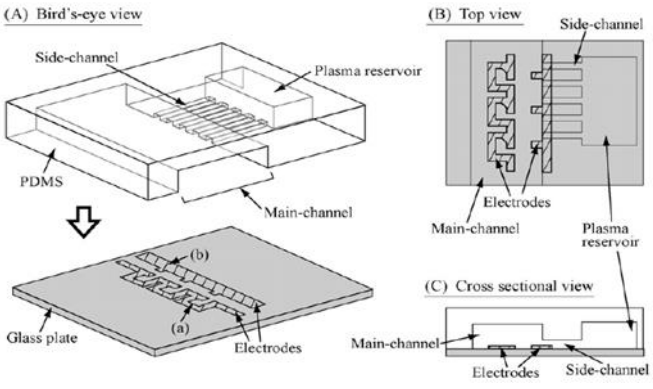

Figure 5. Design of a plasma filter to separate diluted blood using dielectrophoresis and capillarity [33].

Chang and Cho [34] presented a continuous, size-dependent particle separator that used negative dielectrophoresis based on a virtual pillar array of electrodes to separate red blood

cells (5.4 ± 1.3 μm diameter) and white blood cells (8.1 ± 1.5 μm diameter) with separation purity over 99%, see Figure 6.

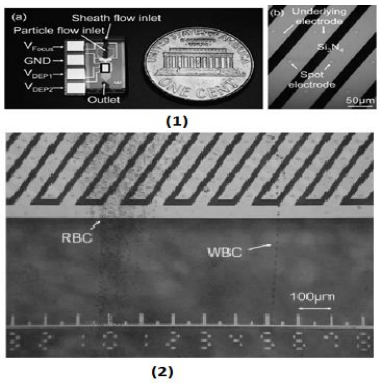

Figure 6. (1) Overall device dimensions of the fabricated device. (2) Separation of red blood cells (RBCs) and white blood cells (WBCs) [34].

Shyng Leu et al [37] presented a micro separator with different dilution ratios and flow rates conditions, to extract the cell-free plasma from whole blood samples. To obtain plasma an arrangement of embedded electrodes was used inside the channel, see Figure 7. The effect of different dilution ratios (1:0, 1:1, 1:2, 1:3) for focusing on cells in the middle of channel was investigated.

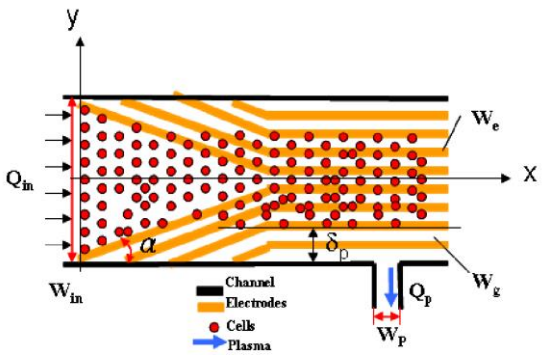

Figure 7. Principle of a DEP micro separator [37].

In this paper, the minimum dilution ratio that could be depleted of RBC cells was 1:3, even though they also worked with whole blood demonstrating an efficiency of 20%.

The microelectrodes array can be fabricated with small dimensions to generate high electric field by applying low voltages. However, eDEP method has important drawbacks such as the fact that the fabrication process of the electrodes is time consuming and expensive, while it does not avoid the hydrolysis of biological cells. The fouling of particles can affect electrode performance. Moreover, bubble generation, thermal convection and cell damaging due to

high electric field are other disadvantages of embedded electrode inside the channel in eDEP devices [16].

2.1. Insulator–based di-electrophoresis devices

Insulator–based DEP offers an alternative by utilizing 3- dimensional insulating posts made out of PDMS (Polydimethylsiloxane), PMMA (Poly methyl methacrylate) or thiolene resins (such as NOA 63 from Norland Optical Adhesives) inside the fluidic channel to change the path track and generate a non-uniform electric field between two external electrodes. The iDEP devices can be deep and therefore be utilized as high throughput micro devices. This is because the electric field gradient is not confined on the embedded electrodes wall surface of channel [38]. Moreover, the majority of iDEP devices that employed the DC-electric field can produce an electroosmotic flow (EOF) that eliminates the need of an external driving force [39, 40]. The use of just two simple electrodes placed in the channel inlet and outlet offers other advantages such as a straightforward fabrication process, devices that are less prone to fouling and minimum bubble generation inside the channel, less electrochemical reactions [41] and the process is more appropriate for metal-sensitive organic samples.

The iDEP method has been successfully employed for different application: separations & concentration of live and dead bacteria [3], E.coli bacteria [36], and separation of white blood cell [42], RBCs [43], or blood cell separation in a sawtooth microchannel [44] (see the review of DC-iDEP studies [45]). The main drawback of DC dielectrophoresis (DC –DEP) device is the undesirable electrolysis on the surface of electrodes. DC-iDEP manipulates the cell or particle by applying spatially non-uniform electric field independent of frequency [3].

2.1.1. Dc- iDEP for non-viable cells

Cummings and Singh [8] in 2003 used glass micro-channels thermally bonded with three different post shapes (diamonds, square and circles). DC electric fields ranging from 250 till 1000 V/cm were applied for trapping 0.1-µm-radius latex particles.

Kang et al. [5] in 2006 used PDMS channels (240×130 µm) and rectangular posts separated 60 microns to separate carboxylate-modified polystyrene particles with different diameters 2.85, 5.125 and 7.85 µm. The electric field varied from 500 to 900 V/cm.

Barbulovic-Nad et al. [46] in 2006 presented separation of fluorescent polystyrene particles (0.5, 2.85 and 7.85 µm) in DI water solution.

Ozuna-Chacon et al. [7] in 2008 presented a strong negative DEP force based device for trapping 0.5-µm-radius carboxylate polystyrene microspheres in a 25-100 µS/cm-medium-

conductivity. The device was made in glass with 440-µm-diameter cylindrical posts separated 550 µm center to center and a DC electric field ranging from 200 till 800 V/cm.

Roberto C. Gallo et al. [47] in 2011 presented DC -iDEP for the separation and discrimination of a mixture 1 and 4 µm polystyrene microspheres particles in 5.7-pH and 1.15 mS/cm-conductivity suspending medium. Figure 8 shows the device design that comprises a main channel, two side channels and two sections of cylindrical posts with different diameters. The microparticles were separated and concentrated at the same time and then redirected to different outlets applying 1000 V.

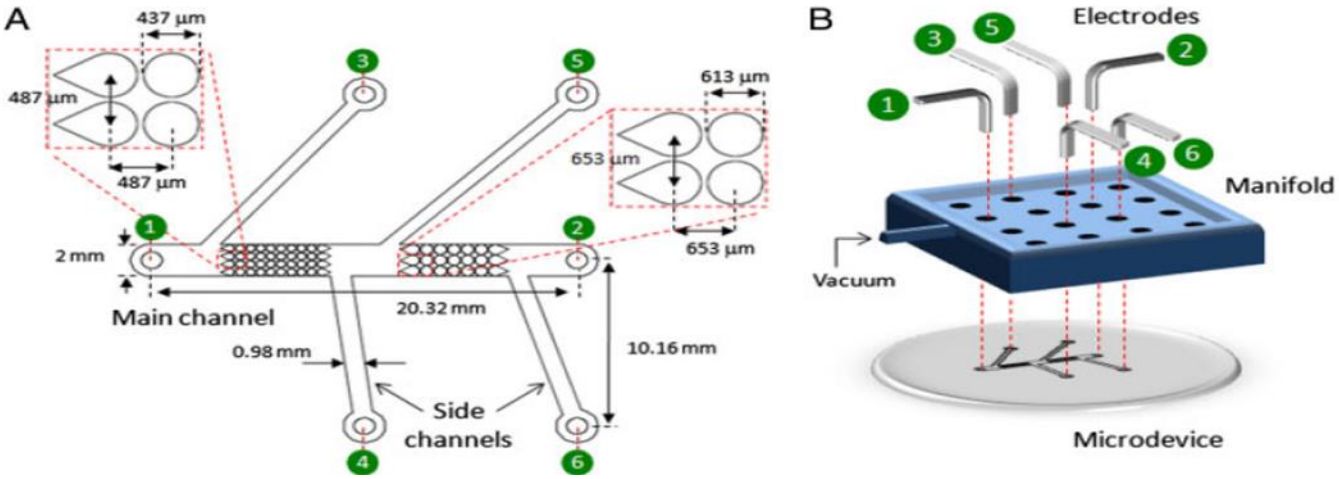

Figure 8. Schematics of (DC)-iDEP design for particle separation. (A) The microdevice employed contains cylindrical insulating posts arranged in two sections with different diameter sizes; (B) a flow manifold is placed on top of the glass microdevice so its openings are aligned with the channel reservoirs, electrodes are then introduced to generate the electric fields [47].

The experiments resulted in trapping and discrimination of the polystyrene particles as it can be seen in Figure 9.

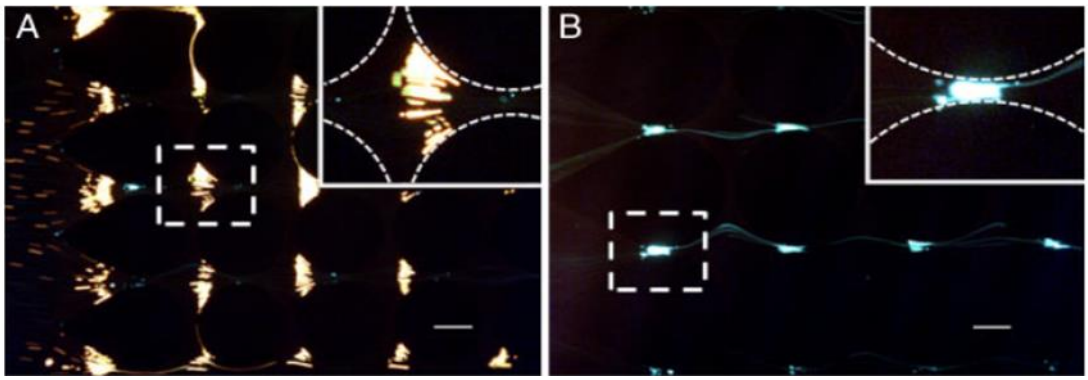

Figure 9. (A) Picture of red particles (4-µm) trapping between post (437- µm-diameter); (b) Picture of green particles (1-µm) trapping between post (613-µm-diameter).

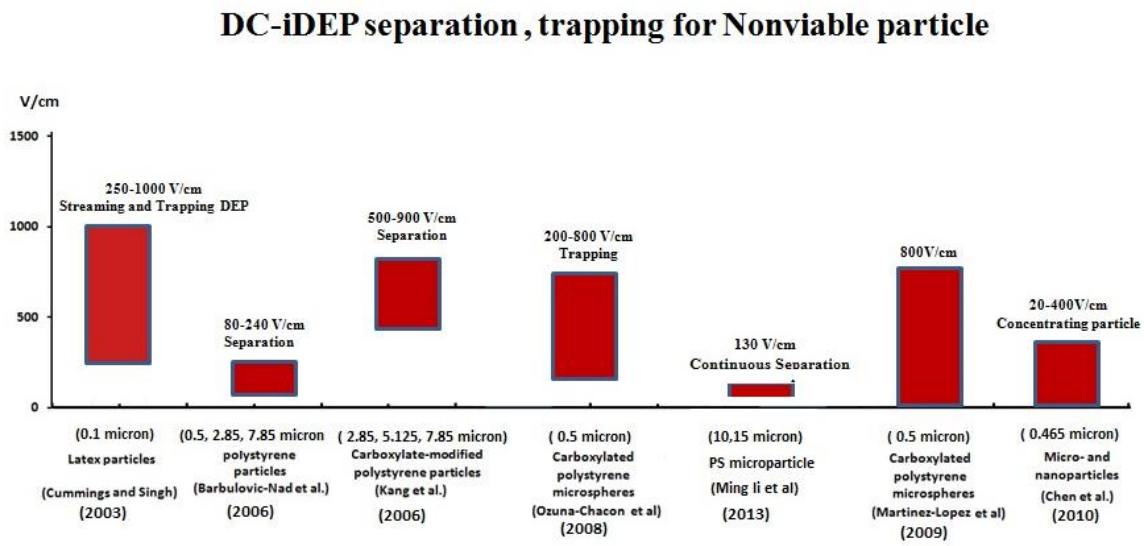

Figure 10. Summary of DC insulator based dielectrophoresis devices for trapping and separation of particles. (Cummings and Singh [8], Barbulovic-Nad et al. [46], Kang et al. [5], Ozuna-Chacon et al. [7],Ming li et al [48], Martínez-López et al. [49] and Chen et al. [50] are previous works of non-viable particles separation (the particle size is in microns).

From Figure 10, previous work has been able to trap particles in the range of red blood cells (2-10 microns) applying high electric fields, but there are other parameters such as the geometry of the channel or the posts, medium and particle conductivities that play an important role to achieve trapping. In the case of red blood cells, the minimization of the voltage required is important and this is directly related to the particle size since the DEP force is proportional to the cube of the particle diameter. Since the RBC size is standard, to minimize the voltage, the channel design is a key parameter, because other parameters such as medium and particle conductivities cannot be modified either.

2.1.2. Dc- iDEP for viable cells

Researchers have found two major problems when trying to apply DC-iDEP for a live cell trapping: force induced by the electric field and the Joule heating effects on the membrane [51]. The DEP force is a function of the intensity of the electric field gradient. Strong DC electric field imposes a great stress on the cell membrane when they transit through narrow constrictions. For instance, Kang et al. in 2008 observed that live cancer cells died in a short time after going through a rectangular obstacle when 343 V were applied [42]. Therefore, it is not possible to increase the voltage to speed up the separation process or to improve the separation efficiency [51].

The temperature rise due to Joule heating cannot be avoided in DC-iDEP experiments, but it can be minimized. To this end, electric current was monitored during the experiment [52] by Feeney et al. [53]. They noticed that thermal decomposition had generated free radicals and cell membranes were damaged under the application of high voltage.

The first separation and concentration of live and dead bacteria was rendered by Lapzico-Encinas et al. [3], in year 2004. Glass microchannels with square, triangular, and circular insulating post of 200-µm diameter and 250-µm distance between two posts were used. Deionized (DI) water was used as electrolyte with 2.25 µS/cm of conductivity and high electric fields between 0-2000V/cm were applied, see Figure 11.

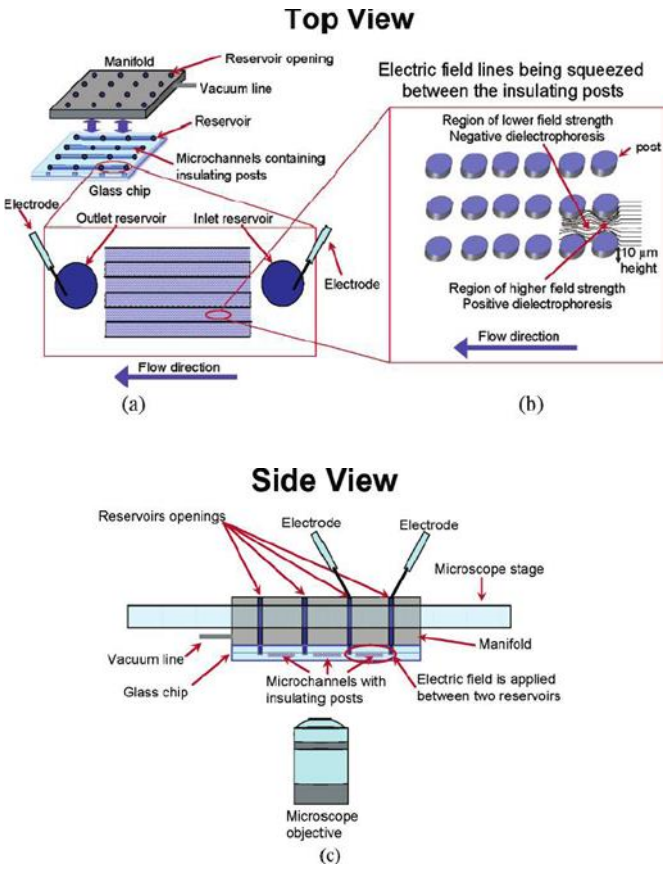

Figure 11. Schematic representation of the experimental setup: (a) top view, showing the manifold, glass chip, an enlargement of the flow microchannels; (b) Electric field lines between the insulating posts; (c) side view showing the manifold and glass chip on the microscope stage [3].

Kang et al. [54] in 2008 used DC-iDEP combined with electrostatic flow for continuously separate a mix of biological cells of tens of micrometers difference in diameter into different collecting wells.

In this research, the particles were white blood cells from HIV-infected subjects and live mammalian breast cancer cells. Two different solutions were used where the particles where in suspension: lysis buffer (1× DMEM, Mediatech, #10-013-CV, Herndom, VA) for fixing the white blood cells by ranging from 8 to 14 µm and other components (platelets, lysis RBC debris, etc.) smaller than 5 µm and nutrition solution (10 mMTris, pH 7.5, 50 mM NaCl, 250 mM Trehalose, and 0.02%EDTA) with 1 million/ concentration for the cancer cells (cell line MCF7) with diameters in the range of 20 to 60 µm. Target cells via specific size were separated by applying the required voltage see Figure 12.

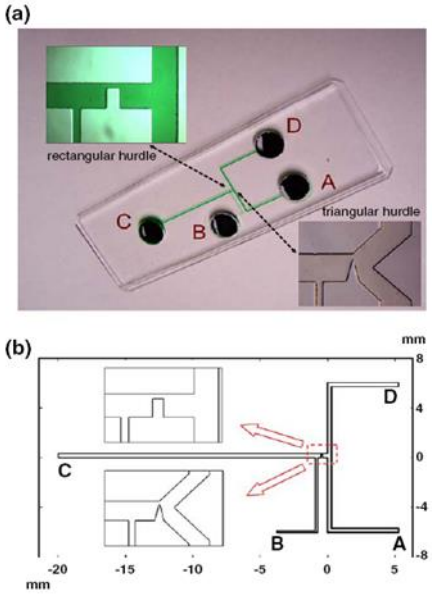

Figure 12. (a) Chip design for cell separation; (b) Dimensions of the microdevice and the inner structure [54]

White blood cell separation was achieved through 31 V applied to the inlet while breast cancer cell separation was achieved when 56 V were applied.

Gallo-Villanueva et al. [55] in 2009 applied negative DEP for immobilizing and concentrating linear DNA particles (pET28b) with 0.001 µm radius and medium with 10.8-11.15 PH and 100-120 µS/cm conductivity. They utilized PDMS microchannels with rectangular insulating post (470-µm width) and 510 µm-distances between the posts. The DNA immobilization occurred with an electric field of 500-1500 V/cm and DNA concentration happened in the electric field of 2000 V/cm.

Cho et al. in 2009 [36] presented a device that concentrated 1.5-µm-radius E.coil cells (bacteria) when 1280 V/cm-AC-field was applied in 0.5 mS/m-medium-conductivity. The microchannel was done out of Honeycomb –type (hexagonal) pores made of SU8 2100.

Srivastava et al. [43], in 2011 presented a PDMS direct current insulator dielectrophoresis (DC-iDEP) device for red blood cell sorting of the eight blood types (A+, A-, B+, B-, A+, AB-, O+, O-) in different conductivity buffers (0.52–9.1 mS/cm). They applied DC electric fields between 17.1 and 68.5 V/cm and used 400 ×170 rectangular insulating obstacles to create spatial non-uniformities in a 1.46-cm long, 200-µm wide,73-µm deep channel with one inlet (200-µm wide) and four outlets (50- µm wide), as shown in Figure 13.

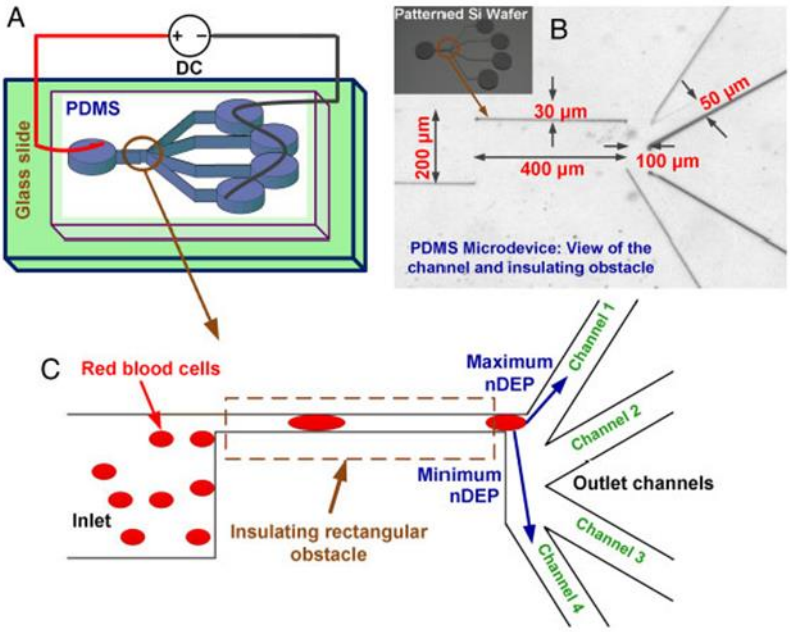

Figure 13 (A) Schematic of PDMS DC- iDEP microfluidic RBC sorter. (B) Overall dimensions (C) Expanded view and the direction of nDEP on the erythrocyte as it flows through this region of the microdevice [43].

Figure 14 shows the RBC trapping before and after applying the electric field. Srivastava proposed an optimum allowable electrical field for separation or trapping viable erythrocyte in lower conductivity mediums of <68 V/cm and in high conductivity mediums of <34 V/cm.

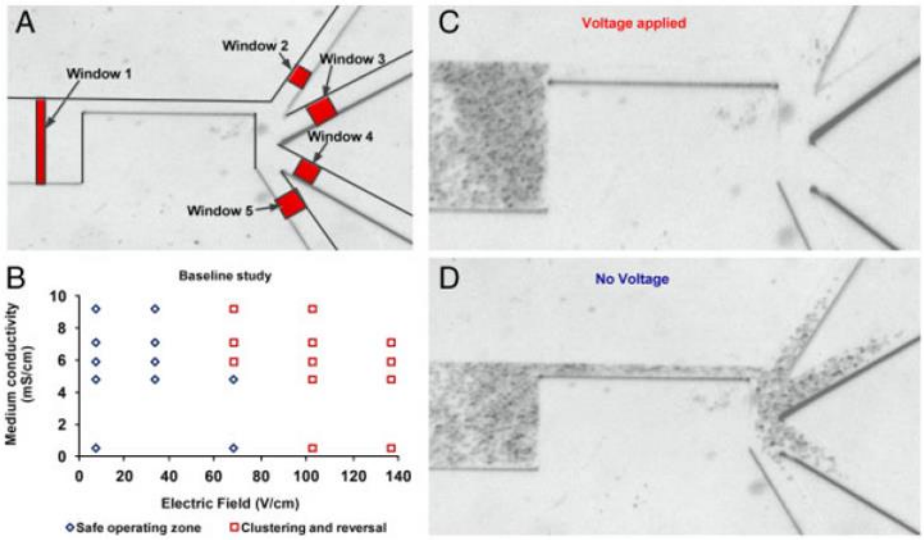

Figure 14. (A). Different cross section channel (B) Viable and nonviable erythrocytes in different field (C) voltage is applied. (D) no voltage is applied [43],

Figure 15 summarizes the previous DC –iDEP works for the separation and trapping of different viable cells showing the maximum electric field used.

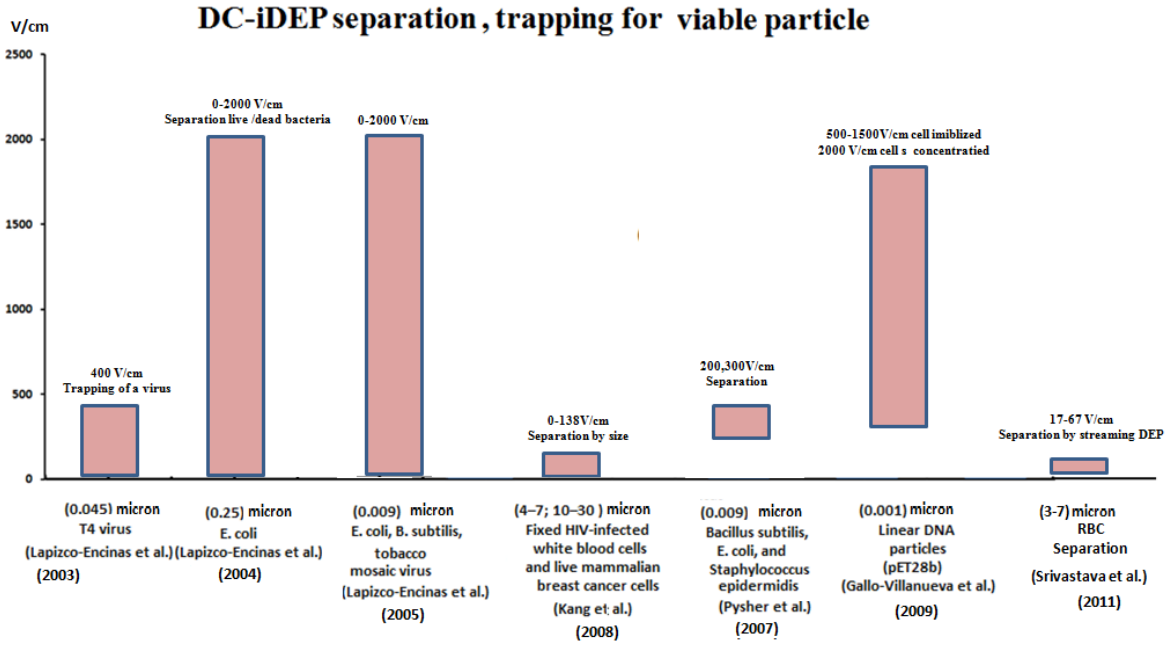

Figure 15. Summary of DC insulator based dielectrophoresis devices for trapping and separation of viable cells (Lapizco-Encinas et al.(virus trapping) [4], Lapizco-Encinas et al.(coli separation) [3], Lapizco-Encinas et al.(E.coli,B.subtilis,virus) [56], Kang et al. [54], Pysher et al [57], Gallo-Villanueva et al. [55] and Srivastava et al. [43], are previous works of viable particles separation (The particle size is in microns).

The main drawback of previous studies is the use of dilution to control different parameters such as conductivity, pH and the ratio of particles in the medium. Since this thesis pretends to design a POC device that filtrates a drop of the real blood. Blood treatment and dilution is not an option to achieve filtration, therefore this thesis will focus on the proper microfluidic design to achieve high throughput plasma filtration without dilution and pretreatment in a reasonable time.

3. Electrokinetics

The Electrokinetic phenomena include several different effects in the presence of an electrical field, as it can be seen in Table 1.

Table 1 .Electrokinetic effects

	Type	Cause	Type of Field
Electro kinetic Effects	Electro-osmosis	Interaction between free charge in electrical double layer and tangential electric field	AC/DC
	Electrophoresis	Charge in electric field	DC
	Dielectrophoresis	Induced dipole in non-uniform field	AC/DC
	Electro-orientation	Interaction between dipole and electric field	AC/DC
	Electro rotation	Dipole lags in rotating electric fields	AC
	Traveling-wave Dielectrophoresis	Dipole lags in traveling electric fields	AC

3.1. Electroosmosis

Whenever a polar fluid (such as water) and a solid are brought into contact, the surface of the solid (wall) gets an electric charge. The charge attracts counter ions and forms a thin layer near the wall called *stern layer*. This layer is stationary and generates another layer called diffuse layer or *Gouy-Chapman* layer. Diffuse layer moves under influence of electric field and both layers are called Electric Double Layer (EDL). The interface between the stationary and the moving layer is called *shear surface* and the potential at the shear plane is called Zeta potential ζ . Both glass [58] and polymer-based microfluidic devices [59] tend to have negatively charged surface chemistries what means that EDL is positively charged. For instance, according to [45] PDMS potential is $\zeta_{PDMS} = -82 \pm 2mV$. If a voltage across the channel is applied, motion of ionized liquid is generated. That is called Electroosmotic flow. Schematics of ion distribution and electroosmotic flow, are shown in Figure 16.

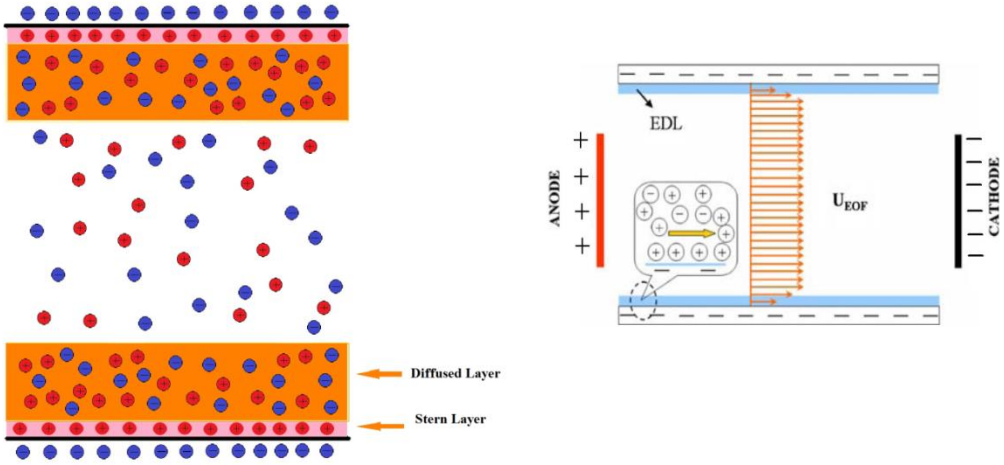

Figure 16. Ion distribution and electroosmotic flow.

Electroosmotic velocity (EOF) [60] is:

$$\vec{V}_{eo} = \mu_{eo}\vec{E} = \frac{\varepsilon_m \zeta_w}{\eta}\vec{E} \quad (1)$$

where μ_{eo} is electro-osmotic mobility of the ionic fluid and $\vec{E}$ is the local electric field. Electro-osmotic mobility is a function of the surface potential between the solid and the liquid phase (ζ), the viscosity (η), and the permittivity (ε_m) of the fluid.

3.2. Electrophoresis

An electric double layer (EDL) will additionally form around a charged particle placed in an infinite ionic liquid under a uniform field. The particle will then be driven towards the region of highest potential by a Coulombic force (Fc) which is proportional to the net charge of the particle (q) and equal to

$$\vec{F}_c = q\vec{E} \quad (1)$$

(Kang and Li 2009 [61]). This force is known as electrophoresis and the resulting electrophoretic velocity (Vep) of a spherical particle can be calculated applying the Huckel equation (Tandon et al. 2008 [62]).

$$\overrightarrow{V_{ep}} = \mu_{ep}\vec{E} \quad (2)$$

This velocity is a function of the electrophoretic mobility (μ_{ep}) of the cell and E the local electric field. The electrophoretic mobility for a spherical particle is defined by the Smoluchowski equation (Baylon-Cardiel et al. 2009 [63]

$$\mu_{ep} = \frac{\varepsilon_m \zeta_p}{\eta} \quad (3)$$

μ_{ep} is a function of the surface potential between the particle and the zeta potential of particle (ζ_p), the permittivity (ε_m) and the viscosity (η) of the surrounding media. The net velocity of the cell as result of these two forces is referred to as the electrokinetic (EK) velocity (Vek) (Baylon-Cardiel et al. 2009; Kwon et al. 2008 [64]).

$$\overrightarrow{V_{ek}} = \mu_{ek}\vec{E} = (\mu_{EO} - \mu_{EP})\vec{E} \quad (4)$$

3.3. Dielectrophoresis

An A charged or neutral particle placed in an infinite ionic liquid under a non-uniform field will become polarized and develops a charge distribution across the volume of the particle. The

cell will then be driven towards or away from the regions of maximal field gradient by a translational dielectrophoretic force (F_{DEP}) (Pohl 1958 [65])

$$F_{DEP} = 2\pi\varepsilon_m r_p{}^3 \mathrm{Re}[f_{CM}]\nabla(E_{RMS}.E_{RMS}) \quad (5)$$

Where r_p is the radius of the cell, $\mathrm{Re}[K(\omega)]$ is the real part of the Clausius–Mossotti (CM) factor and E_{RMS} is the amplitude of the electric field. The direction of the translational displacement is dependent on the sign of the CM factor, which is theoretically bound between -0.5 and 1.0 for spherical particles. A hydrodynamic force, F_{DRAG} is exerted on the particles as they translate through the fluid

$$F_{DRAG} = 6\pi\eta r_p V \quad (6)$$

where V is the velocity of the particle relative to the suspending medium.

The steady-state velocity of the particles is determined by a balance between the dielectrophoretic forces and Stoke's drag in summation with the EK velocity. In this preliminary study, the effect of acceleration is considered negligible, and the relationship for particle translation is given by:

$$U = V_{ek} + \frac{\varepsilon_m r_p{}^2 \mathrm{Re}[f_{CM}]}{3\eta}\nabla(E_{RMS}.E_{RMS}) \quad (7)$$

Where r_p is the radius of the spherical particle, ε_m the solution permittivity and ω the filed angular frequency (rad/sec). The parameter f_{CM} is the Clausius-Mossotti factor, which is given by:

$$f_{CM} = \frac{\tilde{\varepsilon}_p - \tilde{\varepsilon}_m}{\tilde{\varepsilon}_p + 2\tilde{\varepsilon}_m} \quad (8)$$

Where $\tilde{\varepsilon}_P$ and $\tilde{\varepsilon}_m$ are the complex permittivity of the particle and the solution respectively. For an isotropic homogeneous dielectric, the complex permittivity is:

$$\tilde{\varepsilon} = \varepsilon - \frac{\sigma}{\omega}i \quad (9)$$

Where ε is the permittivity, σ is conductivity of the dielectric and *i* is the square root of -1.

Limitation of Clausius-Mossotti factor f_{CM} parameter is:

$$-\frac{1}{2} < \mathrm{Re}[\, f_{CM}\,] < 1 \qquad (10)$$

Table 2. Advantages and disadvantages of p-DEP and n-DEP

Advantage and disadvantage of positive and negative DEP Force for trapping cell [66]	
Positive DEP Force $\mathrm{Re}[\, f_{CM}\,] > 0$	**Negative DEP Force** $\mathrm{Re}[\, f_{CM}\,] < 0$
CM factor can go to +1 (+)	CM factor can go to -0.5 (-)
Less heating (+)	More heating (-)
Typically easier to trap by pulling (+)	Typically easier to trap by pushing (-)
DEP force is toward higher electrical fields and cells go to maximum electric field (-)	DEP force is toward lower electrical fields and cell go to minimum electric field (+)
Trap usually get stronger as V increases(+)	Trap often doesn't get stronger as V increases (-)
Particles collect at electrode edges and can damage the electrode (-)	Particles are repelled from electrode edges (+)
Must use low medium conductivity (-)	Can use saline or other high salt buffer (+)
Particles collect at electrode edges and can damage the electrode (-)	Particles are repelled from electrode edges (+)
Must use low medium conductivity (-)	Can use saline or other high salt buffer (+)

Two parameters, frequency of the applied field and complex permittivity of the medium have a key role in the definition of the Clausius-Mossotti factor. The DEP force is classified as

either positive or negative depending on the sign of the real part of f_{CM} . The classifications are given in Table 2 [66].

3.3.1. Insulator based dielectrophoresis.

Total particle velocity due to non-uniform electric field is:

$$\vec{V}_{Tot} = (\mu_{EO} - \mu_{EP})\vec{E} + \mu_{DEP}\nabla\vec{E^2} \quad (11)$$

Where $\vec{V}_{TOT}$ is the total velocity, $\vec{E}$ is electric field, $\nabla\vec{E}^2$ is the gradient of the squared modulus of the electric field, μ_{EO} is the electroosmosis mobility , μ_{EP} the electrophoresis mobility and μ_{DEP} the dielectroporesis mobility. The direction of the EO flow is from the positive electrode to the ground electrode and the direction of the EP flow is from the ground to positive electrodes for negatively charge particles and from the positive electrode to the ground electrode for positively charged particles. μ_{EP} can be neglected compared to μ_{EO} thus the EK flow is mainly dominated by EOF and particles move from positive to negative electrodes (RBCs have small net negative charge and their EP mobility is small to compared with EO mobility) [7].

Frequency is zero in DC-iDEP and the Clausius-Mossotti factor depends on particle and medium conductivity. The Clausius-Mossotti factor :

$$f_{CM} = \frac{\sigma_P - \sigma_m}{\sigma_P + 2\sigma_m} \quad (12)$$

where σ_P , σ_m are the particle and medium conductivity. Negative f_{CM} presents negative DEP, where particles concentrate at field minima, and positive f_{CM} presents positive DEP, where particles concentrate at field maxima.

The DEP velocity relationship depends on the electric field gradient, Clausius-Mossotti factor, medium viscosity, and medium permittivity. $\vec{V}_{DEP}$ is the dielectrophoretic velocity and μ_{DEP} is the dielectrophoretic mobility which, can be expressed as [67, 68]:

$$\vec{V}_{DEP} = -\mu_{DEP}\nabla\vec{E}^{2} = \frac{d^{2}\varepsilon_{m}f_{CM}}{12\eta}\nabla\vec{E}^{2} \quad (13)$$

Where d is the particle diameter, ε_m is the permittivity of medium, f_{CM} is Clausius-Mossotti factor, η is the viscosity of medium and $\nabla\vec{E}^{2}$ is the gradient of the square modulus of the electric field. The net DEP force for a spherical particle is:

$$F_{DEP} = 2\pi\varepsilon_{m}r_{p}^{3}f_{CM}\nabla(\vec{E}.\vec{E}) \quad (14)$$

Where ε_m permittivity of the medium, r is is radius of the particle and ∇E^{2} is the gradient of the square modulus of the electric field.

The particle flux j can expressed in term of the electrokinetic velocity $\overrightarrow{V_{ek}}$ an the dielctrophoretic $\overrightarrow{V_{dep}}$ velocities as

$$\vec{j} = C(\overrightarrow{V_{ek}} + \overrightarrow{V_{dep}}) \quad (15)$$

Where C is the concentration of particles. Trapping of particles happens when the contribution of DEP to the particle flux is greater than the contribution of EK. Therefore, in the region of trapping, total particle flux j along the electric field line is zero.

$$\vec{j}.\vec{E} = 0 \quad (16)$$

Combined with Eq 14, 12 can be expressed as:

$$(\mu_{EK}\vec{E} - \mu_{DEP}\nabla\vec{E}^{2}).\vec{E} = 0 \quad (17)$$

Thus, the condition for trapping due to DEP for a spherical particle is:

$$\frac{C\mu_{DEP}\nabla(\vec{E}.\vec{E}).\vec{E}}{\mu_{EK}\vec{E}.\vec{E}} > 1 \quad (18)$$

Where the DEP mobility overcame on EK mobility in the trapping DEP zone and the EK mobility exceeds the DEP mobility in the EO flow zone and C is a correction factor that accounts for unconsidered phenomena and measurement errors.

3.4. Human Blood

Blood is a very inhomogeneous material, which includes different components: plasma (serum and fibrin) (55%) and suspended micro-particles (45%). According to Kokoris et al. [69], micro particles are: almost 45% erythrocytes (red blood cells-RBCs), 1% leukocytes (white blood cells -WBCs) and 0.5% thrombocytes (platelets). Plasma consists of 90 % (w/w) water, 7% (w/w) proteins. According to Rosenson et al. [70] plasma behaves like a Newtonian fluid with a constant viscosity of $\mu_{plasma} 1.36 \pm .08 \times 10^{-3}\, pa.s$. The mean blood viscosity at shear rates of 100, 50, and 1 s^{-1} were 3.26 ± 0.43,4.37 ± 0.60, and 5.46 ± 0.84 mPa s, respectively. Men had significantly higher blood viscosity values than women at each shear rate.

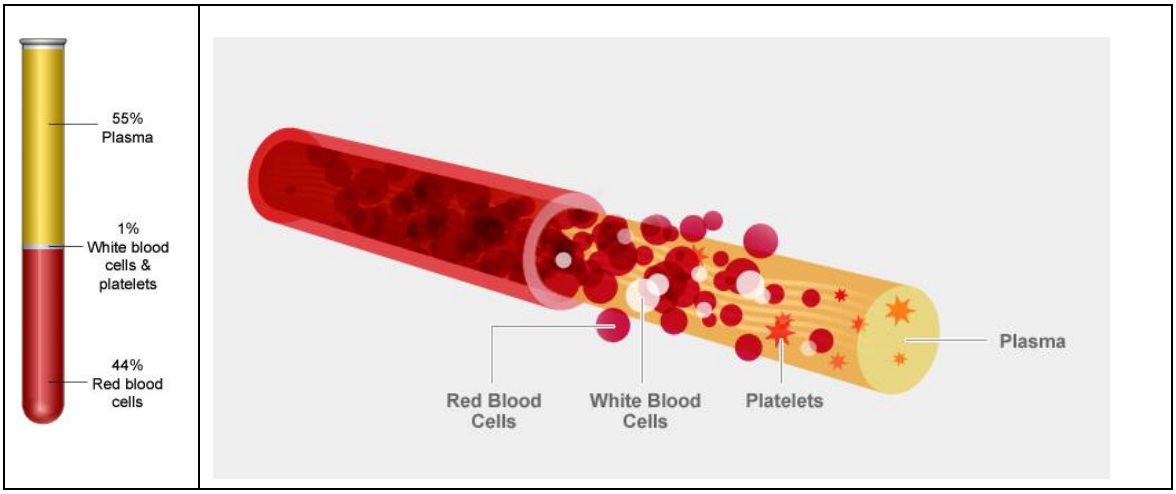

RBCs are biconcave in shape with a diameter of 6–8 µm. They carry hemoglobin and assist to respiratory gases transportation. They are responsive to the small changes in pH and temperature of solvent conditions. WBC have a diameter between 8 and 12 µm and they avoid infections and diseases. The other components in the blood are platelets, which have diameters between 2.65 to 2.9 µm and they can aggregate to clot.

3.4.1. Electrical properties of blood

Mature RBCs grow up in the bone marrow before being released into blood stream circulation. They lack of nucleus, which is important dielectrophoretically because polarization across a nuclear membrane will not occur. RBCs have a net negative charge with a nonconductive (µS/m) outer membrane and conductive (S/m) interior [71, 72].

Regarding to plasma Jones et al in 2011 [44] measured plasma relative permittivity as , and plasma conductivity as 1.2S/mat at 24℃ and 1.57S/mat at 37℃. Yong at al. [73] measured

the change of blood conductivity and resistivity related to percentage of RBCs, see Figure 17.

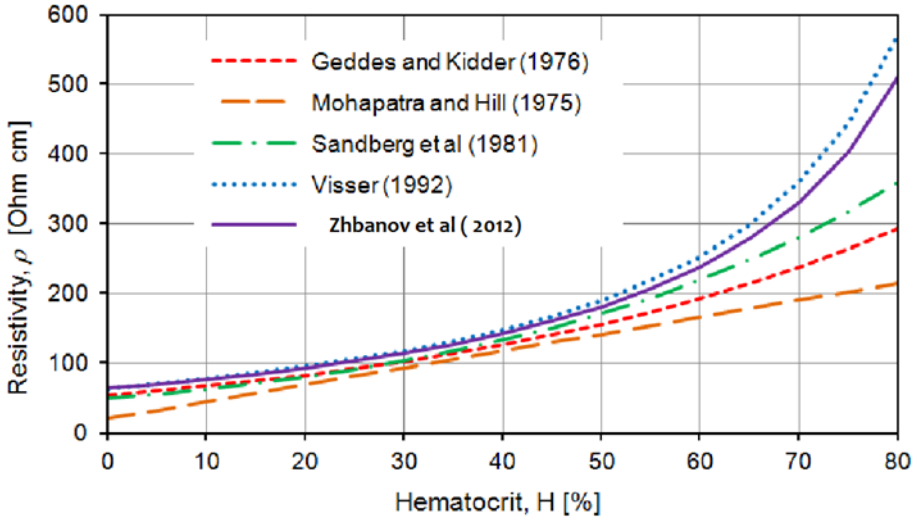

Figure 17. Dependence of the blood resistivity on hematocrit concentration [73].

Dielectrophoretic particle separation efficiency is strongly related to its electrical properties. Therefore it is important to analyze these properties in red blood cells. S. Abdalla [74] in 2011 presented electric and dielectric properties of human blood along a large frequency range (10 Hz–10 GHz). The direction of the electric field has an effect on electrical resistivity of flowing blood and on Rouleaux phenomena formation.

3.5. REFERENCES

[1] Frost Sullivan. Co “Top Technology Trends in Health and Wellness (Technical Insights),” June 2012.

[2] Curtis D. Chin, Vincent Linder and Samuel K. Sia, "Commercialization of microfluidic point-of-care diagnostic devices," *Lab Chip,* vol. 12, pp. 2118–2134, 2012.

[3] Lapizco-Encinas BH, Simmons BA, Cummings EB, Fintschenkoy "Dielectrophoretic concentration and separation of live and dead bacteria in an array of insulators" *Anal. Chem.,* vol. 76(6), pp. 1571-9, 2004.

[4] Lapizco-Encinas BH, Simmons BA, Cummings EB, Fintschenkoy “High throughput electrodeless dielectrophoresis ofviruses in polymeric microdevices "Squaw Valley, CA, USA,, 5–9 Oct 2003.

[5] Kang KH, Kang Y, Xuan X, Li D " Continuous separation of microparticles by size with direct current-dielectrophoresis" *Electrophoresis,* vol. 27, pp. 694–702, 2006.

[6] Lapizco-Encinas BH, Ozuna-Chacon S, Rito-Palomares M "Protein manipulation with insulator-based dielectrophoresis and direct current electric fields" *J Chromatogr (1),* vol. A 1206, pp. 45–51, 2008 .

[7] Ozuna-Chacón S, Lapizco-Encinas BH, Rito-Palomares M,Martínez-Chapa SO, Reyes-Betanzo C "Performance characterization of an insulator-based dielectrophoretic microdevice" *Electrophoresis,* vol. 29, pp. 3115–3122, 2008.

[8] Cummings EB, Singh AK "Dielectrophoresis in microchips containing arrays of insulating posts: theoretical and experimental results " *Anal. Chem,* vol. 75, pp. 4724-4731, 2003.

[9] Sollierb, Maı ¨wenn Kersaudy-Kerhoasa and Elodie"Micro-scale blood plasma separation: from acoustophoresis to egg-beaters," *Lab Chip,* vol. 13, pp. 3323, 2013.

[10] S. J. Vella, P. Beattie, R. Cademartiri, A. Laromaine, A. W. Martinez, S. T. Phillips, M. K. A. and G. M. Whitesides, "Measuring Markers of Liver Function Using a Micropatterned Paper Device Designed for Blood from a Fingerstick," *Anal. Chem.,* vol. 84, pp. 2883–2891, 2012.

[11] Xiaoxi Yang, Omid Forouzan, Theodore P. Brown and Sergey S. Shevkoplyas" Integrated separation of blood plasma from whole blood for microfluidic paper-based

analytical devices," *Lab Chip,* vol. 12, pp. 274, 2012.

[12] Temsiri Songjaroen, Wijitar Dungchai, Orawon Chailapakul, Charles S. Henrye Wanida Laiwattanapaisal"Blood separation on microfluidic paper-based analytical devices," *Lab Chip,* vol. 3392–3398, pp. 12, 2012.

[13] Mary Amasia, Marc Madou, "Large-volume centrifugal microfluidic device for blood plasma separation" *Bioanalysis,* vol. 2(10), pp. 1701–1710, 2010.

[14] Robert Gorkin, a Jiwoon Park,b Jonathan Siegrist,a Mary Amasia,a Beom Seok Lee,c Jong-Myeon Park,cd, "Centrifugal microfluidics for biomedical applications" *Lab Chip,* vol. 10, pp. 1758–1773, 2010.

[15] Nicole Pamme, Andreas Manz, "On-Chip Free-Flow Magnetophoresis: Continuous Flow Separation of Magnetic Particles and Agglomerates" *Anal. Chem,* vol. 76, pp. 7250-7256, 2004.

[16] Talukder Z. Jubery, Soumya K. Srivastava, Prashanta Dutta, "Dielectrophoretic separation of bioparticles in microdevices: A review" *Electrophoresis,* vol. 35, pp. 691-713, 2014.

[17] Nuttawut Lewpiriyawong, Chun Yang, "Dielectrophoresis Field-Flow Fractionation for Continuous-Flow Separation of Particles and Cells in Microfluidic Devices" *Advances in Transport Phenomena,* vol. 3, pp. 29-62, 2014.

[18] Filip Petersson, Lena A¡ berg,Ann-Margret Swa1rd-Nilsson, Thomas Laurell, "Free Flow Acoustophoresis: Microfluidic-Based Mode of Particle and Cell Separation" *Anal. Chem,* vol. 79, pp. 5117-5123, 2007.

[19] Per Augustsson, Cecilia Magnusson,Maria Nordin,Hans Lilja,Thomas Laurel, "Microfluidic, Label-Free Enrichment of Prostate Cancer Cells in Blood Based on Acoustophoresis" *Anal. Chem.,* vol. 84, pp. 7954−7962, 2012.

[20] Ching chou wo, ling zong hong,chun Ting ou, "Blood cell -free of plasma separated from blood sample with cascading weir taype microfilterusing dead end microfilter," *Journal of Medical and Biological Engineering,* vol. 32 No.3, pp. 163-168, 2012.

[21] Xing Chen∗, Da Fu Cui, Chang Chun Liu, Hui Li, "Microfluidic chip for blood cell separation and collection based on crossflow filtration" *Sensors and Actuators B ,* vol.

130 , pp. 216–221, 2008.

[22] Tae Goo Kang, Yong-Jin Yoon, Hongmiao Ji, Pei Yi Lim,Yu Chen, "A continuous flow micro filtration device for plasma/blood separation using submicron vertical pillar gap structures" *J. Micromech. Microeng,* vol. 24 , pp. 087001, 2014.

[23] A. Karimi, S. Yazdi, and A. M. Ardekani, "Hydrodynamic mechanisms of cell and particle trapping in microfluidics" *Biomicrofluidics,* vol. 7, pp. 021501, 2013.

[24] Elodie Sollier, Derek E. Go, James Che, Daniel R. Gossett, Sean O'Byrne, Westbrook M. Weaver, Nicolas Kummer, Matthew Rettig, Jonathan Goldman, Nicholas Nickols, Susan McCloskey, Rajan P. Kulkarni and Dino Di Carlo, "Size-selective collection of circulating tumor cells using Vortex technology" *Lab Chip,* vol. 14, pp. 63–77, 2014.

[25] J. Steigert, T. Brenner, M. Grumann ,L. Riegger ,S. Lutz , R. Zengerle , J. Ducrée"Integrated siphon-based metering and sedimentation of whole blood on a hydrophilic lab-on-a-disk" *Biomed Microdevices ,* vol. 9, pp. 675–679, 2007.

[26] J. Steigert, T. Brenner, M. Grumann ,L. Riegger ,S. Lutz , R. Zengerle , J. Ducrée, "Gravitational Sedimentation Induced Blood Delamination for Continuous Plasma Separation on a Microfluidics Chip" *Anal. Chem,* vol. 84, pp. 3780−3786, 2012.

[27] Stefan H. Holm, Jason P. Beech, Michael P. Barrettb, Jonas O. Tegenfeldt, "Separation of parasites from human blood using deterministic lateral displacement" *Lab Chip,* vol. 11, pp. 1326–1332, 2011.

[28] Angeles Ivón Rodríguez-Villarreal, Martin Arundell, Manuel, "High flow rate microfluidic device for blood plasma separation using a range of temperatures" *Lab on a chip,* pp. 211-219, 2010.

[29] Munn, Abhishek Jainab, Lance L, "Biomimetic postcapillary expansions for enhancing rare blood cell separation on a microfluidic chip" *Lab Chip,* vol. 11, pp. 2941–2947, 2011.

[30] Pizziconi, Timothy A. Crowley, Vincent, "Isolation of plasma from whole blood using planar microfilters for lab-on-a-chip applications" *Lab On A Chip,* vol. 5, pp. 922-929, 2005.

[31] Sung Yang, a Akif Undar and Jeffrey D. Zahn, "A microfluidic device for continuous, real time blood plasma separation" *Lab On A Chip,* vol. 6, pp. 871-880, 2006.

[32] Wheeler, D. Clague, "Dielectrophoretic manipulation of macromolecules: The electric field," *Phys. Rev. E,* vol. 64, pp. 026605, 2001.

[33] Yuta Nakashima, Sakiko Hata, Takashi Yasuda, "Blood plasma separation and extraction from a minute amount of blood using dielectrophoretic and capillary forces," *Sensors and Actuators,* vol. B 145, pp. 561–569, 2010.

[34] Cho, Sunghwan Chang and Young-Ho, "A continuous size-dependent particle separator using a negative dielectrophoretic virtual pillar array" *Lab-On-A-Chip,* vol. 8, pp. 1930-1936, 2008.

[35] Sanchari Bhattacharya, Tzu-Chiao Chao, Alexandra Ros, "Insulator-based dielectrophoretic single particle and single cancer cell trapping" *Electrophoresis ,* pp. 32, 2550–2558, 2011.

[36] Yoon-Kyoung, Cho1 Suhyeon Kim, Kyusang, Lee, Chinsung Park, Jeong-Gun Lee, Christopher Ko, "Bacteria concentration using a membrane type insulator-based dielectrophoresis in a plastic chip" *Electrophoresis,* vol. 30, pp. 3153–3159, 2009.

[37] Liao, Tzong-Shyng.Leu and Zhi-Feng, "Separation plasma and blood cells by dielectrophoresis in microfluidic chip" *International Journal of Modern Physics: Conference Series,* vol. 19, p. 185–189, 2012.

[38] W. a Braff, A. Pignier, C. R. Buie, "High sensitivity three-dimensional insulator-based dielectrophoresis," *Lab Chip,* vol. 12, no. 7, pp. 1327–31, Apr. 2012.

[39] J. Regtmeier, R. Eichhorn, M. Viefhues, L. Bogunovic, and D. Anselmetti, "Electrodeless dielectrophoresis for bioanalysis: theory, devices and applications," *Electrophoresis,* vol. 32, no. 17, pp. 2253–73, Sep. 2011.

[40] Singh, E. B. Cummings and A. K., "Dielectrophoresis in Microchips Containing Arrays of Insulating Posts: Theoretical and Experimental Results," *Anal. Chem,* vol. 75, no. 18, pp. 4724–4731, Sep. 2003..

[41] S. K. Srivastava, J. L. Baylon-Cardiel, B. H. Lapizco-Encinas, and A. R. Minerick, "A continuous DC-insulator dielectrophoretic sorter of microparticles" *J. Chromatogr. A,* vol. 1218, no. 13, pp. 1780–9, Apr. 2011..

[42] Y. Kang, D. Li, S. a Kalams, and J. E. Eid, "DC-Dielectrophoretic separation of biological

cells by size" *Biomed. Microdevices,* vol. 10, no. 2, pp. 243–9, Apr. 2008.

[43] S. K. Srivastava, A. Artemiou, and A. R. Minerick, "Direct current insulator-based dielectrophoretic characterization of erythrocytes: ABO-Rh human blood typing," *Electrophoresis,* vol. 32, no. 18, pp. 2530–40, Sep. 2011.

[44] P. V Jones, S. J. R. Staton, and M. a Hayes, "Blood cell capture in a sawtooth dielectrophoretic microchannel" *Anal. Bioanal. Chem.,* vol. 401, no. 7, p. pp. 2103–11, Oct. 2011.

[45] S. K. Srivastava, A. Gencoglu, and A. R. Minerick, "DC insulator dielectrophoretic applications in microdevice technology: a review" *Anal. Bioanal. Chem,* vol. 399, no. 1, p. pp. 301–21, Jan. 2011.

[46] Barbulovic-Nad I, Xuan X, Lee JSH, Li D "DC dielectrophoretic separation of microparticles using an oil droplet obstacle" *Lab Chip,* vol. 6(2), pp. 274–279, 2006.

[47] Roberto C. Gallo-Villanueva, Victor H. Pe´ rez-Gonza´ lez1,Blanca H. Lapizco-Encinas, "Separation of mixtures of particles,in a multipart microdevice employing,insulator-based dielectrophoresis" *Electrophoresis,* vol. 32, pp. 2456 2465, 2011.

[48] Ming Li, Shunbo Li,Weihua Li,Weijia Wen,Gursel Alici, "Continuous manipulation and separation of particles using combined obstacle- and curvature-induced direct current dielectrophoresis" *Electrophoresis,* vol. 34, pp. 952-960, 2013.

[49] Martínez-López JI, Moncada-Hernández H, Baylon-Cardiel JL,Martínez-Chapa SO, Rito-Palomares M, Lapizco-Encinas BH, "Characterization of electrokinetic mobility of microparticles in order to improve dielectrophoretic concentration" *Anal Bioanal Chem,* vol. 394, pp. 293–302, 2009.

[50] Chen D, Du H, Tay Cy, " Rapid concentration of nanoparticles with DC dielectrophoresis in focused electric fields" *Nano Res Lett ,* pp. 5:55–60, 2010.

[51] Joel Voldman, "Electrical force for microscale cell manupulation" *J., Annu. Rev. Biomed. Eng,* vol. 8, pp. 425-454, 2006.

[52] Xiangchun Xuan, " Joule heating in electrokinetic flow" *Electrophoresis,,* vol. 29 , pp. 33-43., 2008.

[53] L. Feeney, E.R. Berman "Oxygen toxicity:membrane damage by free radicals" *Invest.*

Ophthalmol, vol. 15, pp. 789 , 1976.

[54] Kang Y, Li D, Kalams SA, Eid JE, "DC-dielectrophoretic separation of biological cells by size" *Biomed Microdevices,* vol. 10(2), pp. 243-9, 2008.

[55] Gallo-Villanueva RC, Rodriguez-Lopez CE, Diaz-de-la-Garza RI,Reyes-Betanzo C, Lapizco-Encinas BH " DNA manipulation by means of insulator based dielectrophoresis employing direct current electric fields" vol. 30, 2009.

[56] Lapizco-Encinas BH, Davalos RV, Simmons BA, Cummings,EB, Fintschenko Y, "An insulator-based (electrodeless) dielectrophoretic concentrator for microbes in water" *J Microbio Meth ,* vol. 62, pp. 317–326, 2005.

[57] Pysher MD, Hayes MA " Electrophoretic and dielectrophoretic field gradient technique for separating bioparticles" *Anal Chem 79,* vol. 12, pp. 4552–4557, 2007.

[58] christoph Erbacher, Fion G. Bessoth, Michael Busch, Elisabeth Verpoorte, Andreas Manz, "Towards Integrated Continuous-Flow Chemical Reactors" *Mikrochimica Acta vol. 131,* pp. 19-24, 1999.

[59] JensBranebjerg, , Peter Gravesen, Jens Peter Krog, Claus Rye Nielsen "Fast Mixing by Lamination," in *Proceedings of MEMS'96, 9th IEEE International Workshop Micro Electrochemical System*, San Diego ,CA, Feb 11-15, 1996.

[60] Soumya K. Srivastava, Andreas Artemiou,Adrienne R. Minerick "Direct current insulator-based dielectrophoretic characterization of erythrocytes: ABO-Rh human blood typing" *Electrophoresis,* vol. 32, pp. 2530–2540, 2011.

[61] Kang Yj, Li Dq" Electrokinetic motion of particles and cells in microchannels" *Microfluid Nanofluid,* vol. 6, pp. 431–460, 2009.

[62] Tandon V, Bhagavatula SK, Nelson WC, Kirby BJ "Zeta potential and electroosmotic mobility in microfluidic devices fabricated from hydrophobic polymers: 1. The origins of charge" *Electrophoresis ,* vol. 29, pp. 1092–1101, 2008.

[63] Baylon-Cardiel JL, Lapizco-Encinas BH, Reyes-Betanzo C, Cha ´vez- Santoscoy AV, Martı ´nez Chapa SO, "Prediction of trapping zones in an insulator-based dielectrophoretic device" *Lab Chip,* vol. 9, pp. 2896–2901 , 2009 .

[64] Villanueva RG, Sano M, Encinas BL, Davalos R “Joule heating effects on particle immobilization in insulator-based dielectrophoretic devices. " Electrophoresis 35: 352–361, 2014

[65] Herbert Ackland Pohl, " Some effects of nonuniform fields on dielectrics" *J Appl Phys,* vol. 29, pp. 1182–1188, 1958.

[66] Herbert Ackland Pohl, The behavior of neutral matter in non-uniform electric field, Cambridge University Press, 1978.

[67] Brian J. Kirby, Micro- and Nanoscale Fluid Mechanics Transport in microfluidic, New York: Cambridge University Press, 2010.

[68] Javier L. Baylon-Cardiel, Blanca H. Lapizco-Encinas, Claudia Reyes-Betanzo, Ana V. Ch,avez-Santoscoy, "Prediction of trapping zones in an insulator-based dielectrophoretic device" *Lab Chip,* vol. 9, pp. 2896–2901, 2009.

[69] Kokoris M, Nabavi M, Lancaster C, Clemmens J, Maloney P, Capadanno J, Gerdes J, Battrell CF., "Rare cancer cell analyzer for whole blood applications: automated nucleic acid purification in a microfluidic disposable card" *J Cell Physiol,* pp. 371-380, 2000.

[70] Robert S. Rosenson, Amy Mccormick, Eugene F. Urtiz, "Distribution of blood viscosity values and biochemical correlates in healthy adults" *ClinicalChemistry 42:8,* pp. 1189-1195 , 1996.

[71] Adrienne R.Minerick "The rapidly growing field of micro and nanotechnology to measure living cells. " *AIChE J,* vol. 54, pp. 2230 - 2237, 2008.

[72] Gascoyne, P., Satayavivad, J, Ruchirawat, M, "Microfluidic approaches to malaria detection" Acta Tropica, vol. 89, pp. 357-369, 2004.

[73] Alexander Zhbanov, Sung Yang, “Effect of Erythrocyte Sedimentation and Aggregation on the Conductivity of Blood in a Miniature Chamber" in *The Sixth International Conference on Quantum, Nano and Micro Technologies*, 2012.

[74] S. Abdalla, "Complex permittivity of blood cells and E. coli suspensions," *Journal of Molecular Liquids,* vol. 160 , pp. 130–135, 2011.

4. Research goal and approach

Point-of care diagnostics tests (POCT) are tests that do not require clinical equipment and therefore can be done on the side of the patient. The majority of diseases can be diagnosed or monitored through blood assays. The growth of new infectious diseases or chronic disease in elderly population increase the interest for blood assays performed in the POCT format. But in most diagnostic procedures, plasma or serum (plasma deprived of clotting agents) must be extracted from full blood samples prior to analysis. Thus, the best opportunities for microfluidic POCT systems reside on those that provide separation of plasma from the components of blood. Nevertheless, the ability to analyze a whole blood sample with the requirements for a point-of-care (POC) device such as robustness, friendly use and simple handling, remains unmet.

To achieve this goal cell and particle separation in microfluidic systems has recently gained significant attention in many sample preparations for clinical procedures. Our previous work has put emphasis on the development of microfluidics filters in which capillary forces are used to move liquids in microstructures and filter RBCs [1]. But the amount of gathered plasma was not enough to implement more than one test in a single microfluidic chip. Direct-current insulator-based dielectrophoresis (DC-iDEP) is a well-known technique that benefits from the electric field gradients generated by an array of insulator posts for separating, moving and trapping biological particle samples and it could provide a tool to extract more plasma from the initial sample, without the need of an external driving force.

As mentioned in the state-of-art, previous studies that employed dc-iDEP mostly do not take into account the requirements of a POCT device.

This thesis is focused on the use of DC-iDEP technique to separate RBCs from whole blood without hemolysis to produce microfluidic based POCT that can be manufactured using current microtechnology procedures and can work with just a single droplet of blood. In order to achieve this goal;

First, the post-array distribution in a microfluidic channel should be analyzed using parametric optimization. This optimization is aimed at maximizing trapping of RBCs while minimizing the required voltage and maintaining a similar footprint and manufacturable dimensions. A mathematical trapping condition along the central line of the transversal distance between posts can be used to obtain an optimum radius of the posts. COMSOL Multiphysics finite element software is used to analyze different post-array geometric models. The results depend only on the geometry of the array and are valid for any particle or medium properties, to be useful for microfluidic designers. If so, the optimization can be used to reduce the electric field required to achieve effective trapping and, therefore, avoid the

negative effects of Joule heating, which is a critical point when trying to trap viable cells. See Figure 1.

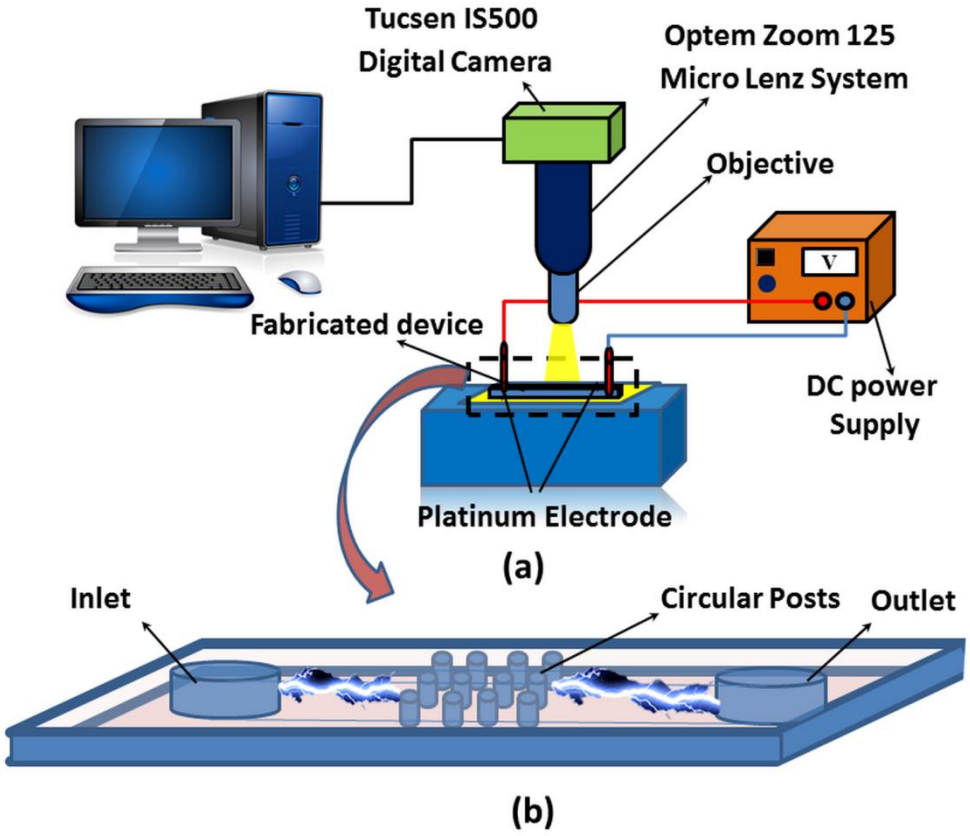

Figure. 1 (a) The illustration, experimental setup (b) And DC iDEP microdevice.

After, the optimized transversal distance between posts will be used in the proposal of a novel combination of hydrodynamic and dielectrophoretic techniques to achieve plasma separation in a microfluidic channel from fresh blood. The microchannel proposed is based on a set of dead-end branches at each side, see Figure 2, and is initially filled using capillary forces. During this process, stagnation zones are generated at the dead-end branches that can partially trap RBCs. Later, an electric field can be applied and, due to the design of the first constriction, dielectrophoretic trapping of RBCs prevent more RBCs from entering into the channel. Moreover, an electroosmotic flow sweeps the rest of the RBCs from the central part of the channel. Consequently, an RBC-free zone of plasma is formed in the middle of the channel, allowing real-time monitoring of the proposed assay.

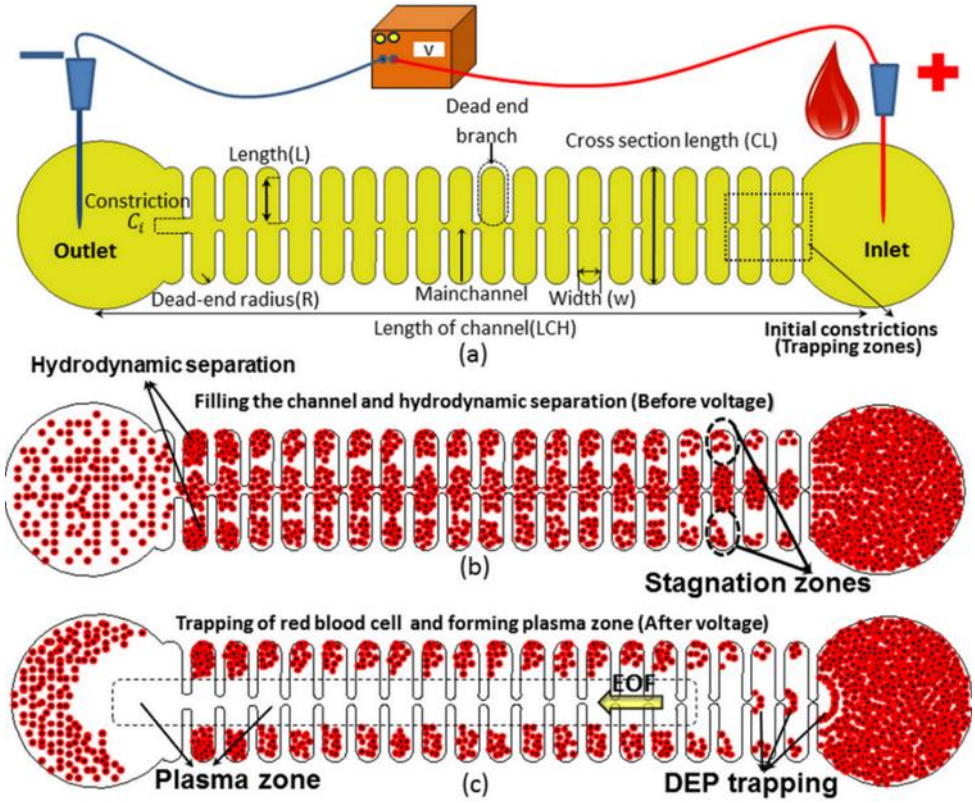

Figure 2 (a) Schematic illustration of a corrugated microchannel for RBCs trapping using hydrodynamic and DC-iDEP, (b) Hydrodynamic trapping generated during capillary filling, (c) Free zone of plasma generation due to DC-iDEP RBC trapping in the initial constrictions and sweeping of the remaining RBCs using EO flow.

Finally, the previous microfluidics designs will be combined with conventional lateral flow immune chromatography to extract enough plasma to perform a blood panel in a simple and portable device. The microfluidic chip design combines cross-flow filtration with a reversible electroosmotic flow that prevents clogging at the filter entrance and maximizes the amount of separated plasma. The proposed design should work with a small amount of sample (a single droplet ~10 µL) and gather a considerable amount of plasma (more than 1µL) with high purity (more than 99%) in a reasonable time (5 to 8 minutes). The results obtained from the microfluidic system should be comparable to previous commercial lateral flow assays but requiring less sample and providing more information (possibility to implement multiple tests) see Figure 3 (a-c).

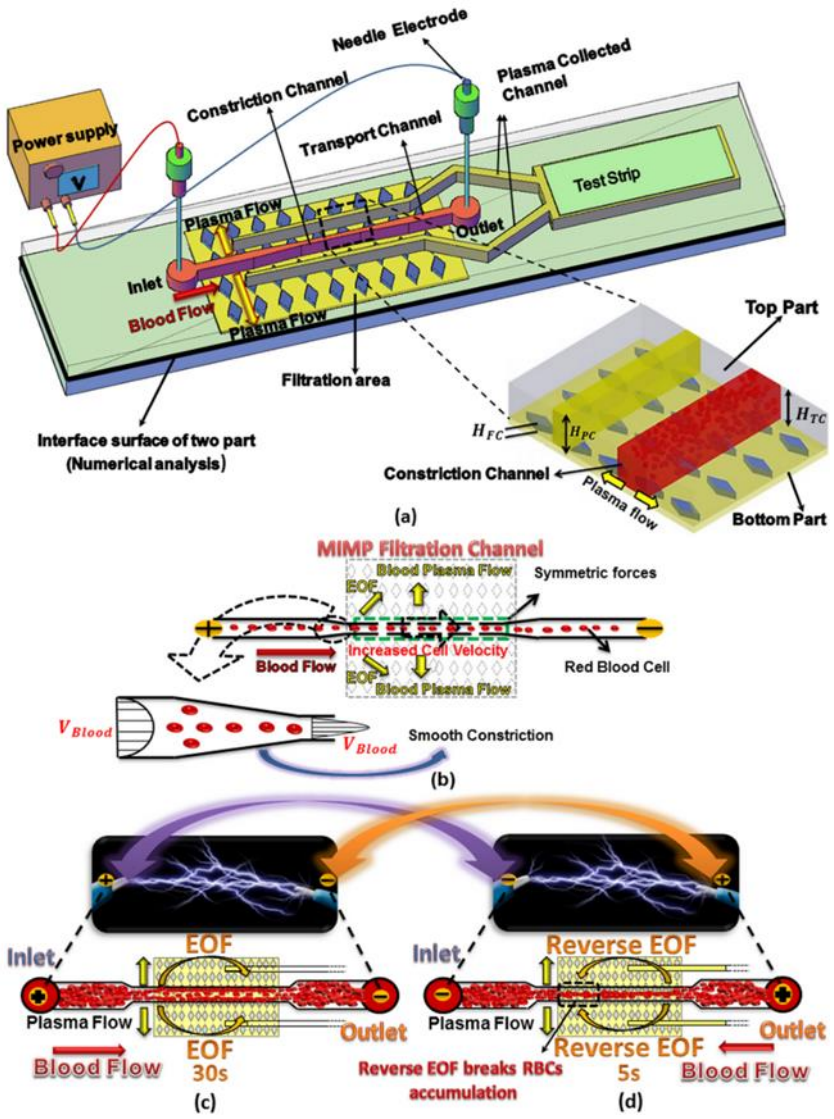

Figure 3 (a) Schematic diagram of the blood plasma separation microdevice. (b) Detail of the transport channel constriction. (c) and (d) Electroosmotic flow and RBCs flow directions depending on electrode polarization.

The research approach in this process is presented in Figure 4.

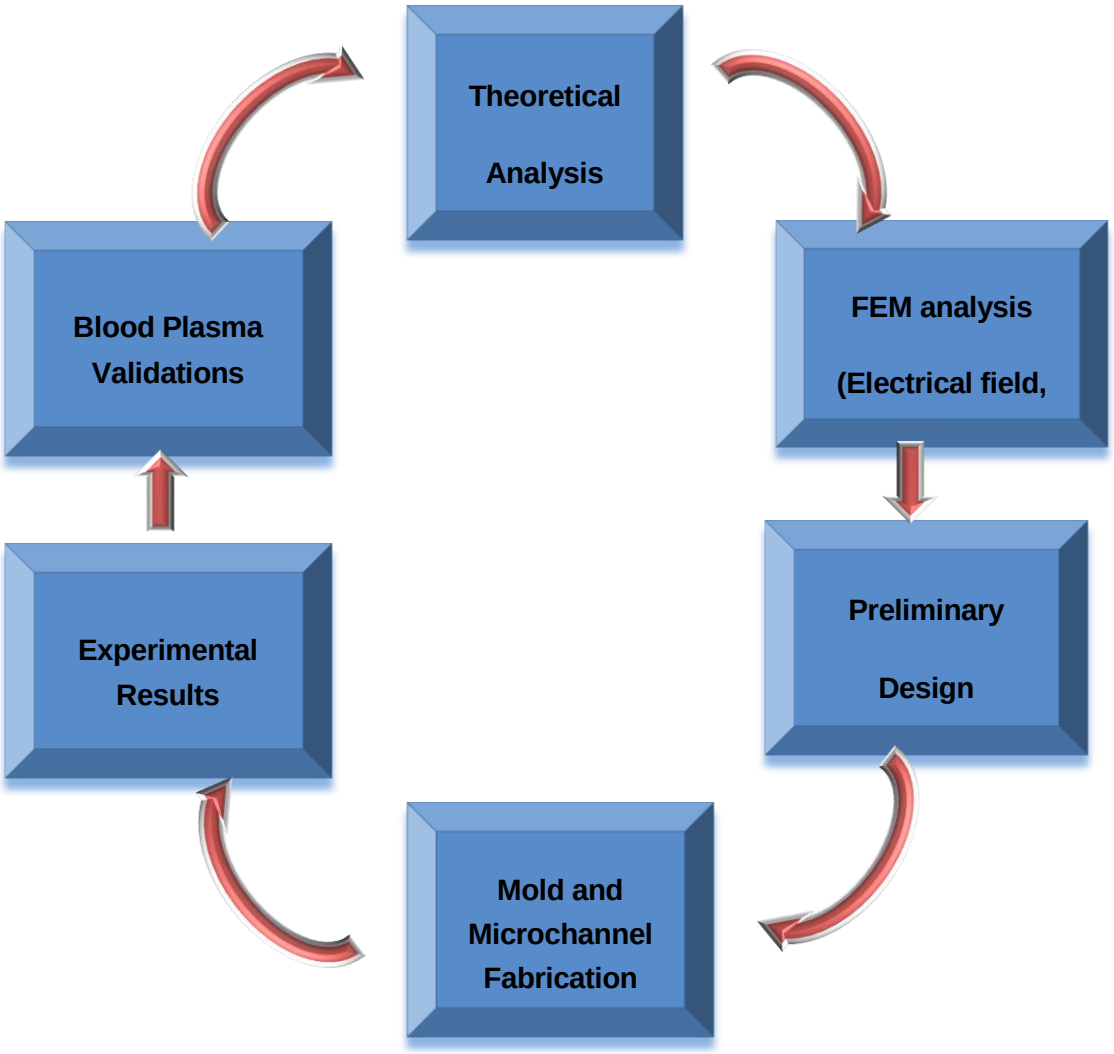

Figure 4. Schematic demonstration of thesis steps.

4.1. References

[1] Hojat madadi, Jasmina caslas, Mahdi mohammadi, "Self-driven efficient blood plasma separator microfluidic chip for point of care testing," *Biofabrication Journal,* vol. accepted, Feb,2015.

5. Numerical optimization of post-array geometries for enhanced direct-current insulator-based dielectrophoretic trapping

Cell and particle separation in microfluidic systems has recently gained significant attention in many sample preparations for clinical procedures. Direct-current insulator-based dielectrophoresis (DC-iDEP) is a well-known technique that benefits from the electric field gradients generated by an array of posts for separating, moving and trapping biological particle samples. We propose a strategy for optimizing the post-array distribution in a microfluidic channel. It is aimed at maximizing the trapping condition, while minimizing the required voltage, with a similar footprint and channel thickness. In order to maximize a dielectrophoresis trapping condition that takes the form of a mathematical inequality, a parametric optimization has been done focusing on the geometric parameters of the post-array. It is found that the trapping condition along the central line of the transversal distance between posts can be used to obtain an optimum radius of the posts. Different post-array geometric models with transversal distance between posts varying from 10 to 60 µm have been simulated using COMSOL Multiphysics finite element software. Simulations show that, as the radius increases, the trapping condition can be decreased between 56 %- 341 % percent for each transversal distance from 10 to 60 µm. Thus, we used COMSOL simulations to find that the optimum radius should be around 40 µm more than the transversal distance between posts. Some microchannels with embedded post-arrays are manufactured in Polydimetilsiloxane (PDMS) and the trapping patterns of polystyrene particles are measured experimentally and compared to the earlier reported results. Experiments show the same trends as pointed out by the simulations. The dependence on the longitudinal distance between posts is also explored, to find out that it is rather weak and with monotonic behavior. These results depend only on the geometry of the array and are valid for any particle or medium properties. The results show that optimization can be used to reduce the electric field required to achieve effective trapping and, therefore, avoid the negative effects of Joule heating.

5.1. Introduction

Lab-on-a-chip is a powerful tool in analytical chemistry and medical engineering. The lab-on-a-chip integrated with microfluidic systems enables miniaturization, integration, and automation of complex biochemical assays. Their main advantages are reduction of reagent use and portability.

Separation of cells or particles from a fluid is a step required in many biochemical tests. Different microfluidic methods have been developed to this end (see review) [1, 2]. Among these, the dielectrophoresis method (DEP) is a well-known technique to separate particles even in samples of small volume [3].

Dielectrophoresis is a movement of particles caused by a polarization effect when a non-uniform electric field is applied to particles that have different conductivity than the medium. Since the dielectrophoretic force is proportional to a gradient, it can appear either when direct current (DC) or alternate current (AC) is applied. The non-uniform electric field can be generated using an array of electrodes (electrode based, eDEP) [4, 5, 6] or an array of insulating posts (insulator based, iDEP). While eDEP is a more traditional method, iDEP can overcome most of the well-known problems of eDEP, associated to the presence of the electrodes [7], since the high field gradient is obtained changing the path track of the field by means of the insulator obstacles between the electrodes. Moreover, iDEP devices have a higher throughput because the technique allows the design of deeper channels than in eDEP devices that have a limited depth because the electric field is confined on the electrode surface[8]. Finally, most iDEP devices are able to produce an electroosmotic flow (EOF) that eliminates the need of an external driving force [9, 10].

The use of just two electrodes, placed in the channel inlet and the channel outlet, offers other advantages such as a more straightforward fabrication process, less fouling than with embedded electrodes, minimum bubble generation inside the channel and less electrochemical reactions [11]. These devices are more appropriate for metal-sensitive organic samples.

The iDEP method have been successfully employed for different applications: separation and concentration of live and dead bacteria [12, 13] separation of white blood cells [14], red blood cells [15] or blood cell separation in a sawtooth microchannel [16] (see the review [17]).

The geometry of the insulating post-array in the microchannel is one of the most important influencing factors in the performance of iDEP microfluidic devices. The first application of arrays of insulating posts to generate iDEP was presented by Cummings and Singh in 2003. In their studies, they studied a diamond and a circular insulating post-array [10]. Barbulovic-Nad et al. in 2006 used an oil droplet as an adjustable insulating structure to change the distance between the insulating structures and study how this affected to the dielectrophoresis [18]. Kwon et al. in 2007 presented a study focuced on the improvement of the circular-post geometry subject to electrokinetic (EK) and dielectrophoretic forces using a mathematical model. Their results indicated that when the longitudinal spacing between the posts was 0.6 times the post radius, DEP to EK force ratio was larger [19]. Nakano et al. in 2011 demonstrated iDEP-based manipulation of proteins using ellipsoidal and triangular shaped posts. Also their study presented an approximated numerical analysis of the electric

field and the gradient of the electric field at the tip of the insulating posts [20]. Kim et al. in 2014 presented a simulation model to study the effect on protein concentration of circular and square post-arrays, both in-plane and out-of-plane [21]. Lalonde et al. in 2014 reported the effect of geometry on the trapping performance of iDEP. In their study, two different insulating-posts geometries (circle and diamond) were employed with a fixed spacing between them of 50 µm. The results indicated that the highest electric field gradient was achieved when diamond- posts were used [22].

The aforementioned studies provide valuable insight into the effect of geometry on DC-iDEP phenomena but they are focused on a particular geometry or a type of particles. A procedure to obtain the most efficient post-array distribution that minimizes the voltage required to achieve trapping and therefore minimizes the Joule effect based only on geometric conditions would be useful particularly in those applications that require viable cell trapping. The goal of this work is to optimize the geometry of an array of circular insulating posts in such a way that the electric field can be minimized, and therefore, also its side effects and to provide an empirical relationship between parameters such a transversal distance between posts and radius to help microfluidic designers to obtain the maximum advantages of the iDEP.

The current study investigates the optimum value of the radius and the longitudinal distance between posts for a given transversal distance between posts, to enhance particle trapping using the direct current iDEP (DC-iDEP) method. Numerical modeling and experiments are performed to study the effect of these geometrical parameters. The electric field, the electric field gradient and a trapping condition are calculated in more than 300 models to show a significant relation between the transversal distance between posts and the optimum radius of the posts, according to a Figure of merit particularly chosen for this study.

5.2. Materials and methods

According to chapter 3, the total velocity of the particles due to the combined effects of electroosmosis (EO), electrophoresis (EP) and dielectrophoresis (DEP) can be expressed as the superposition of a linear electrokinetic velocity $\vec{V}_{EK}$ (EOF + EP flow) and a nonlinear DEP velocity:

$$\vec{V}_{tot} = \vec{V}_{EO} + \vec{V}_{EP} + \vec{V}_{DEP} = (\mu_{eo} - \mu_{ep})\vec{E} - \mu_{DEP}\nabla\vec{E}^2 \quad (1)$$

where $\vec{V}_{tot}$ is total velocity, $\vec{E}$ is electric field, μ_{eo} is electroosmotic mobility, μ_{ep} is electrophoretic mobility and μ_{DEP} is dielectroporetic mobility. According to Ermolina and Morgan [24] the zeta potential of particles with more than 1 µm is almost 0.04 mV. This

implies that the electrophoretic miobility is $2.84 \times 10^{-7} \mathrm{cm^2 V^{-1} s^{-1}}$. The electroosmotic mobility is measured experimentally by MicroPIV and its value turns out to be $1.12 \times 10^{-4} \mathrm{cm^2 V^{-1} s^{-1}}$, which indicates that electroosmotic mobility is three orders of magnitude higher than electrophoretic mobility.

The direction of the EK flow, as observed experimentally, is from the positive electrode to the negative electrode in the microchannel (electroosmotic direction). To achieve trapping of particles, DEP velocity must overcome EK velocity. Consequently, the net particle velocity along the electric field line is zero in the zone of trapping. The trapping DEP flow condition is [23]:

$$\frac{\mu_{DEP} \nabla(\vec{E}.\vec{E}).\vec{E}}{\mu_{EK}\, \vec{E}.\vec{E}} > 1 \qquad (2)$$

Since we are not interested on the actual extension of the trapping zone, we do not include the DEP and EK mobility terms so the result is independent of the particle and medium properties. Therefore, the scalar field defined by $T \equiv \frac{\nabla \vec{E}^2}{\vec{E}^2}.\vec{E}\,(V/m^2)$ is calculated to observe the effect of trapping for different geometries.

5.2.1. Chip fabrication and experimental setup

Soft-lithography technique is used to fabricate a 1-cm long microchannel and 1-mm wide PDMS microchannels with an embedded insulating post-array 1-mm wide and 2-mm-long in the middle of the channel with different post radius (20- 70 and 150 µm) bonded to a glass cover via an oxygen plasma treatment, see Figure 1. The transversal and longitudinal distances of the fabricated channels are then measured by confocal microscopy. Figure 1 (a) shows a contour plot of the 70-µm-radius post array. The average transversal distance is 30±3 µm and longitudinal distance is 50±3 µm as shown in Figure 1. The post-diameter is 140±6 µm and the post height is 50±5 µm, as expected.

Afterwards, the channels are filled with DI water. Then a 4-µl suspension (2.5% aqueous suspension) of polystyrene red dyed beads with a diameter of 6 µm and a concentration of 2.10 x 108 particles/ml from Polysciences Inc (Warrington, Pennsylvania USA) are diluted in 16-µl of de-ionized water (ε_r=80.1; ρ=~20 kΩcm) [25] and the sample is introduced in the channel inlet.

To ensure about the negative charge of the surface of the PDMS microchannel, new PDMS microchannel are used in each experiment. In order to record the images and videos of the particle response, a digital camera (Tucsen ISH500, 5.0 M pixel,) is connected to a micro inspection lens system Optem zoom 125C (with a broad 12.5:1 zoom range) and a 20X objective.

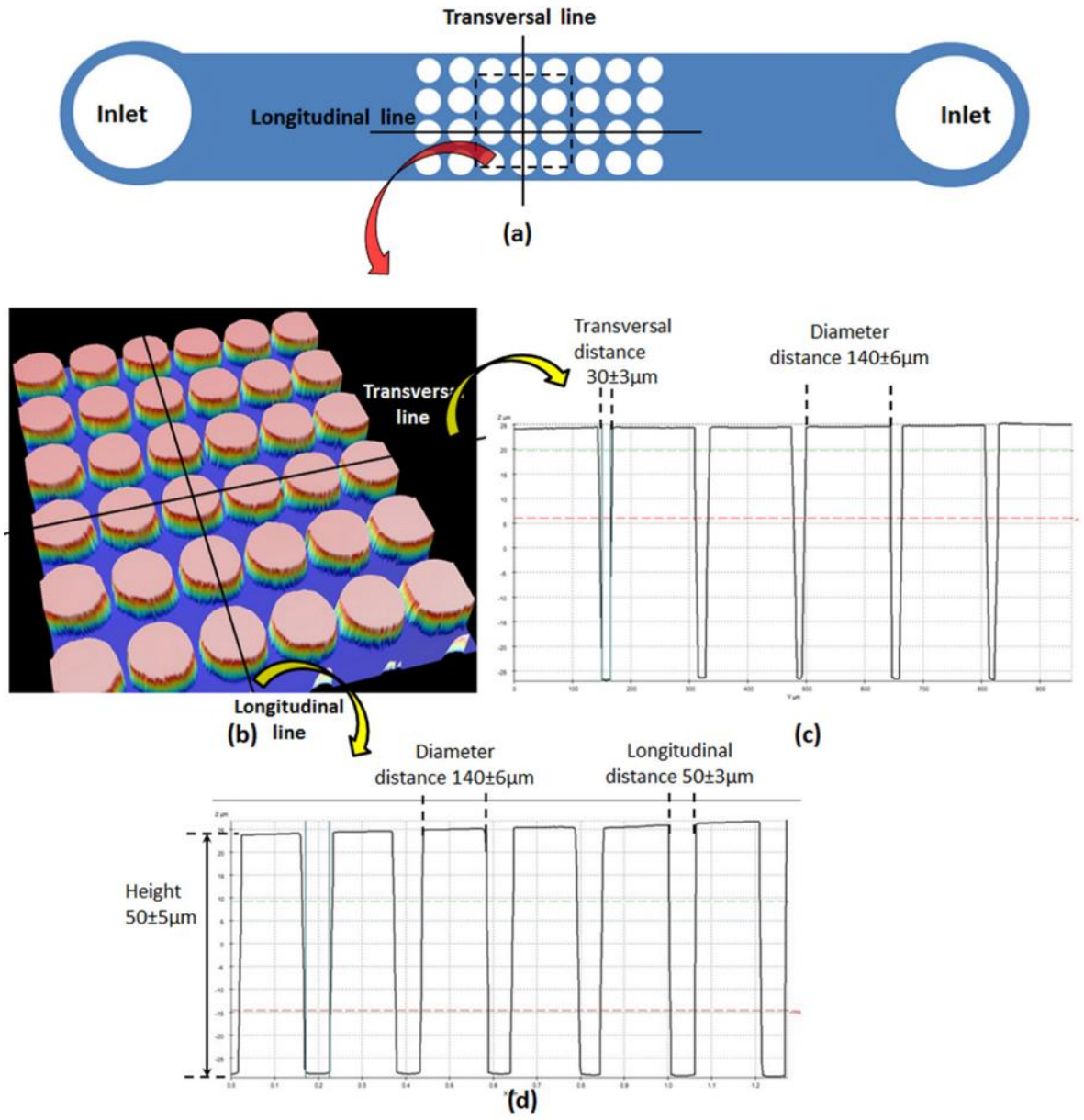

Figure. 1 Confocal microscopy image (a) topography of the 70-µm-radius post-array (b) Transversal distance cross-section (c) Longitudinal distance and post height.

A high DC voltage power supply (SF-9585 PASCO- California-USA) is utilized to generate the electric field. Two Platinum electrodes (Roland Consult-Germany) are placed in the inlet and outlet of the main channel to create the electric field. The microchannel and experimental setup is shown in Figure 2 (a, b).

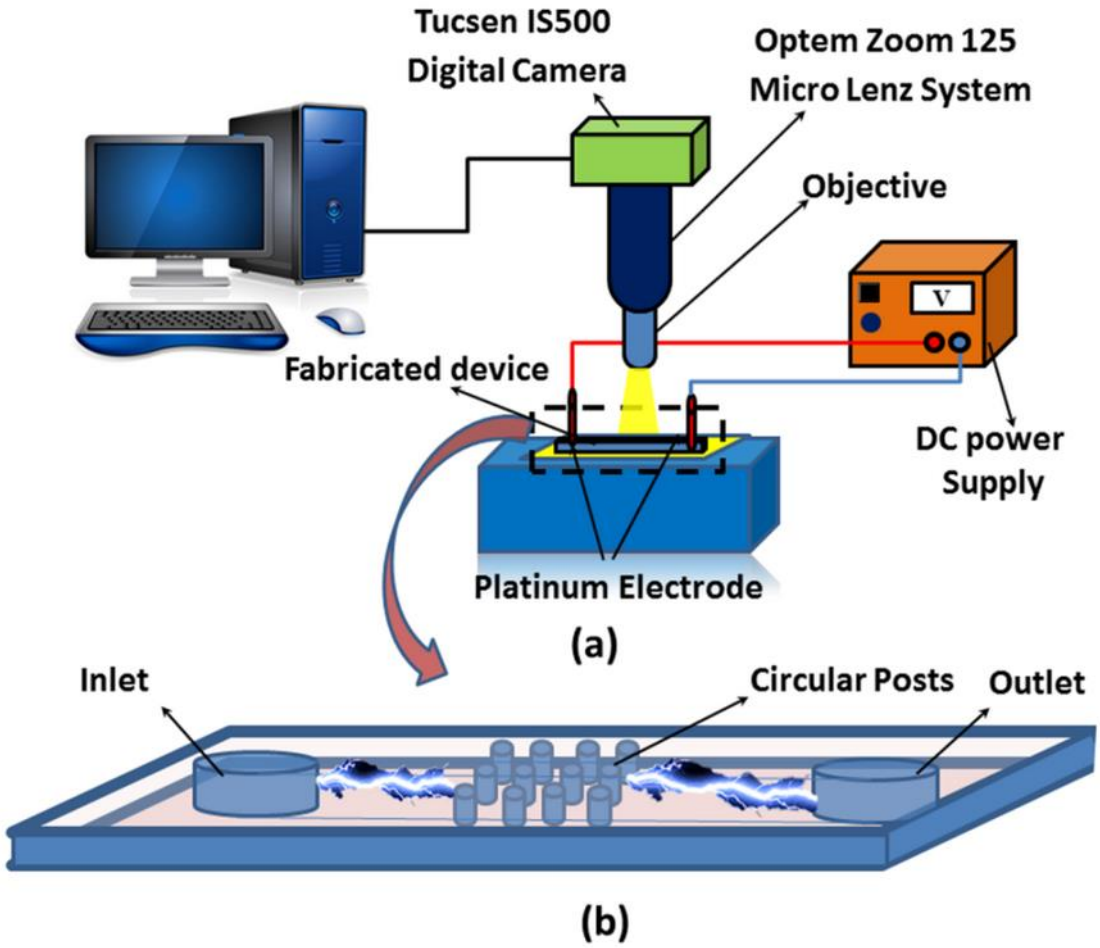

Figure. 2 (a) Experimental set-up and (b) DC iDEP microdevice schematic picture.

5.3. Results and discussion

The geometry of the insulating post-array in the microchannel has a main role in the proficiency of the iDEP micro device. For this reason, we have varied the parameters that define the array in order to find an optimal geometry. These parameters are analyzed in detail to elucidate the influence of geometry on trapping.

5.3.1. Effect of post geometry on the distribution of electric field

The presence of insulators in the microchannel distorts the electric field, producing gradients. Different geometries of insulators result in different electric field distributions. From equation (5) it can be deduced that the dielectrophoretic force exerted on particles in a medium is proportional to the gradient of squared electric field; therefore, it is concluded that the geometry of the microchannel is one of the most important factors that influence the performance of iDEP micro devices.

In order to analyze the posts geometry effect on the distribution of the electric field and of the gradient of squared electric field, a COMSOL model based on finite element methods (FEM) is developed and more than 300 geometries are computed. Grid independency of the predicted electric field simulation was checked to ensure that the solutions were independent of the computational grids. The parameters that define the geometry of the array are shown in Figure 3 where R is the radius of the posts, K is the transversal distance between posts and L is the longitudinal distance between two adjacent posts.

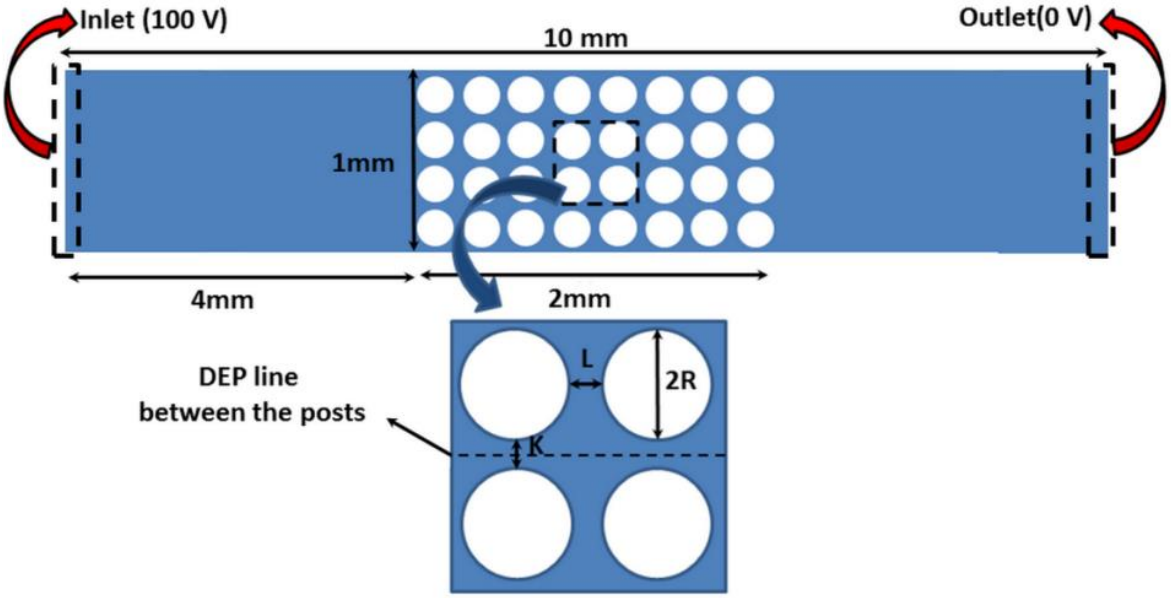

Figure. 3 Schematics of the post-array distribution in the microchannel

A 2D numerical model of a 1-cm long and 1-mm wide microchannel, with a 2-mm long and 1-mm wide array of circular posts located in the middle of the microchannel is defined. 100 V are applied between channel inlet and outlet as boundary condition in COMSOL.

In order to obtain results independent from the particle and medium properties, the quantity $T \equiv \frac{\nabla \vec{E}^2}{\vec{E}^2} \vec{E}$ has been calculated in all simulations. T is a particle- and medium-independent

scalar field that accounts for the trapping capability of each point. The transversal distance (K) and longitudinal distance (L) are kept constant, while the radius of the posts is being varied in the numerical model, to see the effect of R.

Three circular posts with the radius of 20 µm, 70 µm, and 150 µm have been selected to make a preliminary study the iDEP trapping with the purpose of finding a figure of merit that can be optimized. The transversal distance (K) is fixed to 30 µm and L is fixed to 20 µm. The average value of T over the surface between the posts, and the maximum value of T on the line between the posts are shown for each geometry in Table 1.

In case (a), R =20 µm, the higher values of T, as it can be seen in Table 1, are mainly concentrated near the posts but are lower on the line between the two posts.

In case (b), R = 70 µm, presents a more evenly distributed electric field gradient in comparison with R=20 µm. The maximum value of T on the plotted line is $1.11x10^9$, while in case (a) this value is $7.49x10^8$. This means that microparticle trapping occurs at a lower applied voltage for a radius of 70 µm. Note that the average of T over the surface in case (a) is greater than in case (b). This is due to the fact that when the post radius is smaller a greater electric field gradient is obtained. Therefore, the average value of T over the surface will not be a correct criterion for the comparison of microparticle trapping.

As shown in case (c), where the radius of the posts is 150 µm, T is smaller in comparison with case (b). The maximum value of T along the middle line is $9.43\ x10^8$ which is smaller than in case (b). This shows that there will be an optimum value for the radius of the posts.

Instead, the average of T over the surface in this case is about $3.60\ x10^8$ which is smaller than in the two previous cases. It can be seen that as the radius of the posts decreases, keeping transversal and longitudinal distances constant, the T gets more intense and is mainly concentrated near the posts.

K=30 µm L=20 µm V=100V	**(a)** **R=20µm**	**(b)** **R=70 µm**	**(c)** **R=150 µm**
Modeling of $\frac{\nabla\vec{E}^2}{\vec{E}^2}\vec{E}$ (Trapping value)	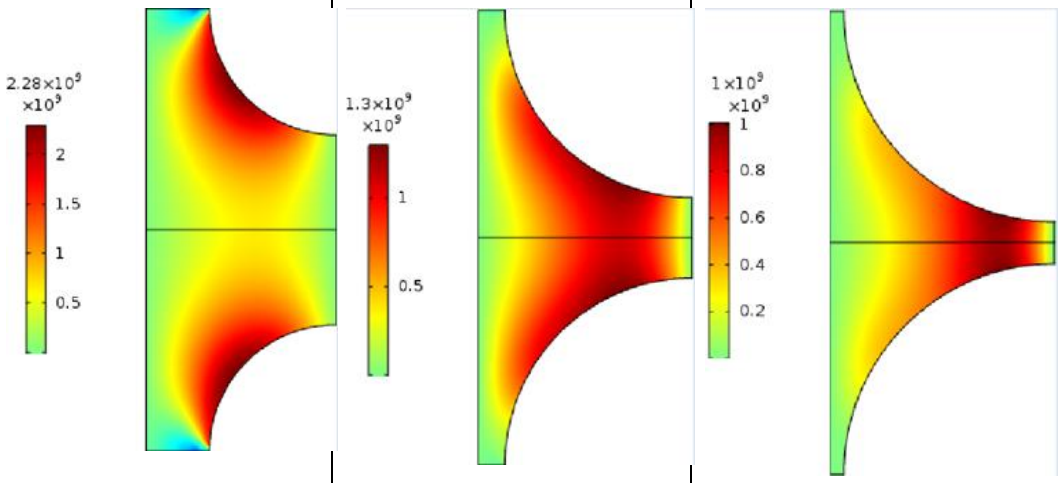		
Maximum value of T over the line	**7.49** x10^8	**1.11** x10^9	**9.43** x10^8
Average value of T over the surface	**7.39** x10^8	**6.63** x10^9	**3.60** x10^8

Table 1. Different numerical modeling of trapping the value by different R and constant K, L and voltage

5.3.2. Experimental validation

To observe the real effect of insulating post-radius on trapping performance, three PDMS microchannel with different insulating radius post-arrays have been fabricated. R is changed between 20, 70, 150 µm, while the transversal distance is 30 µm and the longitudinal distance is 50 µm in all the geometries. The DEP mobility, as presented in equation (3) for current polystyrene particles, is-1.06×⟦10⟧$^{-18}$ m^4/⟦(V⟧^2 s). The negative sign of this value is due to the negative Clausius-Mossotti factor which is assumed as −0.5 for these particles under DC electric fields [22]. 6-µm-diameter polystyrene microsphere particles diluted (1:4) in deionized water have been introduced into the channel to carry out the trapping experiment.

Then, DC voltages of 200, 350 and 500 V have been applied to observe particle trapping for each post-array geometry. Figure 4 shows the performance of trapping for each geometry 30 seconds after the electric field has been applied.

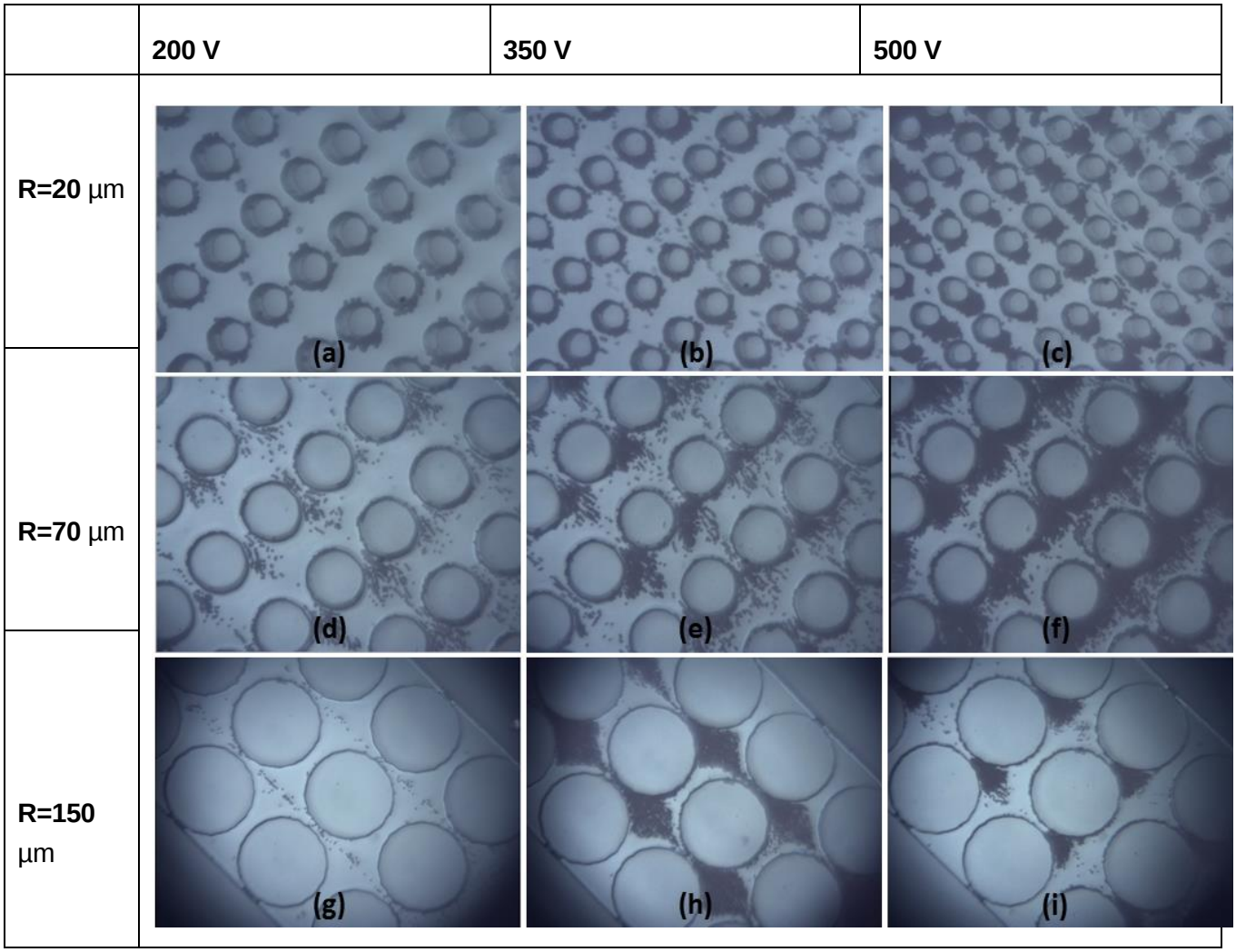

Figure. 4 Particle trapping pictures 30 s after applying 200 V, 350 V and 500 V for polystyrene beads of radius (a-c) 20 µm (d-f) 70 µm, (g-i) 150 µm.

A change in the geometry of the insulator post-array results in a change in the electric field distribution. This has an immediate effect on EK velocity, but also, through the gradient of the squared electric field, affects DEP velocity. Particle trapping can be achieved when the DEP contribution to particle velocity is larger than the one from EK.

The performance of microparticle trapping of an insulating post-array with R=20 µm is shown in Figures 4 (a-c). The experimental pictures present particle trapping confined on the surface of the post and mainly concentrated near the posts. There is no particle trapping

present in the separation between the posts, thus in order to achieve complete separation a high DC voltage is required. Figures 4 (d-f) demonstrate efficient particle trapping starting at 200 V. The observed performance hints that the maximum of T along the line between the posts is a better Figure of merit than the average of T over the surface.

The particle trapping for R=150 µm is depicted in Figures 4 (g-i). Streaming flow appears for 200 V and 350 V and particle trapping is observed only for 500 V. In particular, the DEP velocity is greater than the EO velocity in an insulating post-array with R=70 µm, in which a significant number of particles have been separated with a lower voltage in comparison with R=20 and 150 µm. In addition, experimental results showed that as the radius of the posts decreases, keeping transversal and longitudinal distances constant, trapping of particles gets more intense and is mainly concentrated near the posts.

5.3.3. Optimum radius of the post

In order to find the optimum radius of the post and a relationship between optimum R and K, the maximum value of T on the line between two adjacent posts has been calculated in 220 models. In these models, the value of R varies between 10 µm to 150 µm and the values of the transversal distance (K) changes between 10 µm to 60 µm. The value of L has been fixed to 20 µm and a voltage of 100 V is applied on a 1-cm long channel for all models.

Figure 5 shows the result of the numerical simulation for the maximum value of T on the line between the posts to find the optimum R. There is a specific radius of posts for each K which presents the maximum value of this quantity. This radius is the optimum radius.

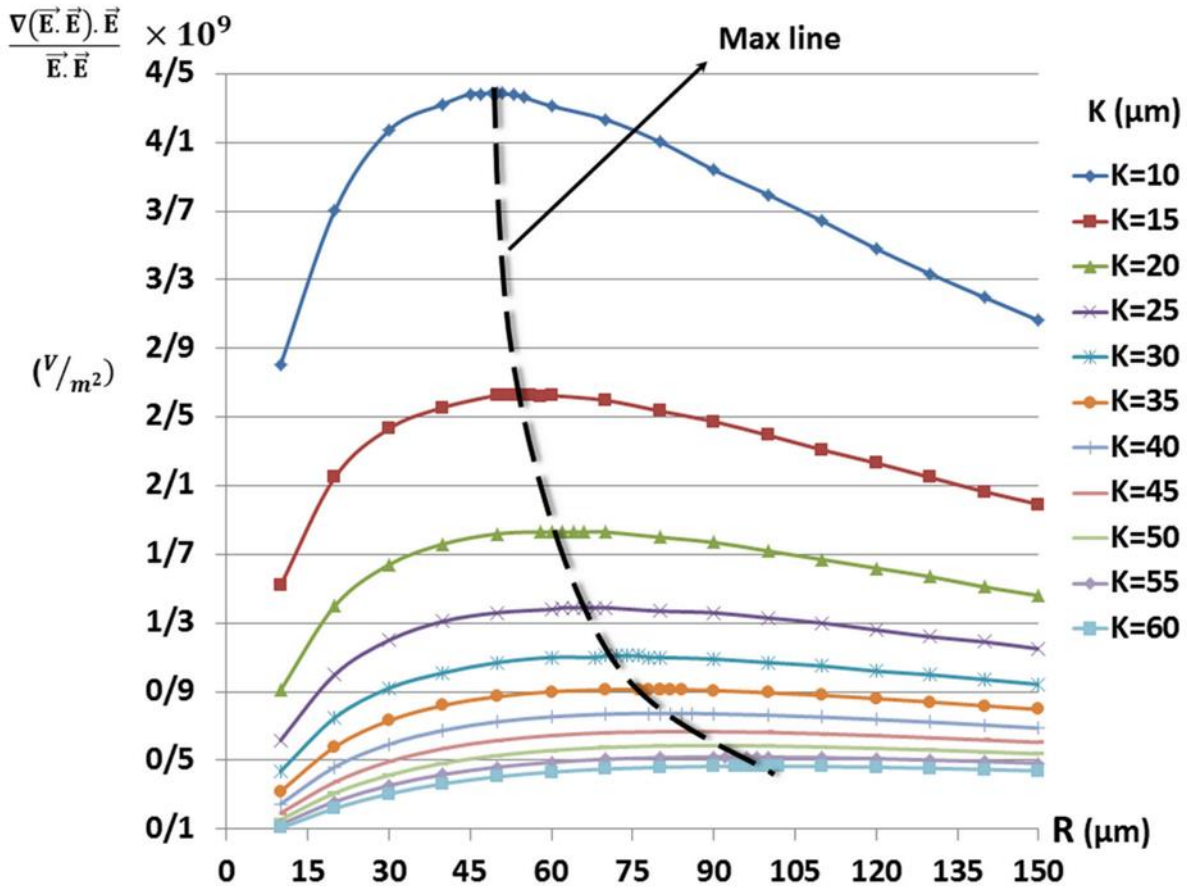

Figure. 5 Trapping versus radius of the posts for different K

The empirical relationship between the optimum radius R and the transversal distance K, according to Figure 5, is.

$$R_{opt} = K + 40 \pm 1 \mu m \qquad (3)$$

This equation is a global equation, which is independent of particle and medium properties.

All optimum values of R and the maximum value of T for each K (transversal distance varies between 10 and 60 µm) are presented in Table 2. In addition, this table shows the evolution of the trapping value T for a given K and its optimum post radius. Last row shows that the increase in the trapping value T from the non-optimized geometry to the optimum post radius can vary between 56% and 341% when the transversal distance varies from 10 to 60 µm.

K (μm)	**10**	**15**	**20**	**25**	**30**	**35**	**40**	**45**	**50**	**55**	**60**
Optimum R (μm)	50	56	60	66	70	76	80	86	90	95	100
The maximum of $\frac{\Delta\vec{E}^2}{\vec{E}^2}\vec{E}\times 10^9$	4/39	2/63	1/83	1/39	1/11	7/74	6/68	5/86	5/20`	5/20	4/67
The minimum of $\frac{\Delta\vec{E}^2}{\vec{E}^2}\vec{E}\times 10^9$	2/81	1/52	9/10	6/18	4/37	3/19	2/46	1/93	1/55	1/27	1/06
Percentage of increase (%)	56.4	72.8	101	125	154	187	215	246	278	309	341

Table 2.Trapping value and optimum R for each K.

5.3.4. Effect of longitudinal distance (L)

The effect of L parameter (Longitudinal distance between post) has been studied for different K and R. The result of the mathematical modeling shows that a variation of T value in terms of L is insignificant when K is smaller than 30 μm. While, the value of trapping is enhanced up to 0.05 %, when L is increased and K is more than 30 μm, which results in a reduction of the voltage required for particle trapping. The effect of L on the value of T for different K and optimum R is plotted in Figure 6. These results can be explained due to the fact that the negative DEP force applied on the particle from the previous post column decreases the trapping value or positive DEP force of the next post column, see Figure 6 (b). This effect enhances the trapping value when the longitudinal distance is increased.

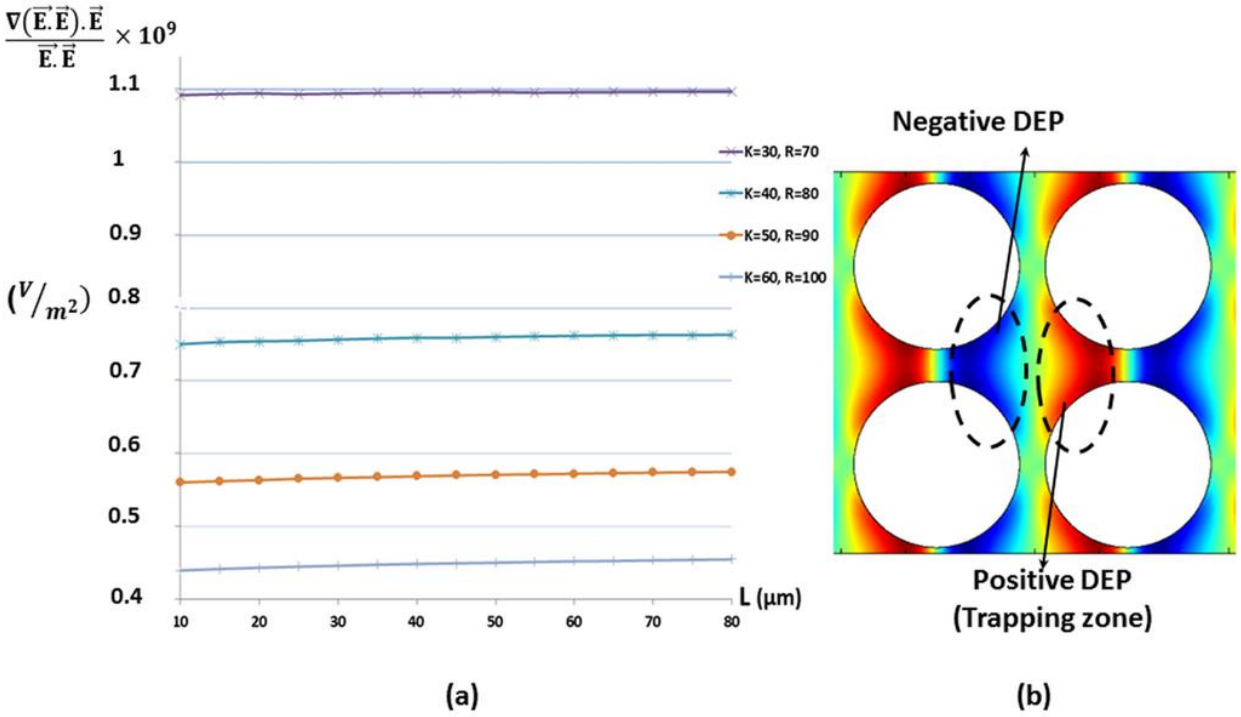

Figure. 6 L versus trapping value for different K.

These results can be explained due to the fact that the negative DEP force applied on the particle from the previous post column decreases the trapping value or positive DEP force of the next post column, see Figure 6 (b). This effect enhances the trapping value when the longitudinal distance is increased.

5.3.5. Discussion

Overall, the results obtained from the numerical simulations are independent of particle and medium properties and can be applied to all particles and mediums. The numerical results show that the modification of geometrical parameters of the post-array can significantly reduce the electric potential required to achieve effective enrichment and particle trapping. The performance of two different insulating post-array geometries (circle and diamond) have been previously studied [22]. Also circular and square post-arrays have been used in-plane and out-of-plane for protein concentration [21] and ellipse and triangle-shaped posts have been used for manipulation of proteins [20] and the effect on trapping of varying the angle of a diamond and a circular insulator post-array has been presented [10]. None of these previous studies were based on an independent geometrically optimized design. The use of the empirical relationship (equation 3) to obtain the most efficient post-array distribution could be used in the previous studies to minimize the voltage required to achieve trapping and therefore to minimize the Joule effect. Besides, the set of experimental results validates the

numerical simulation results which show that for constant transversal distance between posts (i.e 30 µm) there is an optimum radius of the post (i.e. for 30 µm is 70 µm).

5.4. Concluding remarks

This study presents a strategy for optimizing the post-array distribution in DC-iDEP microdevices that maximizes the trapping condition, while minimizing the required voltage, similar footprint and the channel thickness. COMSOL Multiphysics software has been used to perform a parametric optimization of the geometric parameters of the post-array based on a new proposed Figure of merit (the maximum of trapping condition along the central line of the transversal distance between posts, T). More than 300 different post-array geometric models with transversal distance between posts varying from 10 to 60 µm have been simulated. The results show that optimization can reduce the electric field required to achieve an effective trapping and, therefore, avoid the negative effects of Joule heating. Numerical results expressed that, there is a specific radius of posts (R) for each transversal (K) which can enhance the trapping condition between (56.1% to 341%) the initial non-optimized design. This behavior has been captured through a proposed empirical relationship between the transversal distance between posts (K) and the optimum radius (R). The effect of longitudinal distance has been studied. The effect of increasing of longitudinal distance (L) on trapping is insignificant when K is smaller than 30 µm but trapping is enhanced when K is more than 30 µm. The numerical results are validated using microchannels with embedded post-arrays, manufactured in Polydimetilsiloxane (PDMS) to trap polystyrene beads. Experiments show the same trends as pointed out by the simulations. The proposed figure of merit and therefore the results depend only on the geometry of the array and show that optimization can be used to reduce the electric field required to achieve effective trapping of any kind of particle and, therefore, avoid the negative effects of Joule heating specially when dealing with biological cells. Therefore, the use of the derived empiric equation can be an important milestone for a wider use of DC-iDEP devices for trapping viable cells.

5.5. References

[1] A. Lenshof and T. Laurell, “Continuous separation of cells and particles in microfluidic systems.,” Chem. Soc. Rev., vol. 39, no. 3, pp. 1203–17, Mar. 2010.

[2] P. Sajeesh and A. K. Sen, “Particle separation and sorting in microfluidic devices: a review,” Microfluid. Nanofluidics, vol. 17, no. 1, pp. 1–52, Nov. 2014.

[3] D. Clague and E. Wheeler, “Dielectrophoretic manipulation of macromolecules: The electric field,” Phys. Rev. E, vol. 64, no. 2, p. 026605, Jul. 2001.

[4] P. Gascoyne and J. Vykoukal, “Particle separation by dielectrophoresis,” Electrophoresis, vol. 23, pp. 1973–1983, 2002.

[5] B. Cetin, Y. Kang, Z. Wu, and D. Li, “Continuous particle separation by size via AC-dielectrophoresis using a lab-on-a-chip device with 3-D electrodes.,” Electrophoresis, vol. 30, no. 5, pp. 766–72, Mar. 2009.

[6] C. Qian, H. Huang, L. Chen, X. Li, Z. Ge, T. Chen, Z. Yang, and L. Sun, “Dielectrophoresis for Bioparticle Manipulation.,” Int. J. Mol. Sci., vol. 15, no. 10, pp. 18281–18309, Jan. 2014.

[7] T. Z. Jubery, S. K. Srivastava, and P. Dutta, “Dielectrophoretic separation of bioparticles in microdevices: a review.,” Electrophoresis, vol. 35, no. 5, pp. 691–713, Mar. 2014.

[8] W. a Braff, A. Pignier, and C. R. Buie, “High sensitivity three-dimensional insulator-based dielectrophoresis.,” Lab Chip, vol. 12, no. 7, pp. 1327–31, Apr. 2012.

[9] J. Regtmeier, R. Eichhorn, M. Viefhues, L. Bogunovic, and D. Anselmetti, “Electrodeless dielectrophoresis for bioanalysis: theory, devices and applications.,” Electrophoresis, vol. 32, no. 17, pp. 2253–73, Sep. 2011.

[10] E. B. Cummings and A. K. Singh, “Dielectrophoresis in Microchips Containing Arrays of Insulating Posts: Theoretical and Experimental Results,” Anal. Chem., vol. 75, no. 18, pp. 4724–4731, Sep. 2003.

[11] S. K. Srivastava, J. L. Baylon-Cardiel, B. H. Lapizco-Encinas, and A. R. Minerick, “A continuous DC-insulator dielectrophoretic sorter of microparticles.,” J. Chromatogr. A, vol. 1218, no. 13, pp. 1780–9, Apr. 2011.

[12] B. H. Lapizco-encinas, B. a Simmons, E. B. Cummings, Y. Fintschenko, S. N. Laboratories, and P. O. Box, “Dielectrophoretic concentration and separation of live and dead bacteria in an array of insulators.,” Anal. Chem., vol. 76, no. 6, pp. 1571–9, Mar. 2004.

[13] Y.-K. Cho, S. Kim, K. Lee, C. Park, J.-G. Lee, and C. Ko, “Bacteria concentration using a membrane type insulator-based dielectrophoresis in a plastic chip.,” Electrophoresis, vol. 30, no. 18, pp. 3153–9, Sep. 2009.

[14] Y. Kang, D. Li, S. a Kalams, and J. E. Eid, “DC-Dielectrophoretic separation of biological cells by size.,” Biomed. Microdevices, vol. 10, no. 2, pp. 243–9, Apr. 2008.

[15] S. K. Srivastava, A. Artemiou, and A. R. Minerick, “Direct current insulator-based dielectrophoretic characterization of erythrocytes: ABO-Rh human blood typing.,” Electrophoresis, vol. 32, no. 18, pp. 2530–40, Sep. 2011.

[16] P. V Jones, S. J. R. Staton, and M. a Hayes, “Blood cell capture in a sawtooth dielectrophoretic microchannel.,” Anal. Bioanal. Chem., vol. 401, no. 7, pp. 2103–11, Oct. 2011.

[17] S. K. Srivastava, A. Gencoglu, and A. R. Minerick, “DC insulator dielectrophoretic applications in microdevice technology: a review.,” Anal. Bioanal. Chem., vol. 399, no. 1, pp. 301–21, Jan. 2011.

[18] I. Barbulovic-Nad, X. Xuan, J. S. H. Lee, and D. Li, “DC-dielectrophoretic separation of microparticles using an oil droplet obstacle.,” Lab Chip, vol. 6, no. 2, pp. 274–9, Feb. 2006.

[19] J.-S. Kwon, J.-S. Maeng, M.-S. Chun, and S. Song, “Improvement of microchannel geometry subject to electrokinesis and dielectrophoresis using numerical simulations,” Microfluid. Nanofluidics, vol. 5, no. 1, pp. 23–31, Aug. 2007.

[20] A. Nakano, T.-C. Chao, F. Camacho-Alanis, and A. Ros, “Immunoglobulin G and bovine serum albumin streaming dielectrophoresis in a microfluidic device.,” Electrophoresis, vol. 32, no. 17, pp. 2314–22, Sep. 2011.

[21] D. Kim, J. Shim, H.-S. Chuang, and K. C. Kim, “Effect of array and shape of insulating posts on proteins focusing by direct current dielectrophoresis,” J. Mech. Sci. Technol., vol. 28, no. 7, pp. 2629–2636, Jul. 2014.

[22] A. Lalonde, A. Gencoglu, M. F. Romero-Creel, K. S. Koppula, and B. H. Lapizco-Encinas, “Effect of insulating posts geometry on particle manipulation in insulator based dielectrophoretic devices.,” J. Chromatogr. A, vol. 1344, pp. 99–108, May 2014.

[23] J. L. Baylon-Cardiel, B. H. Lapizco-Encinas, C. Reyes-Betanzo, A. V Chávez-Santoscoy, and S. O. Martínez-Chapa, “Prediction of trapping zones in an insulator-based dielectrophoretic device.,” Lab Chip, vol. 9, no. 20, pp. 2896–901, Oct. 2009.

[24] I. Ermolina and H. Morgan, “The electrokinetic properties of latex particles: Comparison of electrophoresis and dielectrophoresis,” J. Colloid Interface Sci., vol. 285, pp. 419–428, 2005.

[25] M. Mescher, A. G. M. Brinkman, D. Bosma, J. H. Klootwijk, E. J. R. Sudhölter, and L. C. P. M. de Smet, “Influence of conductivity and dielectric constant of water-Dioxane

mixtures on the electrical response of SiNW-based FETs," Sensors (Switzerland), vol. 14, pp. 2350–2361, 2014.

6. Hydrodynamic and direct-current insulator-based dielectrophoresis (H-DC-iDEP) microfluidic blood plasma separation

Evaluation and diagnosis of blood alterations is a common request for clinical laboratories requiring a complex technological approach and dedication of health resources. In this work, we present a microfluidic device that with a novel combination of hydrodynamic and dielectrophoretic techniques that can achieve plasma separation in a microfluidic channel from fresh blood and for the first time allow optical real-time monitoring of the components of plasma without pre or post processing. The microchannel is based on a set of dead-end branches at each side and is initially filled using capillary forces with a 2-µL droplet of fresh blood. During this process, stagnation zones are generated at the dead-end branches and some red blood cells (RBCs) are trapped there. Later, an electric field is applied and dielectrophoretic trapping of RBCs is used to prevent more RBCs entering into the channel, which works like a sieve. Besides, an electroosmotic flow is generated to sweep the rest of the RBCs from the central part of the channel. Consequently, an RBC-free zone of plasma is formed in the middle of the channel, allowing real-time monitoring of the platelet behavior. To study the generation of stagnation zones and to ensure RBC trapping in the initial constrictions, two numerical models are solved. The proposed experimental design separates up to 0.1 µL blood plasma from a 2-µL fresh human blood droplet. In this study, a plasma purity of 99 % is achieved after 7 minutes, according to the measurements taken by image analysis.

6.1. Introduction

Nowadays there is a growing need for lab-on-a-chip devices, especially in clinical analysis and diagnostics. The first step in most blood tests is plasma extraction from whole blood.

The use of microfluidics technology can change the time response of this procedure and enable test on demand, for instance, in the evaluation and diagnosis of alterations of hemostasis. New oral anticoagulants (NOACs) have been developed to overcome the frequent monitoring and dose adjustment of their predecessors, but now there is a need for methods to measure the anticoagulant effects of these drugs in several clinical scenarios from bleeding patients, patients requiring an urgent invasive procedure or recurrence of thrombotic events or need for thrombolysis. Unfortunately, tests used to determine their effects on coagulation are drug specific, not standardized for each NOAC, and not available to standard clinical labs. Previous studies already take advantage of microfluidics technology, but either required a previous plasma separation step [1] or real time monitoring was not possible due to RBCs interference [2].

Different methods have been developed for cell and particle separation [3, 4]. Current microfluidic studies to separate blood plasma can be divided into three main groups: The CD format, the paper format and the chip format [5, 6]. The CD format technology is limited due to the need for control valves and the fact that the movement of fluid from one chamber to another relies only on the centrifugation speed [6]. On the other hand, the paper format clogs rapidly and is unsuitable for large volume samples, limiting its application to the analysis of highly concentrated analytes, such as abundant proteins [7] or glucose [8].

In the chip format, some authors have used weir-based designs to separate plasma in capillarity-driven dead-end filtration microchannels [9] or comb and weir-type filter structures [10]. However, in weir-based designs, small quantities of plasma are collected due to clogging of the lower channel depth after the weir.

Alternatively, hydrodynamics have been used effectively to achieve particle and cell separation [11, 12]. These studies used microvortices to investigate the shear gradient lift and wall effect forces at different Reynolds numbers to achieve separation. To this end, a channel was filled without particles and afterwards particles were added to study the hydrodynamic behavior.

Most of the aforementioned methods required mechanical driving sources such as pumps to push the fluid in the microchannels.

In recent years, dielectrophoresis (DEP) methods have been used to manipulate inert particles, and biological microparticles[13, 14]. DC insulator–based dielectrophoresis (DC-iDEP) utilizes dielectric and low permittivity posts or obstacles inside the fluidic channel to change the path track of the electric field and generate a non-uniform electric field. Moreover, the DC-electric field can produce an electroosmotic flow (EOF) that eliminates the need for an external driving force. The use of just two simple electrodes placed in the inlet and outlet of the channel offers other advantages such as a straightforward fabrication process, the fact that, the iDEP devices are less prone to fouling than when embedded electrodes are used, minimum bubble generation inside the channel, fewer electrochemical reactions [15, 16] and the fact that the process is more appropriate for metal-sensitive organic samples. However, if high electric field values are used or the exposure time is increased, cell lysis and cell rupture can appear. For example, human erythrocytes (red blood cells, RBCs) are lysed when an electric field exceeds 600 V/cm [17, 18].

The first separation and concentration of live and dead bacteria via DC-iDEP with square, triangular and circular insulating-posts was presented by B. H. Lapizco in 2004 [19]. Since then, DC-iDEP devices has been applied to different cells and conFigureurations such as E.coli bacteria [20], white blood cells [21], RBCs [22] or blood cell separation in a

sawtooth microchannel [23] (see the review of DC-iDEP studies [24]). The aforementioned works provide valuable insight into DC-iDEP phenomena. One drawback is that most of them used a high electric field and a high ratio of diluted blood samples, sometimes with a controlled pH and ratio of particles in the medium.

This study proposes a microfluidic design that can separate plasma from a single blood droplet (1:1 blood and Heparin), applying low voltage and taking advantage of the hydrodynamic effect to improve red blood cell (RBC) trapping through DC-iDEP.

The use of the presented technology together with real time monitoring of the platelet aggregation on the RBC free zone of plasma created in the middle of the channel could be an important milestone since it would allow the evaluation of the anticoagulant effect with a small amount of blood sample and without any further pre or post processing.

The device considered is a straight channel with dead-end branches on both sides at regular intervals (corrugated shape). Hydrodynamically, red blood cells are captured in the dead-end branches before an electric field is applied. Once the electric field is applied, dielectrophoretic trapping of red blood cell is formed in the three constrictions just after the inlet. This prevents the entrance of more RBCs into the channel. At the same time, the electroosmotic flow generated in the center of the channel sweeps the remaining RBCs. Consequently, an RBC-free zone of plasma is formed in the middle of the channel.

Finite Element Methods are used to validate the length of the dead-end branch for hydrodynamic trapping. A similar methodology is used to determine the achievable constriction width that can trap RBCs without lysis.

The device described in this study takes the advantage of hydrodynamic effects to improve blood plasma separation through a DC-iDEP microfilter. This methodology can speed up DC-iDEP particle separation. The proposed combination of both methods can be utilized for separation of both viable and non-viable particles.

6.2. Design principle of H -DC-iDEP device

The device consists of a 50-µm-deep (H) and 1-cm long (LCH) microfluidic channel with a set of dead-end branches on both sides at regular intervals that generate 20 constrictions (Ci). The dead-end branch is a perpendicular channel initially straight with a constant width (w=200-µm) and the same depth as the main channel (H=50-µm). The length of each branch finishes with a semicircular shape of a dead-end radius (R=100-µm). One inlet port is located at the beginning of the main channel and one outlet at the end. Two electrodes are placed at these locations; Figure 1 (a) shows a schematic view of the microfluidic device considered.

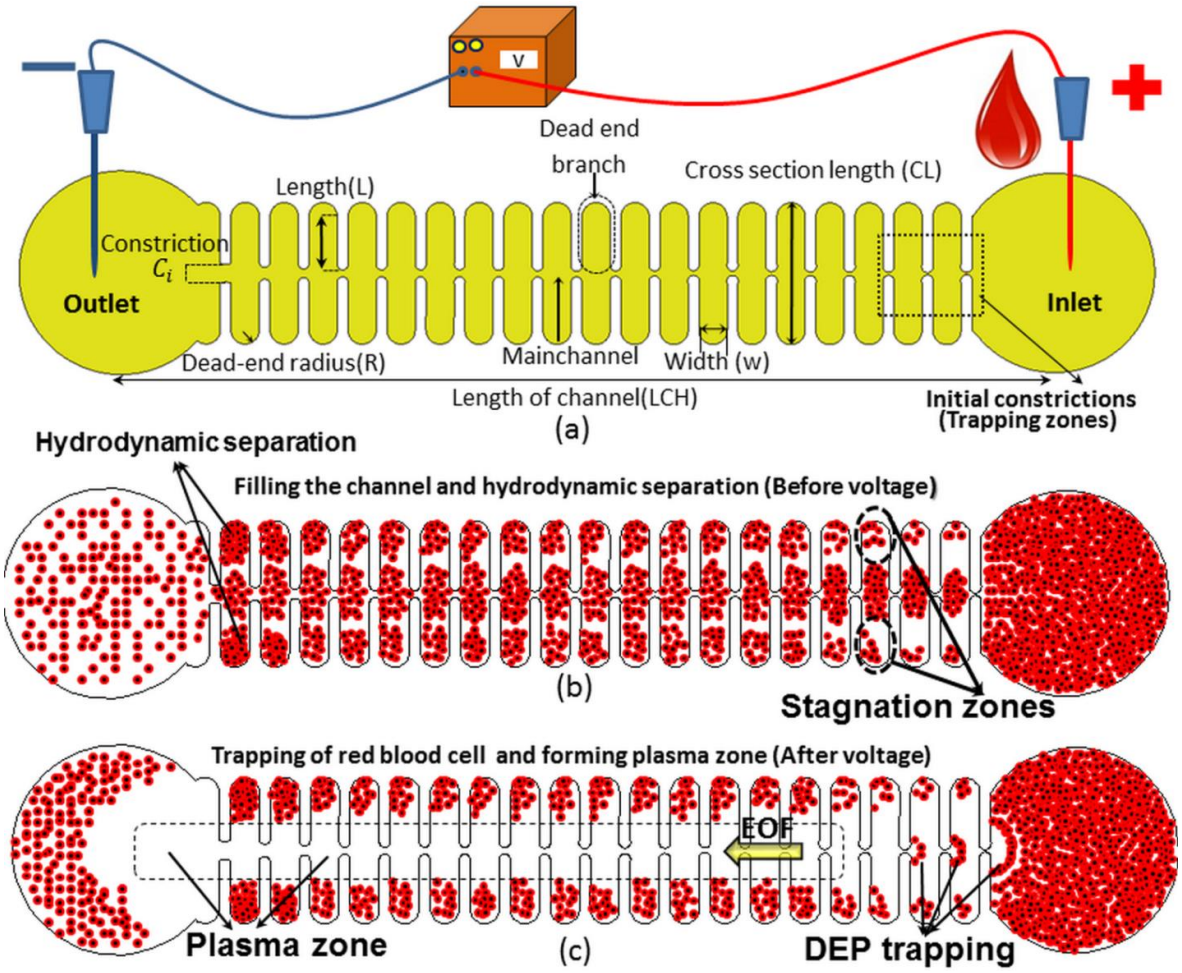

Figure 1 (a) Schematic illustration of a corrugated microchannel for RBCs trapping using hydrodynamic and DC-iDEP, (b) Hydrodynamic trapping generated during capillary filling, (c) Free zone of plasma generation due to DC-iDEP RBC trapping in the initial constrictions and sweeping of the remaining RBCs using EO flow.

Operation of the device is shown in Figure 1 (b) and (c). First, the channel is filled using only capillary force that drives blood through the dry channel up to the end of the dead-end branches. There, the RBCs are trapped hydrodynamically in the stagnation zones generated at the dead-end branches, as it can be seen in Figure 1 (b).

Then, the voltage is applied between the inlet and the outlet. The constrictions where the DC-iDEP force can trap RBCs are the three constrictions just after the inlet, that we call the initial constrictions. The location of the initial constrictions is shown in Figure 1 (a). This prevents more RBCs entering the channel. In this way, DC-iDEP trapping allows the EO flow to sweep the RBCs from the middle of the channel. As a consequence, an RBC-free zone of plasma is generated in the central part of the channel; see Figure 1 (c).

6.3. Materials and methods

6.3.1. Chip fabrication and experimental setup

Polydimethylsiloxane (PDMS) is used to manufacture the microdevice. SU-8 (GM 1060, Gersteltec Sarl, Switzerland) is a negative tone photo-epoxy that is used to create a master mold. SU-8 is chosen since it can be used in thin films between 6 and 50 µm. The prepared mask design is printed in high-resolution film. Microscopy glass slides 75×25 mm are utilized as substrates, which are first cleaned using the Piranha cleaning process (3:1 of H2SO4 + H2O2) and preheated on the hot plate at 200°C for 30 minutes to ensure that the glass slide has dried completely. After cooling the substrate, a 50-µm layer of the photoresist (SU-8) is spin coated at 565 RPM. After 15 minutes relaxation time, the coated substrate is soft-baked in two steps: 10 minutes at 65°C and 60 minutes at 95°C and cooled down to the room temperature. The structures are patterned through the high-resolution printed photo mask by using UV exposure lamp. The coated substrate is post-exposure baked in two steps: 10 minute at 65 °C and 30 minutes at 95 °C, which finally achieves fully cross-linking. After 10 minutes delay time, the structure is cleared through the development process in PGMEA (Propylene glycol methyl ether acetate) for 2 minutes and used as a mold.

To make the PDMS microchannel, Dow Corning Sylgard 184 silicone elastomer and curing agent are thoroughly mixed 10:1 by weight. To obtain a uniform distribution, the mixture is blended and then degassed in a vacuum chamber for 10 minutes to get rid of trapped air bubbles in the sample. In order to ensure the easy peel-off of the channels once cured, the mold is silanized. After that, the mixture is poured on the SU-8 master mold and finally, it is cured for 30 minutes at 120ºC.

The main PDMS microchannel (Top Part) and the cover glass are bonded via an oxygen plasma treatment. A pressure of 1 Torr is set in the oxygen plasma chamber (Gambetti, Germany) and the plasma runs for 30 seconds. The oxygen plasma parameters are chosen to achieve the maximum bond strength. Figure 2 (a) shows a photograph of the completed blood plasma separation microfluidic device.

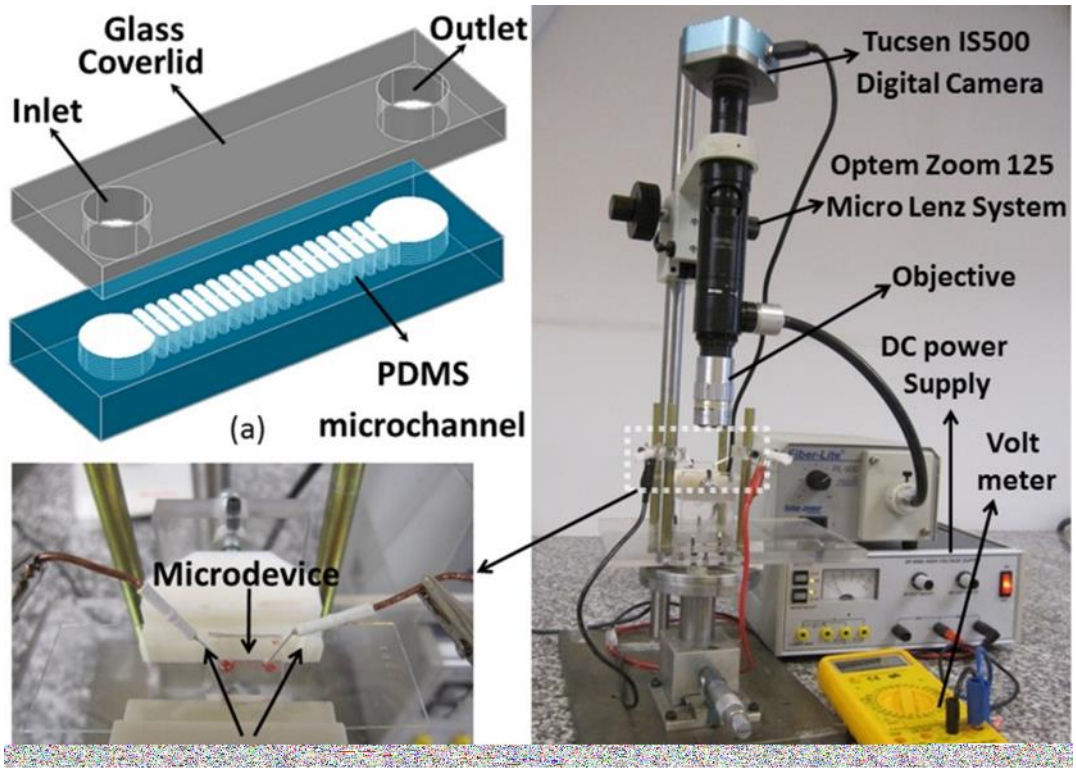

Figure 2 (a) The schematic illustration of the H-DC-iDEP device and (b), (c) The experimental setup

In order to record the images and videos of the blood plasma separation process and analyze the results, a digital camera (Tucsen ISH500, 5.0 M pixel,) is connected to the micro inspection lens system Optem zoom 125C (with a broad 12.5:1 zoom range) and a 20X objective.

A high DC voltage power supply (SF-9585 PASCO- California-USA) is utilized to generate the electric field. Two Platinum electrodes (Roland Consult-Germany) are allocated in the inlet and outlet of the main channel to create the electric field. The experimental setup is shown in Figure 2 (b, c).

6.4. Results and discussion

6.4.1. Numerical hydrodynamic modeling

In order to investigate the hydrodynamic effect of the dead-end branch length (L), numerical analysis of different corrugated microchannels are performed using the Ansys CFX 14.5 software, which is based on the finite element method (ANSYS Academic Research, CFX 14.5 User's Guide, ANSYS, Inc. 2014).

To simulate the blood flow when the voltage is applied, according to Johnston et al [30, 31],who compared five different non-Newtonian blood models, the one that best fitted the experimental data was the Carreau model with the following constants:

$$\mu = \mu_\infty + (\mu_0 - \mu_\infty)\left[1 + (\lambda\dot{\gamma})^2\right]^{(n-1)/2} \quad (1)$$

where $\lambda = 3.13s$ is the time constant, μ is fluid viscosity, $\dot{\gamma}$ is strain rate tensor, $\mu_0 = 0.56\mathrm{P}$ is zero strain viscosity (1P=0.1Ns/m^2), $\mu_\infty = 0.0345\mathrm{P}$ is infinite strain viscosity and n=0. 3568 is an empirical exponent[30, 31].

An inlet electroosmotic velocity of 145 µm/s is defined and the outlet is kept at atmospheric pressure as a boundary condition. The electroosmotic mobility of PDMS and blood flow is measured, $\mu_{eo(PDMS)} = 2.8 \times 10^{-8}\,(m^2/sV)$.

In order to investigate the hydrodynamic effect of the dead-end branch length, L (branch length) has been varied from 0 to 400-µm. The common parameters in all channel models are summarized in Table 1.

Table 1 Constant design parameters of the corrugated channel

Design Parameter		Value
Channel depth	H	50 µm
Dead-end radius	R	100 µm
Dead-end channel width	W	200 µm
Range of constrictions' width	C_i	16-127 µm
Microchannel length	LCH	1 cm

The length of the dead-end branch (L) and the associated cross section (CL) used in the different models are summarized in Table 2.

Table 2 Variable parameters of the model geometry

Model	L (µm)	CL(µm)
A	0	200
B	50	300
C	100	400
D	200	600
E	300	800
F (experimental device)	400	1000

Also, to compare the effect of the dead-end branch length, the velocity streamlines of the tenth dead end branch of each model are shown in Figure 3 (a-f).

The circular dead-end branch without an initial perpendicular straight channel (L=0, dead-end radius =100 µm) is used as the initial geometry (Model A), see Figure 3 (a). The following models add the perpendicular straight channel to this circular shape dead-end branch (Models B-F), see Figure 3 (b-f). Closed loop streamlines are formed on the dead-end branches when the length of the dead-end branch is more than 100 µm, showing velocities approaching to zero in these zones and complete symmetry on both sides of the channel, see Figure 3 (c-f).

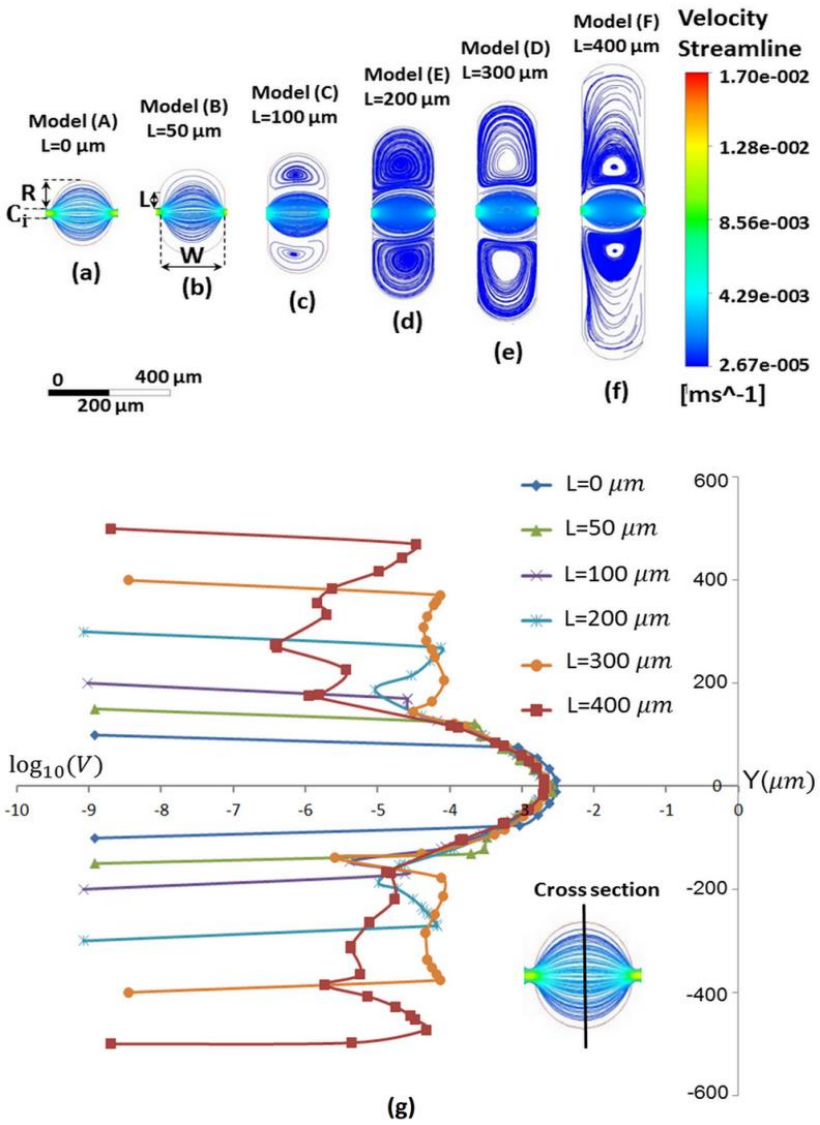

Figure 3 Ansys CFX results. (a-f) Streamline velocity in dead end branch for dead-end radius =100 µm and a varying length L. (g) Plot of the velocity logarithm versus cross section.

Figure 3 (g) shows the logarithm of velocity through the cross section in dead-end branches, and the location of the cross section (in the tenth branch of the channel). It can be seen that appreciable stagnation zones are created 200 microns further from the channel center. Moreover, in 400-µm-length dead end branch, the velocity in the middle is almost 100 times lower than in the 200-µm-long dead-end branch. The stagnation zone length of each cross section (stagnation zone value is selected<50µm/s) is shown in Table 3. This phenomenon increases as the dead end branch length rises, but nevertheless the 400-µm-long dead-end branch is selected for practical reasons, since according to experience, limiting ourselves to this length would ensure RBC trapping without significant air bubble formation.

6.4.2. Numerical DC-iDEP modeling

In order to analyze which constriction width generates RBC trapping without lysis, electric field simulations are performed via ANSYS Multiphysics and post processed.

The widths of the constrictions along the channel vary from the inlet to the outlet starting at 16 µm (Ci) and increasing 6 µm with each step to evaluate the potential for RBC trapping using the DC-iDEP method. In the simulated channel, 50 V are applied between the inlet and the outlet, generating electroosmotic and dielectrophoretic flow.

Figure 4 (a) shows calculated values of equation 18 (Chapter 3) in the first five constrictions (16-40 µm). According to equation 18 (Chapter 3), there are appreciable trapping zones only in the three initial constrictions, where the trapping region is shown in red. In the other constrictions, the streaming flow prevails. The opposite direction of electroosmotic and dielectrophoretic velocities before the constriction, shown in Figure 4 (b), creates a trapping zone before the constriction (regarding experimental results, the correction factor of 10, is defined in equation 18 (Chapter 3)).

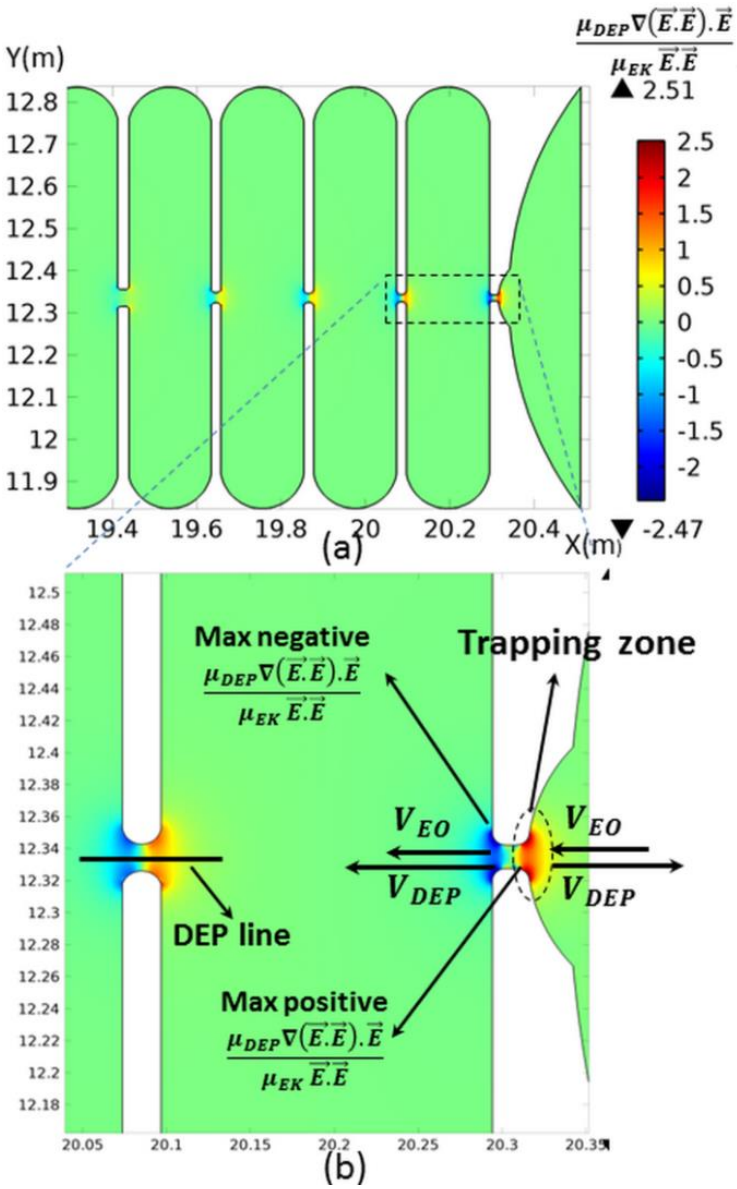

Figure 4 (a) Trapping zones in the five initial constrictions, (b) Schematic plot of electroosmotic and dielectrophoretic velocities in a constriction (correction factor (c) of 10 in Equation (18,chapter 3)).

To ensure that the application of an electric field does not affect hydrodynamic separation, the electric field plot of the tenth dead-end branch (in the middle of the channel) of each model is shown in Figure 5 (a to f).

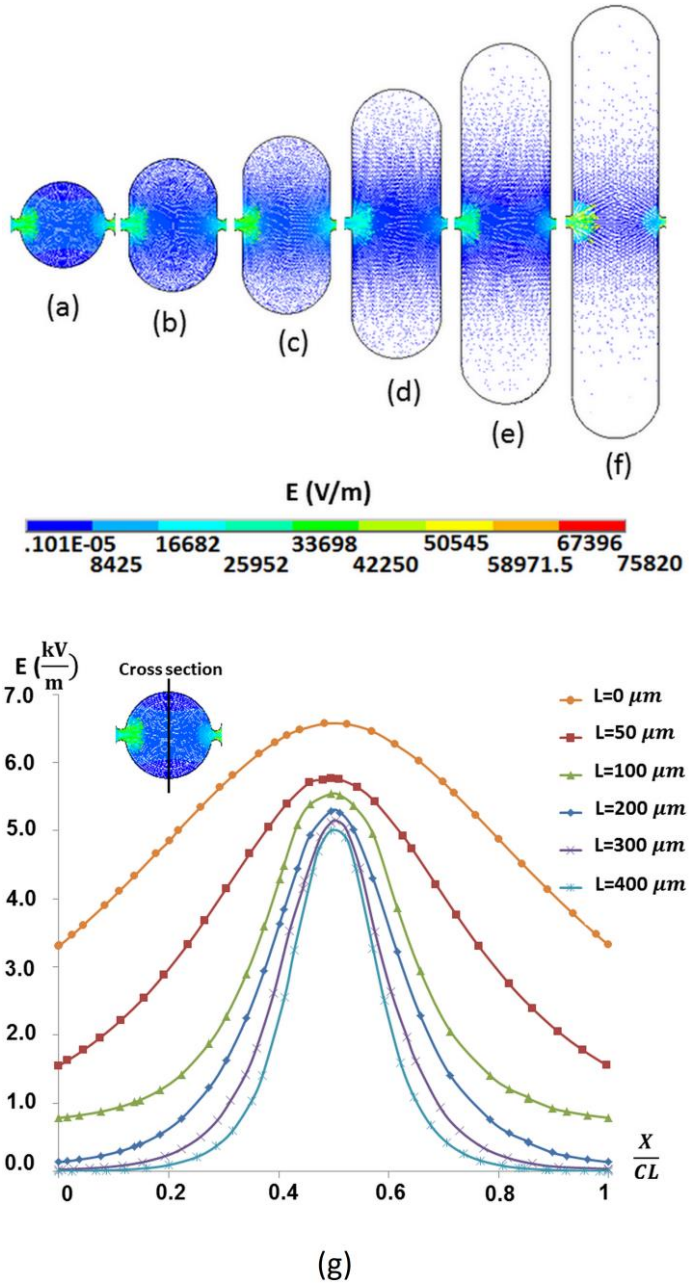

Figure 5 (a-f) Electric field plots of the tenth dead end branch when 50 V are applied between the inlet and the outlet of the corrugated channel for different dead-end branch's length (L), (g) Electric field variation in a dead-end-branch cross section.

Figure 5 (g) shows the variation of the electric field when the dimensionless value X/CL is changed over a cross section of the channel (see Figure 5 (a)) (X is vertical location and CL is the cross section length of each model). The increasing dead-end branch length results in an attenuation of the electric field at the end of the dead-end branch. Since electroosmotic velocity is a function of the electric field, the reduction of the electric field

can lead to a decrease in the electroosmotic velocity in this area and help RBCs to remain in the stagnation zone.

To measure the length of the minimum electric field zone, the electric field is considered minimum when it is lower than 200 V/m in the cross section. See results in Table 3.

Table 3 Variable parameters of the model

Model	Stagnation zone Length <50 µm/s (%)	Numerical stagnation zone length (µm)	Experimental stagnation zone length (µm)	Zero Electric Field Length <200 V/m in cross section (%)
A	0.00%	0	0	0.0%
B	0.00%	0		0.0%
C	0.12%	50		0.0%
D	0.26%	160		0.05%
E	0.35%	280		0.20%
F	0.70%	700	600± 50µm	0.50%

Numerical analysis results highlighted the advantages of dead-end branches of 400-µm-long to separate more red blood cells.

6.4.3. Numerical model validation

In order to validate the above strategy and simulations, the particle trapping in corrugated channels with the same dimensions as the models simulated previously, are measured experimentally and the results are compared with the numerical models. First, a microfluidic chip with two corrugated microchannels of 1-cm long, 0.05-mm deep, 0.02-mm long for Model A and 1-mm long for Model F, with the dead-end branch length according to the Model A and F in Figure 3, are fabricated in PDMS. After surface activation by plasma treatment, the PDMS channels are sealed on a glass slide. See Materials section for further details.

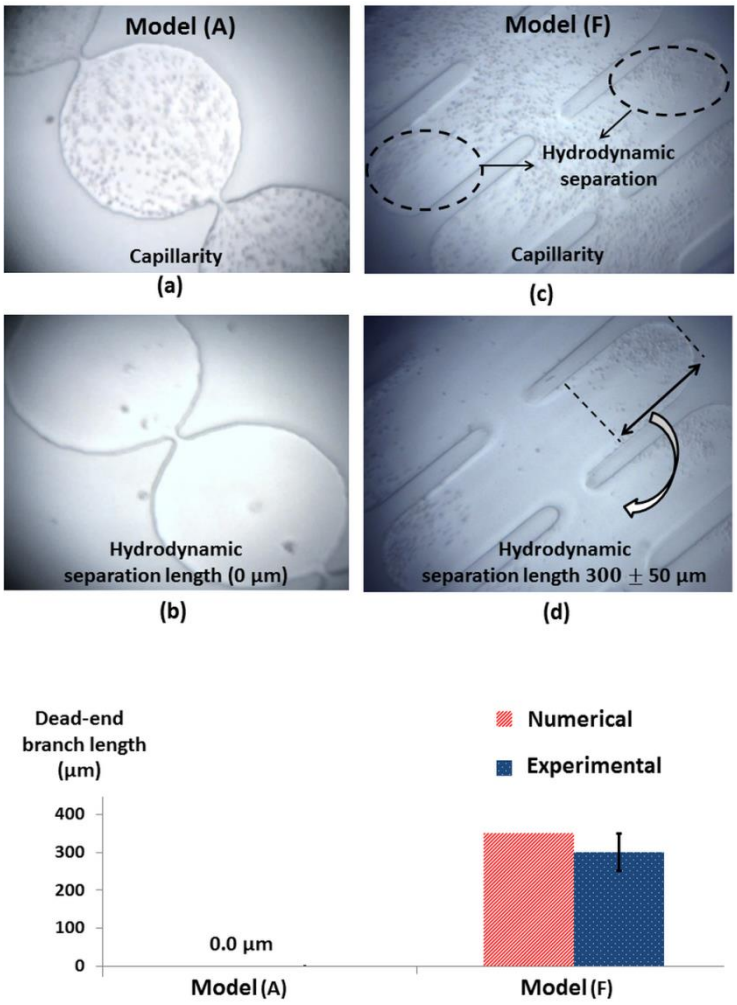

Figure 6 Hydrodynamic behavior comparison between corrugated channels with varying dead-end branch length (a) L=0 µm during capillary filling, (b) L=0 µm under EO flow (Voltage=50 V), (c) L=400 µm during capillary filling, (d) L=400 µm under EO flow (Voltage=50 V).

The two channels are first filled by capillarity due to the plasma activation. Figure 6 (a) and (b) shows the particle distribution in the channels. In agreement, with numerical simulations, Model A with L=0 does not show any dead-end zone and therefore there is no cell trapping during the initial filling by capillarity and when the EO flow is generated. In Model F, the dead-end branch length is increased (L= 400 µm). During the filling by capillarity, the generation of the stagnation zone enables the trapping of some cells at the end of the dead-end branch, see Figure 6 (c), which are kept there, even after, the EO flow is generated, see Figure 6 (d). This experiment is repeated 5 times with channels from the same run and the average values and standard deviation of the length of the stagnation zone are compared to the numerical model results, see Table 3.

To experimentally validate which constriction-width generates RBC trapping without lysis, a voltage of 50 V is applied between the inlet and outlet to the Model F used in the previous test. The max value of the trapping condition (equation 18, chapter 3) over the

axial line (DEP line) of the constriction is calculated being 2.2±0.2, 1.6±0.2, 1.2±0.2, 0.6±0.2 in the manufactured constrictions of 16± 2µm, 22± 2µm, 28± 2µm 34± 2µm. Figure 7 shows a comparison between the numerically calculated trapping zones and the particles being trapped in the experiments with equivalent results.

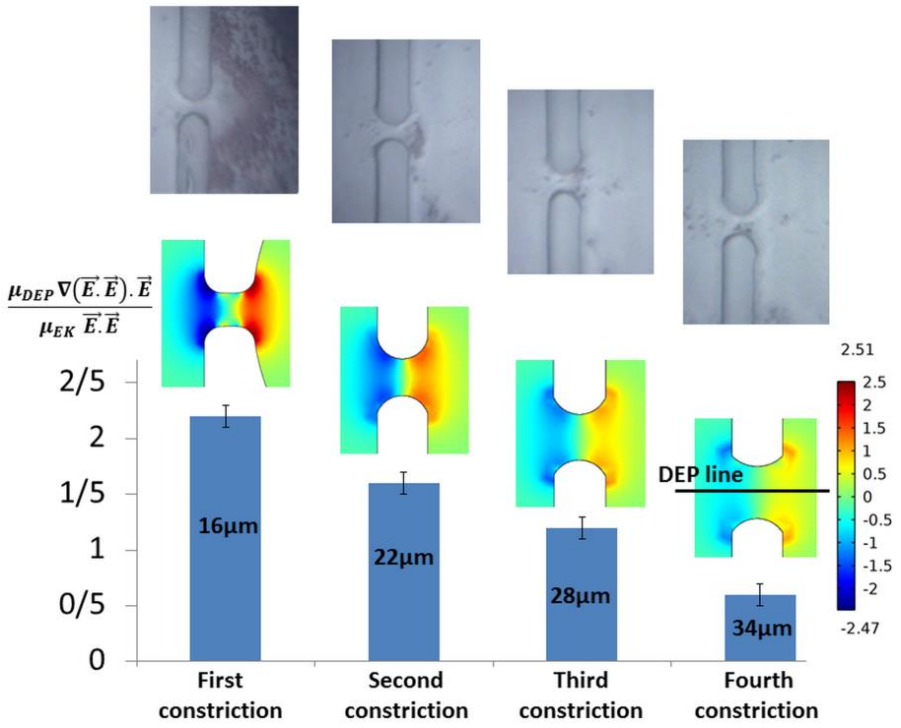

Figure 7 The trapping value and the trapping performance of the first four constrictions.

6.4.4. Experimental test and validation

Finger pricked fresh blood samples from healthy volunteers with almost 40% hematocrit are collected. 2µL of blood is mixed with 2µL Heparin Sodium (1.000UI/ml) to avoid clotting during the experiment. As suggested by numerical results, the final device is fabricated with 400-µm-long dead-end branches.

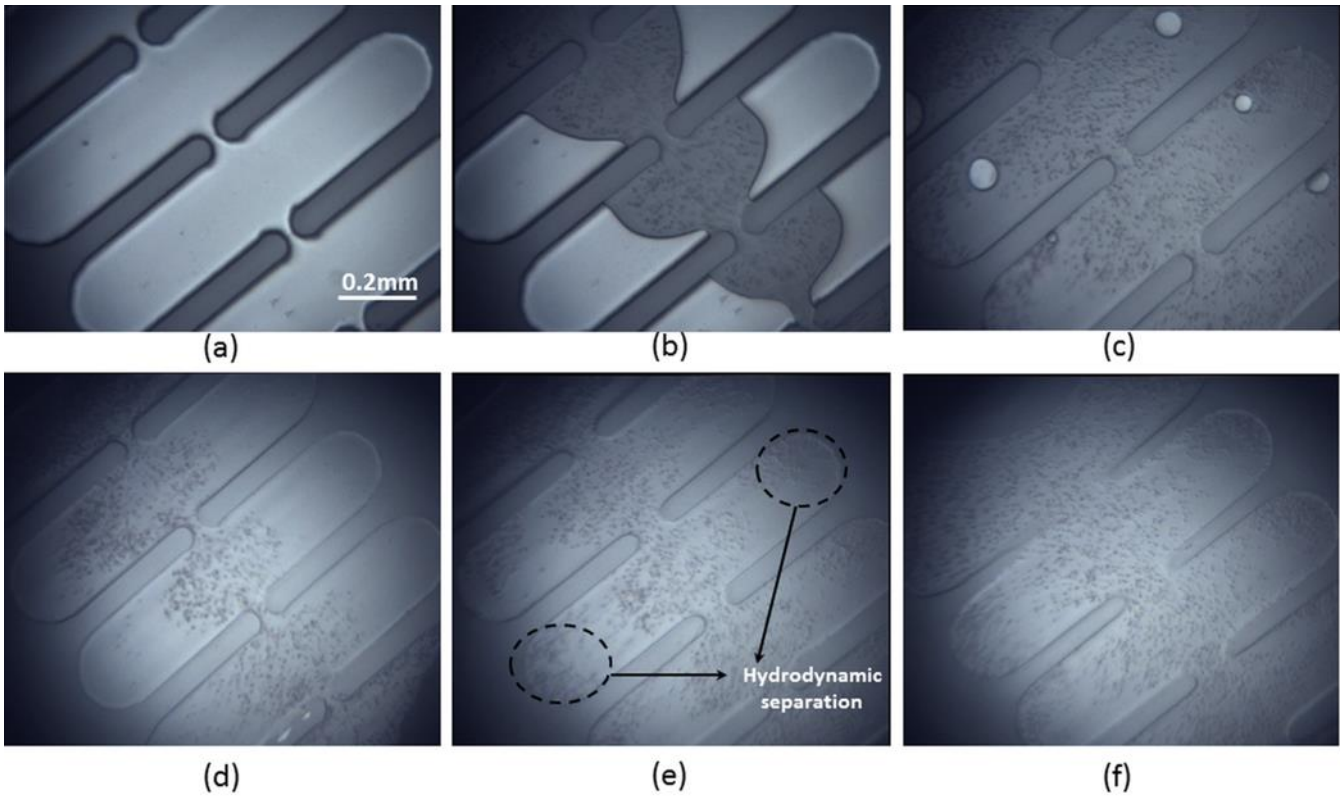

Figure 8 Experimental hydrodynamic separation in a 400-µm- dead-end branch corrugated microchannel (before applying the electric field), (a) Empty channel (b) Filling process, (c) Air bubble generation and hydrodynamic RBC trapping in dead-end branch, (d) Channel inlet, (e) Middle of channel, (f) Channel end.

A blood sample is dropped into the inlet of the microchannel and the blood fills the microchannel through capillary forces. Small air bubbles are formed at the ends of each branch, but since PDMS is gas permeable, the air bubbles disappear after 30 seconds. During the capillary filling, RBCs are trapped at the end of dead-end branches. The average filling velocity field decreases as the constriction width increases.

Therefore the number of RBCs that are trapped at the dead-end branches increases as we move from the inlet to the outlet. Figure 8 (a) shows the empty channel. Figure 8 (b) shows the filling procedure and Figure 8 (c) shows some generated bubbles which vanish in the following images. Figure 8 (d) to (f) shows the initial, middle and end part of the channel where RBCs are trapped at the end of dead-end branches before applying voltage. Secondly, a 1-µL droplet of fresh blood is dropped into the outlet to avoid a hydrostatic pressure difference in the main channel before applying an electric field. The direct current (DC) voltage is set to 50V to achieve trapping and avoid hemolysis during the experiment, since the maximum achievable electric field is 600 V/cm [12, 13].

As expected from Figure 4 (b), the counter play between the electroosmotic and the negative dielectrophoretic flows retains the RBCs just before the initial constrictions.

The trapped RBCs before the initial constriction prevent additional RBCs into entering the channel so this constriction works like a sieve. Figure 9 shows the time evolution of the separation. For instance, the trapping of RBCs at the three initial constrictions after 1, 10, 20 and 30 seconds, respectively. In addition, the improvement of the trapping zone after 2 and 7 minutes are shown in Figure 9 (a) to (f). The directions of EO and DEP velocities before and after the first constriction are shown in Figure 9 (b).

EO flow assisted hydrodynamic separation through the generation of stagnation zones that kept the RBCs at the end of branches.

Due to the streaming flow generated in the corrugated microchannel, the RBCs located in the middle of the channel are swept to the outlet. Consequently, an RBC-free zone of plasma is created in the middle of the channel after 2, 4 and 7 minutes, see Figure 9 (g-i). Also a large RBC- free zone of plasma is formed at the end and outlet of the microchannel after 2, 4 and 7 minutes, see Figure 8 (j-l). Note that, the separated plasma is heparanized plasma. This experiment is repeated five times and average data is obtained for the amount of plasma, time and purity, which are shown in Table 4.

The purity of the separated blood plasma is defined as:

$$Purity = 1 - \frac{C_P}{C_M} \qquad (2)$$

where, C_M is the number of RBC in the channel before applying voltage and C_P is the number of RBC in the separated plasma in the middle and end parts of the channel.

Analyzing the average number of RBCs at the center of channel in Figure 5 (e-f), before applying voltage, and the average number of RBCs that remain in Figure 9 (i-l), after applying voltage, shows that the purity of the separated blood plasma from whole blood in the corrugated channel topology is around 99%, using image processing (The images were analyzed by ImageJ software).

Table 4 Average separated plasma, time and purity.

Parameters	Blood Sample Volume	Volume of the separated plasma (By measurement of plasma zone area)	Time (Minutes)	Purity %
Microchip	~2 µL	0.1 ± 0.02 µL	7±1	> 99

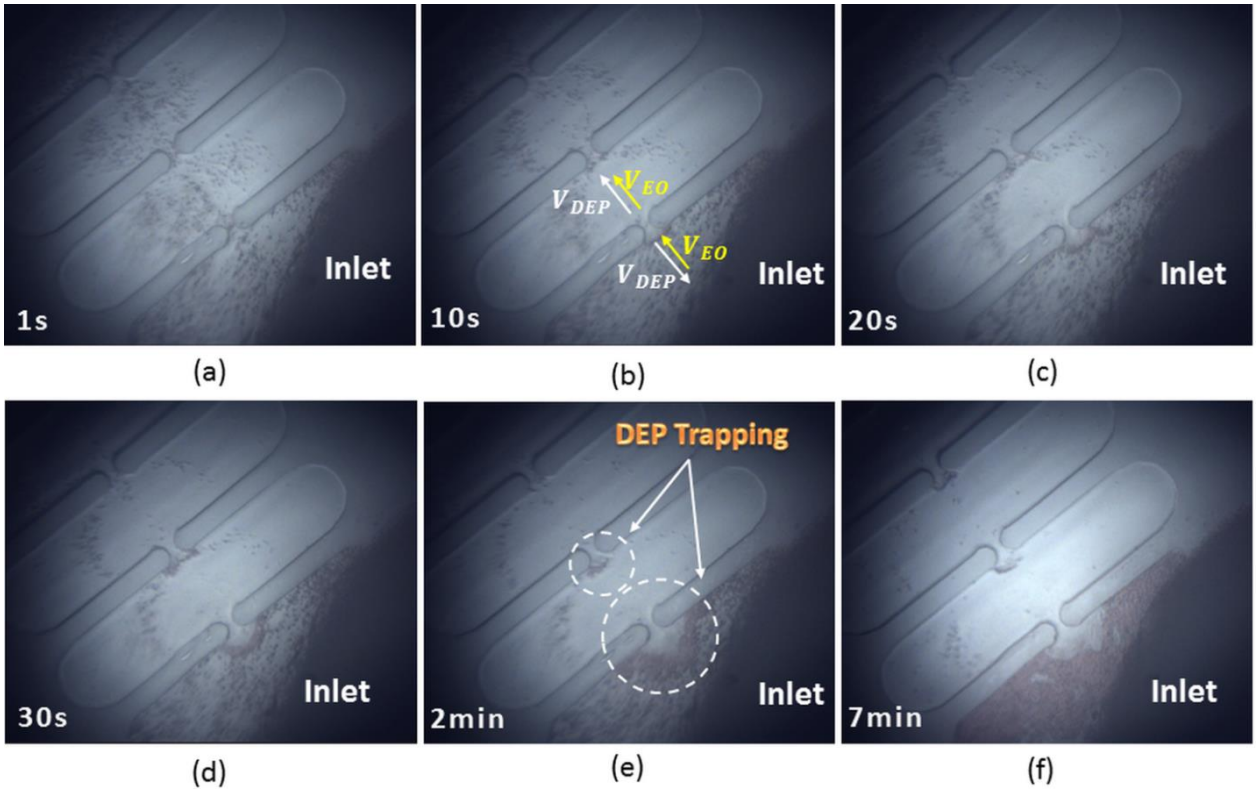

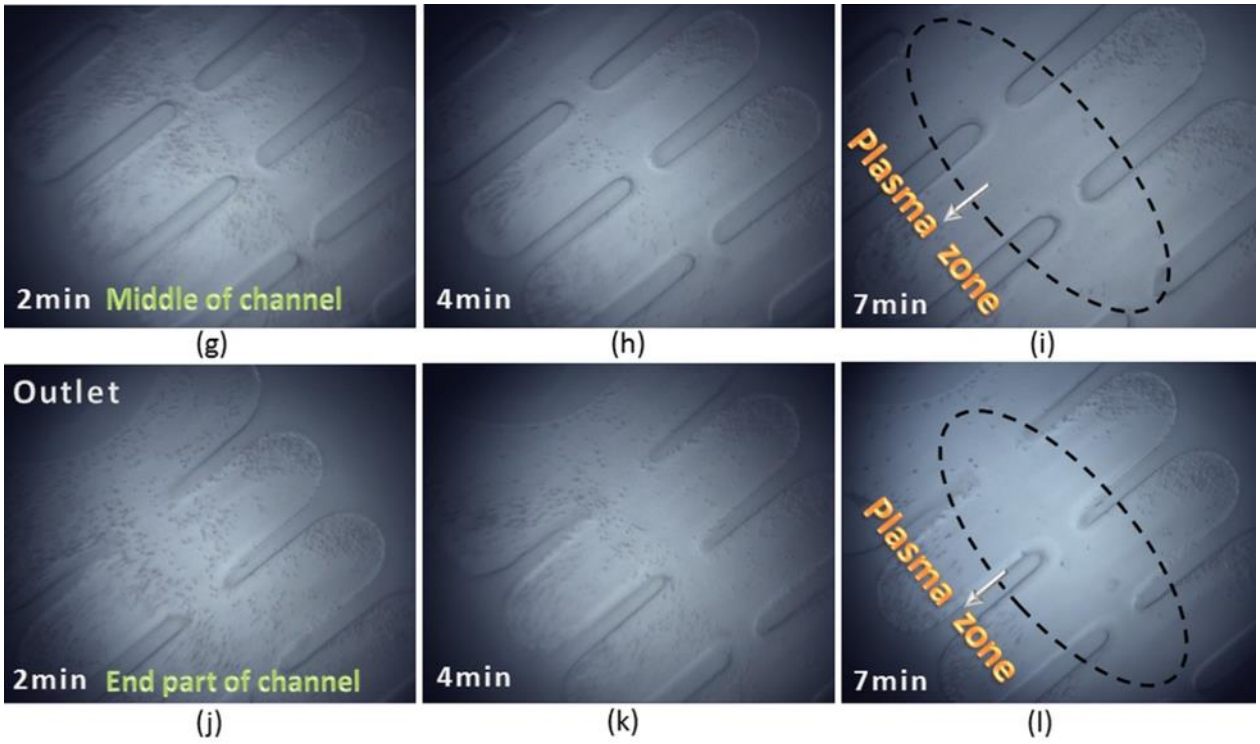

Figure 9 Experimental DC-iDEP RBC separation when 50 V are applied between inlet and outlet. Generation of DEP trapping before initial constrictions after (a) 1 s, (b) 10 s (c) 20 s (d) 30 s, (e) 2 min, (f) 7 min. Plasma zone in the middle of the channel (g) After 2 minutes, (h) After 4 minutes, (i) After 7 minutes. Plasma zone in the channel end, (j) After 2 minutes, (k) After 4 minutes, (l) After 7 minutes.

6.5. Concluding remarks

A microfluidic channel with dead-end branches at each side which combines hydrodynamic and DC-iDEP methods for blood plasma separation featuring 99 % plasma purity from a single 2 microliter blood sample without needs for any external pump, was designed, manufactured and characterized. The microfluidic channel is modeled and designed using Finite Elements Models. In particular, two FEA models are used to model the microfluidic channel and to parametrically investigate the appropriate dimensions to achieve RBC trapping without lysis.

The proposed design has a small area (10 mm × 1 mm) and uses only two external electrodes to generate the required electric field with only 50 V. In this topology 0.1 microliters of plasma can be separated from 2 microliters of blood in less than 7 minutes.

The previous studies related to DC-iDEP phenomena used very high diluted blood samples 1:750 for separating RBCs [22], while our study uses a 1:1 dilution with heparin to avoid coagulation during the test.

Other authors either required precise regulation of four voltages to separate white blood cells [21] or high voltage (200-700 V) was used to separate of blood cells from diluted blood in a sawtooth shape channel [23]. Also, in some cases particles were added after the medium filled the device but in the current study, both particles (blood cells) and medium (heparinized plasma) are simultaneously introduced into the channel.

None of these cases combined the advantages of hydrodynamic separation with DC-iDEP to achieve higher purity in less time, requiring a lower voltage. However, the current study proposes a simple channel design that utilizes a single voltage value (50 V) to enhance hydrodynamic separation using DC-iDEP method for RBC trapping as well as using electroosmotic flow to form an RBC-free zone of plasma in the middle of the channel.

To the authors' knowledge, a hydrodynamic effect enhanced DC-iDEP microfilter for blood plasma separation has been demonstrated in this study for the first time. It is an example of how DC-iDEP can speed up particle separation in biological applications where time can be a constraint.

6.6. References

[1] Okorie U M, Diamond S L (2006) Matrix protein microarrays for spatially and compositionally controlled microspot thrombosis under laminar flow. Biophys. J. 91- 9: 3474–3481

[2] De Witt S M, Swieringa F, Cavill R, Lamers M M E, Kruchten R V, Mastenbroek T, Baaten C, Coort S, Pugh N, Schulz A, Scharrer I, Jurk K, Zieger B, Clemetson K J, Farndale R W, Heemskerk J W M, Cosemans J M E M (2014) Identification of platelet function defects by multi-parameter assessment of thrombus formation. Nature communications 5: 4257

[3] Lenshof A, Laurell T (2010) Continuous separation of cells and particles in microfluidic systems. Chemical Society Reviews 39: 1203–1217

[4] Sajeesh P, Sen A K (2014) Particle separation and sorting in microfluidic devices: a review. Microfluid Nanofluid 17: 1–52

[5] Hou HW, Bhagat A A, Lee WC, Sha Huang S, Han J, Lim CT (2011)Microfluidic Devices for Blood Fractionation. Micromachines 2: 319-343

[6] Kerhoas MK, Sollier E (2013) Micro-scale blood heparinized plasma separation: from acoustophoresis to egg-beaters. Lab Chip13: 3323–3346

[7] Songjaroen T, Dungchai W, Chailapakul O, Henry CS, Laiwattanapaisal W (2012) Blood separation on microfluidic paper-based analytical devices. Lab Chip 12: 3392-3398

[8] Yang X, Forouzan O, Brown TP, Shevkoplyas SS (2012) Integrated separation of blood plasma from whole blood for microfluidic paper-based analytical devices. Lab Chip 12: 274-280

[9] Wu CC, Hong LZ, Ou CT (2012) Blood cell -free of plasma separated from blood sample with cascading weir taype microfilterusing dead end microfilter. Journal of Medical and Biological Engineering32:163-168

[10] Crowley TA, Pizziconi V (2005) Isolation of plasma from whole blood using planar microfilters for lab-on-a-chip applications. Lab Chip 5: 922–929

[11] Karimi A, Yazdi S, Ardekani AM (2013) Hydrodynamic mechanisms of cell and particle trapping in microfluidics. Biomicrofluidics 7:021501-22

[12] Sollier E, Go DE, Che J, Gossett DR, Sean O'Byrne S, Weaver WM, Kummer N, Rettig M, Goldman J, Nickols N, McCloskey S, Rajan P. Kulkarni RP, Carlo DD (2014) Size-selective collection of circulating tumor cells using Vortex technology. Lab Chip14: 63–77

[13] Jubery TZ, Srivastava SK, Dutta P (2014) Dielectrophoretic separation of bioparticles in microdevices: A review. Electrophoresis 35: 691-713

[14] Lewpiriyawong N,Yang C (2014) Dielectrophoresis Field-Flow Fractionation for Continuous-Flow Separation of Particles and Cells in Microfluidic Devices. Advances in Transport Phenomena 3: 29-62

[15] Srivastava SK, Cardiel JB, Encinas BL, Minerick AR (2011) A continuous DC-insulator dielectrophoretic sorter of microparticles. Journal of Chromatography A, 1218: 1780–1789

[16] Qian C, Huang H, Chen L, Li X, Ge Z, Chen T, Yang Z, Sun L(2014) Dielectrophoresis for Bioparticle Manipulation. Int. J. Mol. Sci 15: 18281-18309

[17] Gao J, Yin XF, Fang ZL (2004) Integration of single cell injection, cell lysis,

separation and detection of intracellular constituents on a microfluidic chip. Lab Chip 4: 47-52

[18] Brown R, Audet J (2008) Current techniques for single-cell lysis. J R Soc Interface 5: 131–138

[19] Encinas BL, Simmons B, Cummings E, Fintschenko Y (2004) Dielectrophoretic Concentration and Separation of Live and Dead Bacteria in an Array of Insulators. Anal. Chem 76: 1571-1579

[20] Cho YK, Kim S, Lee K, Park C, Lee JG, Ko C (2009) Bacteria concentration using a membrane type insulator-based dielectrophoresis in a plastic chip. Electrophoresis 30: 3153–3159

[21] Kang Y, Li D, Kalams S, Eid J (2008) DC-dielectrophoretic separation of biological cells by size. Biomed Microdevices vol. 10: 243–249

[22] Srivastava S, Artemiou A, Minerick A (2011) Direct current insulator-based dielectrophoretic characterization of erythrocytes: ABO-Rh human blood typing," Electrophoresis, 32: 2530–2540

[23] Jones P, Staton S, Hayes M (2011) Blood cell capture in a sawtooth dielectrophoretic microchannel. Anal Bioanal Chem 401: 2103–2111

[24] Srivastava S, Gencoglu A, Minerick A (2011) DC insulator dielectrophoretic applications in microdevice technology: a review.Anal Bioanal Chem 399: 301–321

[25] Cardiel JB, Encinas BL, Betanzo CR, Santoscoy AC, Chapa SM (2009) Prediction of trapping zones in an insulator-based dielectrophoretic device. Lab Chip 9: 2896–2901

[26] Kirby B (2010) Micro- and Nanoscale Fluid Mechanics Transport in Microfluidic Devices. Cambridge University Press, NewYork

[27] Chaoco SO, Encinas BL, Palomares MR, Chapa SM, Betanzo CR (2008) Performance characterization of an insulator-based dielectrophoretic microdivice. Electrophoresis 29:3115-3122.

[28] Kwon JS, Maeng JS, Chun MS, Song S (2008) Improvement of microchannel geometry subject to electrokinesis and dielectrophoresis using numerical

simulations. Microfluid Nanofluid 5: 23–31

[29] Villanueva RG, Sano M, Encinas BL, Davalos R (2014) Joule heating effects on particle immobilization in insulator-based dielectrophoretic devices. Electrophoresis 35: 352–361

[30] Chan WY, Ding Y, Tu JY (2007) Modeling of non-Newtonian blood flow through a stenosed artery incorporating fluid-structure interaction. ANZIAM Journal 47: 507-523

[31] Johnston B, Johnston P, Corney S, Kilpatrick D (2004) Non-Newtonian blood flow in human right coronary arteries: steady state simulations. Journal of Biomechanics 37: 709–720

7. Multifunctional Blood Plasma Separator Microfluidics Chip for Point-of-Care Testing based on a Bilateral Electroosmotic Microfilter

A wide range of diseases and conditions are monitored or diagnosed from plasma, but the ability to analyze a whole blood sample with the requirements for a point-of-care (POC) device such as robustness, friendly use and simple handling, remain unmet.

This study presents a novel microfluidic chip for blood plasma separation, which combines microfluidics with conventional lateral flow immune chromatography to extract enough plasma to perform a blood panel in a simple and portable device. The microfluidic chip design is a combination of cross-flow filtration with a reversible electroosmotic flow that prevents clogging at the filter entrance and maximizes the amount of separated plasma. The main advantage of this design is its efficiency, since with a small amount of sample (a single droplet ~10µL) a considerable amount of plasma (more than 1µL) is extracted and collected with high purity (more than 99%) in a reasonable time (5 to 8 minutes). To validate the quality and quantity of the separated plasma and to show its potential as clinical tool, the microfluidic chip has been combined with lateral flow immune chromatography technology to perform a qualitative detection of the TSH (thyroid-stimulating hormone) and a blood panel for measuring cardiac Troponin and Creatine Kinase MB. The results obtained from the microfluidic system are comparable to previous commercial lateral flow assays that required more sample for implementing less tests.

7.1. Introduction

Clinical blood tests are often used to determine or monitor diseases, mineral content, pharmaceutical drug effectiveness and organ function. Multiple tests for specific blood components (such as a glucose test or a cholesterol test) are often grouped together into a blood panel. Although many researchers have developed plasma separation from whole blood utilizing different techniques in microtechnologies, the volume of extracted plasma to implement the test is still one barrier to achieve a reliable miniaturized blood panel.

The blood plasma separation microfluidic methods can be categorized in three formats: paper-based microfluidics, the CD format and the microfluidic chip format [1]. Paper-based

microfluidics, with part of the knowledge coming from lateral-flow assays [2, 3, 4] and a great market potential due to its low cost, is still immature in capabilities typical of microfluidic chip format devices such as the mixing, the need for control over flow rates, interaction times between sample and reagents. The CD based format, as another technology to miniaturize the conventional centrifugation method, has the limitation of requiring numerous valves and specific equipment [5, 6]. Different approaches have been taken in the microfluidics chip format to achieve separation of plasma from whole blood, see the reviews[7, 8, 9]. Initially, most of these microfluidic chips required a syringe pump to control the required flow rate of the microdevice, which is not always available when thinking in a point-of-care device for blood testing near the patient and in general only few nanoliters of plasma could be separated.

The majority of diseases can be diagnosed or monitored through blood assays. The growth of new infectious diseases or chronic disease in elderly population increase the interest in blood assays performed in the POCT format. But diagnostic procedures plasma or serum (plasma deprived of clotting agents) that must be extracted from full blood samples prior to analysis. Thus, the best opportunities for microfluidic POCT systems reside on those that provide separation of plasma from the components of blood and fulfill POC conditions such as short time to result, portability, flexibility and low cost per test, [10].

Electrokinetic (EK) technique has potential to address these issues and create flow by utilizing a voltage difference, which eliminates the need of an external driving force. The previous studies that employed EK techniques to separate cells or particles [11, 12, 13] used either complex electrode geometries, more than two electrodes or a set of different voltages which make it more complicated for the integration of such designs in micro-total analysis system. Furthermore, in particular for biological samples, where cells/particle can not be placed separately, the contamination of the separation channel during the initial filling is problematic.

This study presents a highly efficient blood plasma separator microfluidic chip by taking advantage of a cross-flow filtration method combined with a reversible electroosmotic flow to prevent red blood cell accumulation in the entrance of the filtration area. The use of just two simple electrodes placed in the inlet and the outlet of the microchannel offers advantages such as a straightforward fabrication process and allows the regulation of the flow rate through the voltage. This strategy allows the collection of 1 µL of blood plasma from a 10-µL fresh human blood sample. In the proposed design, two different 50-µm-deep channels are placed in the top part of the microfluidic design to facilitate the detection and readout of multiple blood parameters.

To validate the quality and quantity of the separated plasma and to show its potential as clinical tool, the microfluidic chip has been combined with lateral flow immune chromatography technology to perform two different types of analysis: firstly, a single test for the qualitative detection of the TSH (thyroid-stimulating hormone) and secondly a blood panel for measuring two indicators in the diagnosis of myocardial infarction (MI): Cardiac Troponin (cTnI) and Creatine Kinase MB (CK-MB). Clearly, a combination of both measurements in the same test device increases the efficiency of the diagnosis. The results obtained from the microfluidic system are comparable to previous commercial lateral flow assays that required more sample for implementing less tests. Moreover, the proposed device present interesting characteristics for the POCT such as short time to result, portability, flexibility, low cost per test.

7.2. Materials and methods

7.2.1. Design principle

The proposed microfluidic device is manufactured in two parts, see Figure 1 (a). The top part comprises a main channel (height, H_TC= 50-µm and 500-µm wide with a 150-µm wide constriction in the middle) called transport channel for delivering the blood drop sample and two plasma collected channels allocated symmetrically on both sides of the transport channel which are connected at the end to deliver the separated plasma for the blood test. Figure 1 (b) shows that in the designed constriction of the transport channel, the blood is accelerated to avoid RBCs accumulation in the entrance of the filtration channel (bottom part).

The bottom part includes a symmetric arrangement of diamond microposts (MIMP, Microchannel Integrated MicroPillars), which are H_{FC}= 1.5-µm deep to be ensured of RBCs filtration. This arrangement was previously designed to work as an efficient micropump [14], allowing a fast extraction of plasma.

The blood plasma separation is initially due capillary forces generated by the oxygen plasma treatment and glass MIMP capillarity. But after a while, the blood flow velocity in the transport channel is slowed down which leads to an accumulation of cells in the entrance of the separation area (RBCs clogging). To address this issue and break the RBCs accumulation, an electroosmotic flow is generated connecting the two electrodes placed in the inlet and the outlet respectively, see Figure 1 c.

When a DC electric field is applied between the channel inlet and the channel outlet, the ions from the electrolyte form an electric double layer (EDL) over the wall surface. The ions from the double layer are attracted to the negative electrode producing an electroosmotic liquid flow. The electroosmotic velocity is (EOF) [15].

$$\vec{V}_{eo} = \mu_{eo}\vec{E} = \frac{\varepsilon_m \zeta_w}{\eta}\vec{E} \quad (19)$$

where E is the magnitude of the electric field, $\mu_{eo}$is the electroosmotic mobility of the ionic fluid, ζ_w is the zeta potential of the microchannel, η is the viscosity and ε_m is the permittivity of the fluid.

The total electrokinetic velocity (EK) of the suspended RBCs in the fluid due to the combined effects of electroosmosis (EO) and electrophoresis (EP) can be expressed as:

$$\vec{V}_{EK} = \vec{V}_{EO} - \vec{V}_{EP} = (\mu_{eo} - \mu_{ep})\vec{E} \quad (20)$$

Where $\vec{V}_{EK}$ is the total electrokinetic velocity, $\vec{E}$ is electric field strength, μ_{eo} is the electroosmotic mobility and μ_{ep} is the electrophoretic mobility. The electrophoretic direction of negatively charged particles such as RBCs is from the ground to the positive electrode. According to Srivastava et al. in 2011 [15], RBCs are large with a minor net negative charge, therefore EP mobility is insignificant compared with EO mobility thus μ_{EP} can be neglected. The applied DC electric field creates a net force on the RBCs mainly dominated by EO flow and particles move from positive to negative electrodes [16].

Figure 1 (c) shows how the electroosmotic flow (EOF) generates a higher sheare rate on the clogged RBCs in the entrance area of the separation zone and consequently control the RBCs movements.

In this technique, the direction of this net force is modified by changing the polarity of electrodes (reverse EOF), see Figure 1 (c- d). This reverse DC electric field prevents the RBC accumulation at the entrance of the separation area and allows the filtration process to proceed till the plasma has reached the test zone of the lateral flow assay test strip. Figure 2 (a-b) shows the main dimensions of the proposed design.

This extracted blood plasma is collected in two channels (height, H_{PC}=50-µm) located 500 µm apart from the transport channel in the top part, called plasma collected channels. The

width of these plasma collected channels increases smoothly from 100-µm (in the MIMP filtration channel) up to 400-µm at the end where the blood plasma is gathered to interface with the lateral flow assay test strips.

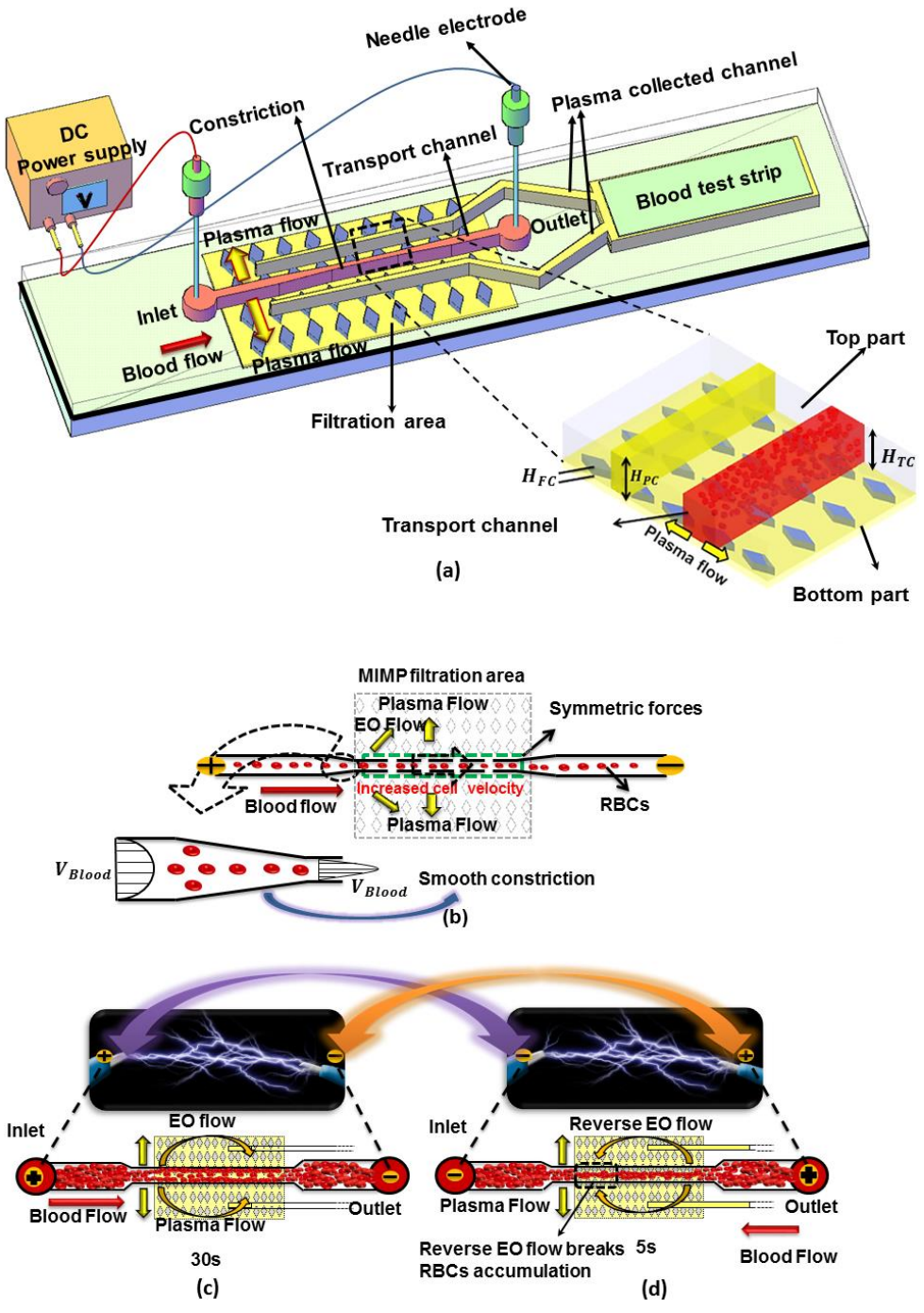

Figure 1 (a) Schematic diagram of the blood plasma separation microdevice. (b) Detail of the transport channel constriction. (c) and (d) Electroosmotic flow and RBCs flow directions depending on the electrode polarization.

7.2.2. Microfluidic chip fabrication and experimental setup

The microfluidic device is manufactured in two main parts: the top part and the bottom part, which are fabricated using different manufacturing processes. After joining the both parts, the lateral flow assays test strips are allocated on the top part and sealed using tape.

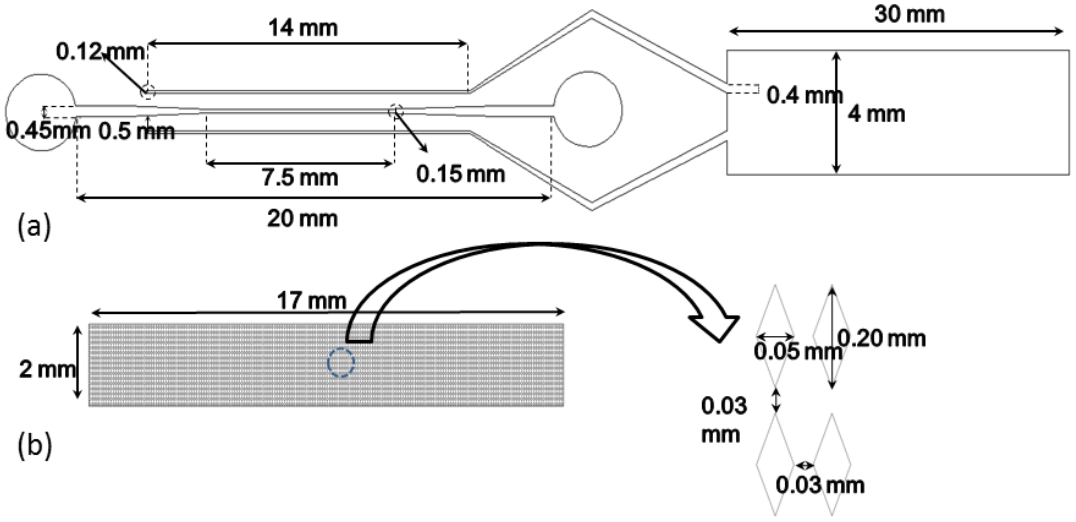

Figure 2 Design dimensions (a) Top part, (b) Down part diamond shaped post-array.

7.2.2.1. Down part fabrication

The microfiltration channel is fabricated on a glass substrate using both photolithography and wet chemical methods. Figure 3 (a to d) illustrates the fabrication steps of the MIMP filtration channel. Glass slides (75×25 mm) cleaned by the Piranha cleaning process are used as a substrate, see Figure 3 (a). S1818 (G2, Dow, Denmark) positive photoresist is spin coated at 2000 revolution per minute during 30 seconds on the top of the glass slide and soft baked at 120 °C for 1 minute. The MIMP structure is patterned through a high-resolution printed photo-mask by using a UV exposure lamp for 5 seconds, see Figure 3 (b). A 52-seconds bath in MF-24A developer (Microposit MF-24, Dow, Denmark) defines the mask features; see Figure 3 (c). Finally, the glass is etched in buffered HF at room temperature for 150 seconds and washed with DI water; see Figure 3 (d).

7.2.2.2. Top part manufacturing process

The transport channel and the plasma collected channel are defined in Polydimethylsiloxane (PDMS) utilizing a conventional soft lithography process. SU-8 (GM 1060, Gersteltec Sarl, Switzerland) is chosen since it is easily patterned on wide range of thicknesses between 6 to

50 micrometers. The designed mask is printed in a high-resolution film. Microscopy glass slides 75×25 mm are utilized as substrates which are firstly cleaned by a Piranha cleaning process (3:1 of H2 SO4 : H2 O2) and then preheated on the hot plate at 200 °C for 30 minutes. After cooling the substrate, a 50-µm layer of the photoresist (SU-8) is spin coated at 540 RPM. In the next step, after 15 minutes of relaxation time, the coated substrate is soft-baked in two steps: 10 minutes at 65 °C and 60 minutes at 95 °C and cooled down to the room temperature. The structures are patterned through the high-resolution printed photo-mask using a UV exposure lamp (650 mJ/cm2). The coated substrate is post-exposure baked in two steps: 10 minute at 65 °C and 30 minutes at 95 °C. Finally, after 10 minutes delay time, the structure is cleared in PGMEA (Propylene glycol methyl ether acetate) for 4 minutes and used as a mold.

To make the PDMS microchannel, Dow Corning Sylgard 184 silicone elastomer and curing agent are thoroughly mixed 10:1 in weight. In order to ensure an easy peel-off of the channels once cured, the mold is silanized. The mixture is poured in the SU-8 master mold and finally, it is cured. The curing process of PDMS was completed after 20 minutes at 125°C. According to our previous study [17] an alternative step can be used to prepare long term self-driven PDMS based microdevices. The use of surfactants can help to produce hyprophilic PDMS, but in this study the hydrophilicity was achieved through an oxygen plasma treatment.

In the last step, the microchannel inlet, outlet, and a window to allocate the test strip were cut; see Figure 3 (e).

7.2.2.3. Microdevice assembly and test strip integration

The top part and the MIMP filtration area (bottom part) are bonded via an oxygen plasma treatment of 30 seconds at 1 Torr. In the test strips, the filtration pad (fiberglass) and the absorption pad from the end have been removed. After, the test strips are allocated in place and sealed with tape.

7.2.2.4. Sample collection and characterization

Fresh blood samples from healthy adults are collected using a lancet from market POCT. A 5-µL drop of fresh human whole blood is mixed with 0.5-µL heparin (purchased from Pfizer Co., Madrid, Spain) as a standard anticoagulant and 5-µL of phosphate-buffered saline (PBS, purchased from Life Technologies S.A., Madrid, Spain).

Since the required volume of the blood plasma for wetting the conjugate pad is relatively high, and according to instruction of test strip company, (Nal Von Minden) 5-µL of phosphate-buffered saline is added to the LFA strips after the plasma has reached the conjugate pad.

Two different types of tests are implemented; one measures TSH level and the other is a blood panel for measuring two indicators in the diagnosis of myocardial infarction (MI): Cardiac Troponin (cTnI) and Creatine Kinase MB (CK-MB).

The TSH test measures the levels of TSH, a hormone that is produced and released by your pituitary gland. The official "normal" range for the Thyroid Stimulating Hormone (TSH) blood test runs from approximately 0.5 to 4.5/5.0 µIU/ml. In this range, a TSH under 0.5 µIU/ml indicated hyperthyroidism (an overactive thyroid), and a TSH over 5.0 µIU/ml indicated hypothyroidism (an underactive thyroid).

The cTnI is a protein found in the cardiac muscle that is released into the blood 4-6 hours after the onset of pain. CK-MB is an enzyme found in the cardiac muscle too, but that is released 3-8 hours after the onset of symptoms, but it lasts up to 72 hours while cTnI can become elevated up to 10 days. Clearly, a combination of both measurements in the same test device increases the efficiency of the diagnosis.

The separated plasma in both plasma-collected channels is driven to the entrance of the test strip.

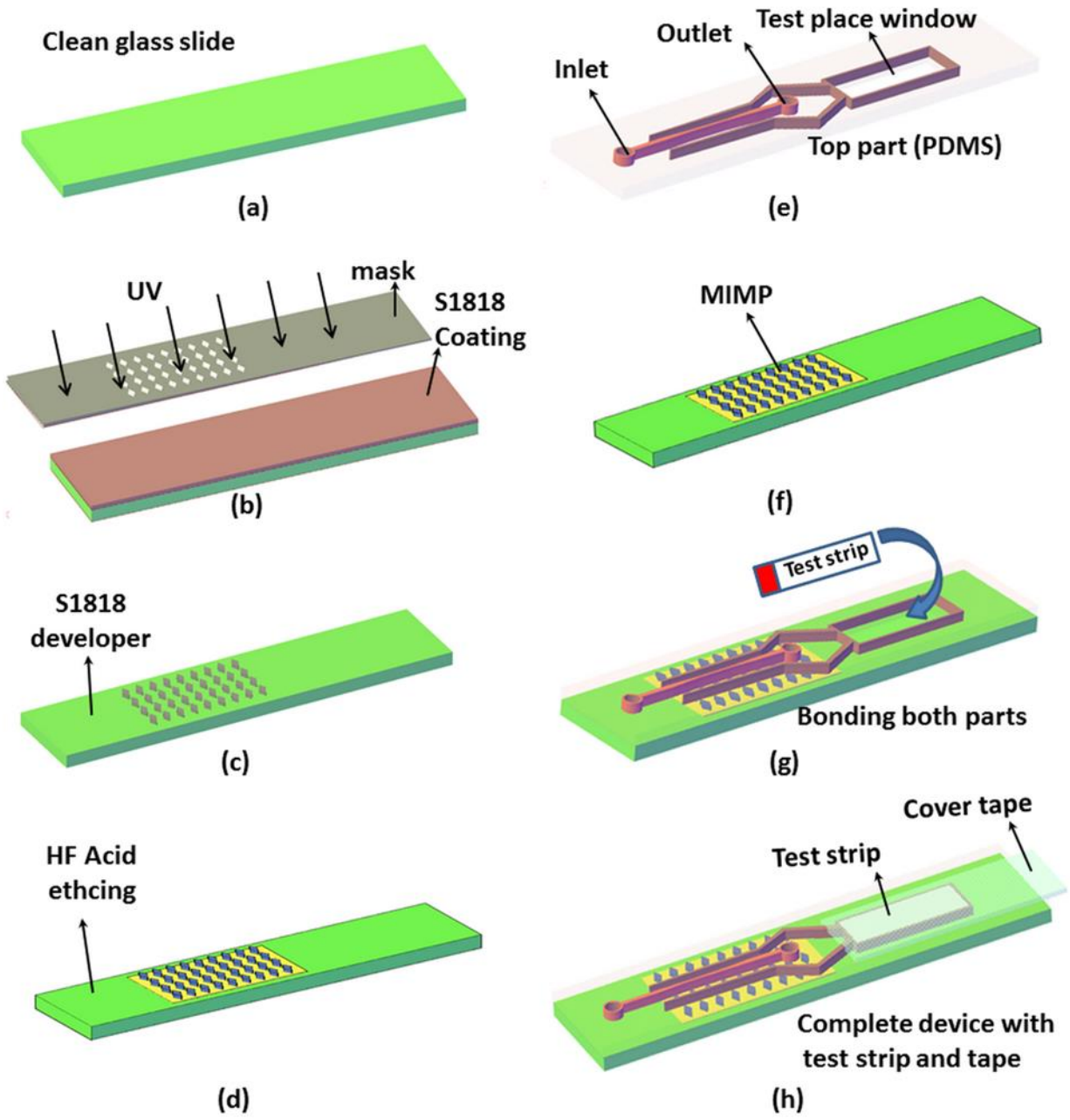

Figure 3 Schematic view of the microdevice fabrication (a-d) MIMP filtration channel manufacturing steps, (e) the microdevice top part with the test window, the channel inlet and the channel outlet (PDMS) (f) the microdevice down part (glass), (g) bonding of both parts, (h) the complete microdevice with the test strip covered with tape.

The test strip gold conjugate pad is overlapped with the blood plasma reservoir and sealed with tape, see Figures 3 (g-h). In the gold conjugate pad, the plasma antigens are recognized and bound to the gold-conjugated antibodies. When the gold nanoparticles complex reach the test line, they form a strong bond with the immobilized antibodies embedded in the nitrocellulose membrane and a colored line will appear, see Figure 6 (b).

If there is enough hormone/protein/enzyme (TSH, cTnI and CK-MB) in the sample a coloured band will form at the test region of the nitrocellulose membrane. The appearance of a coloured band at the control region serves as a procedural control, indicating that the proper volume of specimen has been added.

In order to record images and movies of the blood plasma separation process and analyze the results, a digital camera (Tucsen ISH500, 5.0 M pixel,) is connected to the micro inspection lens system Optem zoom 125C (with a broad 12.5:1 zoom range) and a 20X objective. A high DC voltage power supply (SF-9585 PASCO- California-USA) and two platinum electrodes (Roland Consult-Germany) are employed to generate an electric field.

7.3. Results and discussions

7.3.1. Experimental results

Figure 4 (a) shows the device before introducing the 5-µL droplet of human blood sample into the inlet port of the transport channel. The blood sample is firstly drawn into the microdevice, due to the capillary forces which the oxygen plasma treatment generated. The separation process starts as soon as the blood flows in the transport channel and arrives in the MIMP filtration channel in the down part. The capillary forces are not enough to fill the 50-µm-deep plasma-collected channels.

Therefore, to increase the volume of extracted plasma after 2 minutes, 50 V are applied between the channel inlet and the channel outlet to a 22-mm long microchannel, see Figure 4 (b). The applied electric field creates an EO flow from the inlet to the outlet (positives to negative electrode) that speeds up the filling process of the plasma-collected channels, see Figure 4 (c-d).

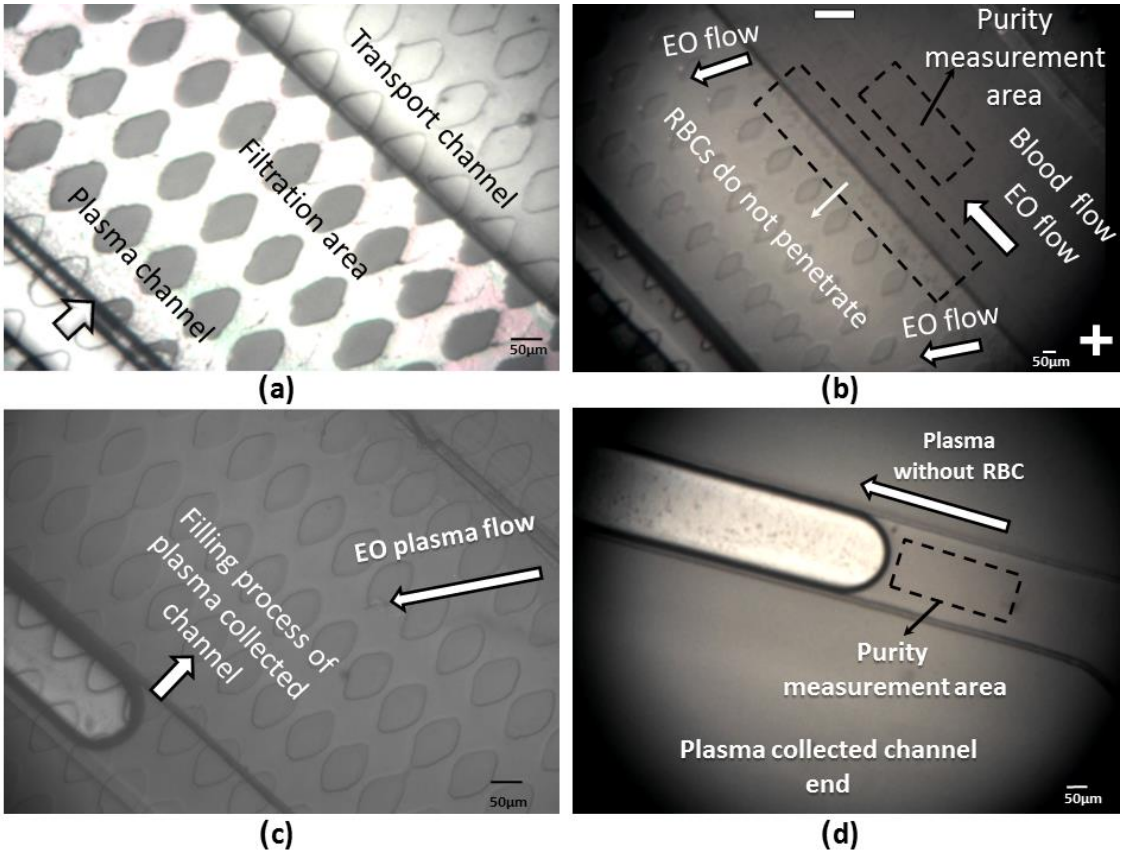

Figure 4 Microdevice performance. (a) Initial empty channel. (b) Filling the transport channel after applying voltage and plasma separation. (c) Filling the plasma-collected channel, (d) End of the plasma-collected channel.

Normally, RBCs clogging is inevitable in the separation zone of blood microfilter, the velocity of blood is decreased in the transport channel which leads to an accumulation of cells in the entrance of the separation area, see Figure 4 (b).

In order to break the accumulation of RBCs and avoid clogging in the entrance of the filtration area, the direction of the electric field is changed every 30 seconds during 5 seconds (outlet to the inlet). Figure 5 (a) shows the direction of EO flow in the transport and MIMP channels and it can be seen that the RBCs clogged the entrance to the MIMP filtration area. Figure 5 (b) shows the backward generated electrosmotic flow when the polarity is changed. This flow pushes the RBCs away from the entrance of the MIMP and breaks the RBCs clogging. The complete opening of the filtration entrance is shown in Figure 5 (c).

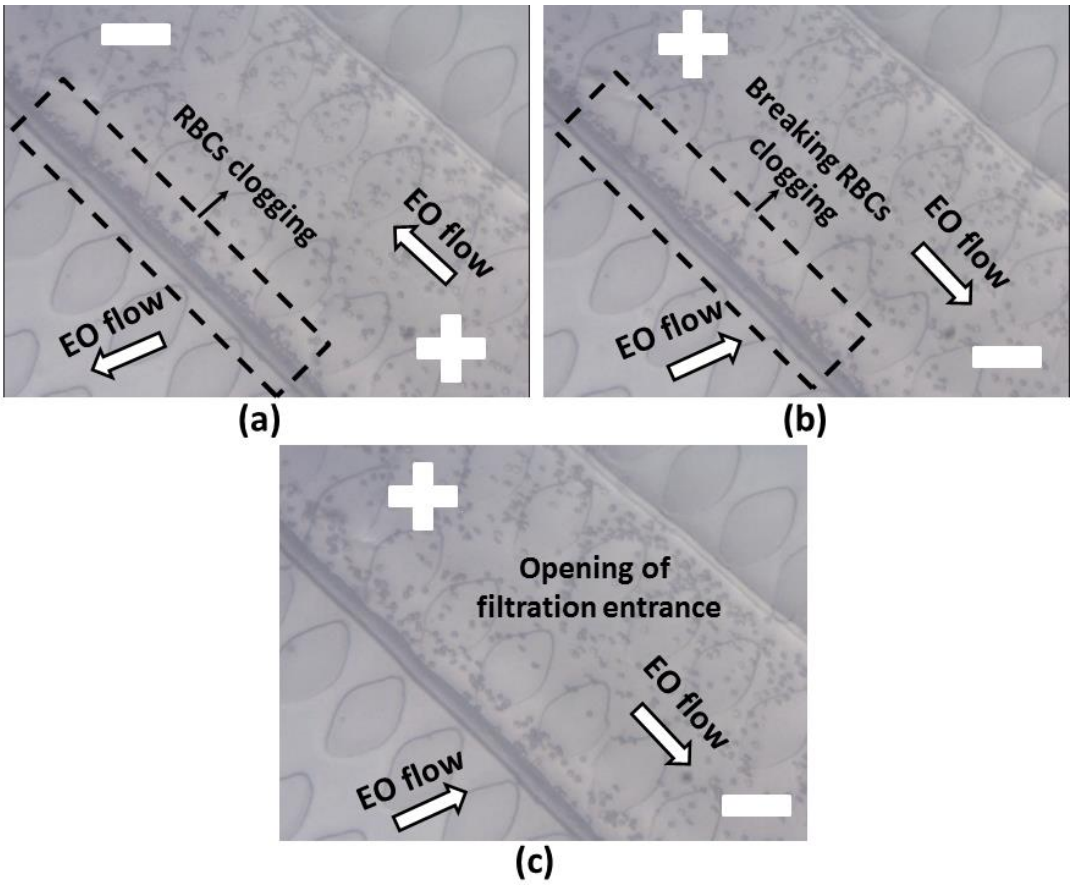

Figure 5 (a) The RBCs clog the entrance of the filtration area. (b) Opening of the entrance of the filtration area using reverse EO flow. (c) The entrance is opened after 5 seconds.

The purity of the extracted blood plasma is defined as:

$$Purity = 1 - \frac{C_P}{C_M} \tag{3}$$

where, C_P is the number of RBC in the plasma collected channel and C_M is the number of RBC in the main channel. Image J is used to compare the number of RBCs in the region marked in Figures 4 (b) and (d). The purity calculated from equation 3 of the extracted blood plasma from whole blood in the plasma channel topology is around 99%.

Calculating the total area filled with plasma, around 1 µL of blood plasma is successfully separated from 10 µL of fresh blood sample in all the tests. According to the results, the plasma collected channel is filled in 8-10 minutes with a purity of more than 99%.

Results of five fabricated devices are summarized in Table 1, showing the average and standard deviation of the recorded data.

Table 1. Average amount of separated plasma, time and purity

Microchip	Blood Sample Volume	Volume of The Extracted Plasma	Time (Minute)	Purity %
Reciprocating electroosmotic	~5µL	1 ± .01 µL	8-10	> 99

7.3.2. Integration of the plasma separator with analyte detection and plasma validation

7.3.2.1. TSH Test

All components of the test strip are shown in Figure 6 (a), notice that the filtration pad and absorption pad have been removed in order integrate the lateral flow assay in the microfluidic chip. The separated plasma reaches to the conjugated pad after 8 minutes and the chromatography process is started. Five test devices are tested; a colored line appears in the control section of the test strip in average 18± 2 minutes after dropping the blood droplet. The schematic view of test strip is shown in Figure 6 (b). It should be highlighted that, the microfluidic chip is shown from the backside view since the test strip is rotated in the implementation process; see Figure 3 (h). Figure 7 (a) shows a picture of the obtained results from the microfluidic chip compared to the standard NADAL® TSH Test.

As it can be seen from both devices, the TSH test result is negative and the appeared coloured line in the control ‘C’ section confirms the correct operation of the TSH test in the presented hybrid microfluidic chip.

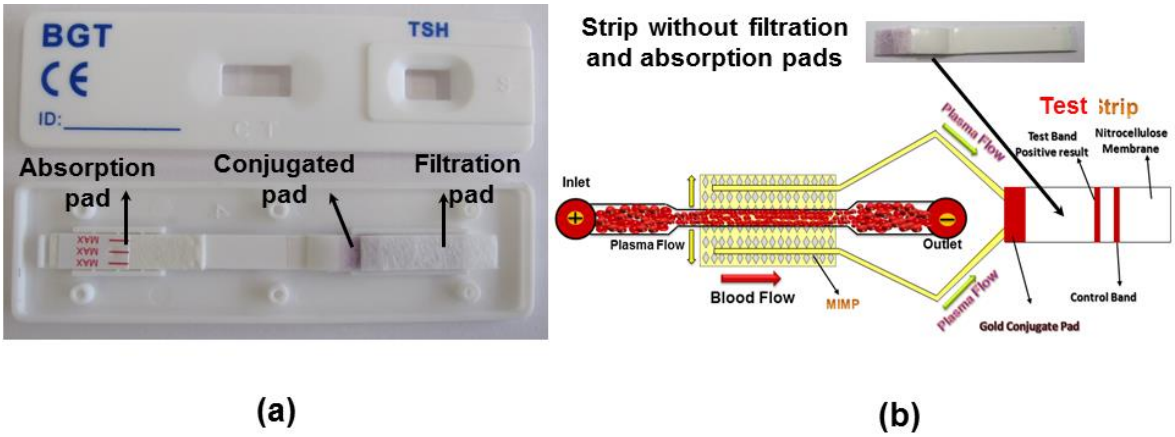

Figure 6 All components of TSH test strip and the test strip without filtration pad (a) schematic view of microdevice with the test strip.

7.3.2.2. Myocardial infarction Test (MI Blood panel)

The capability of the presented microdevice for separating and gathering blood plasma within more than one plasma-collected channel, paves the way for multiplex blood analysis simultaneously in the same device. In order to implement myocardial infarction test, half test strip of Cardiac Troponin cTnI and Creatine Kinase MB (CK-MB) have been placed in test location of the microfluidic device.

Five test devices has been tested; average time for the colored line to appear is 20 ± 2 minutes after dropping the blood droplet. The hybrid microfluidic device with cTnI and CK- also commercial LFA cTnI and CK-MB tests are shown in Figure 7 (b).

For the evaluation of the experimentally obtained results, the gray intensity color of different experiments in microfluidic device and commercial LFA test stripes has been measured by ImageJ software and is presented in Figure 8.

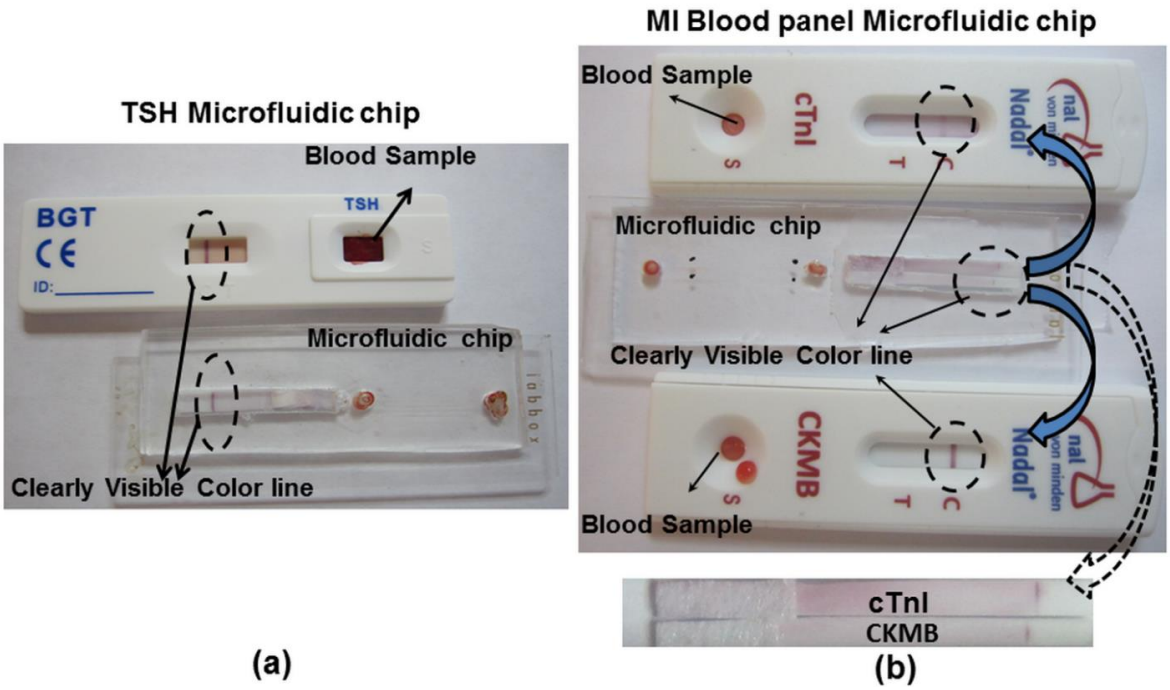

Figure 7 (a) The results of the TSH test using in the microfluidic chip and LFA strip. (b) The results of the myocardial infarction tests using the microfluidic chip and cTnI and CKMB LFA strips.

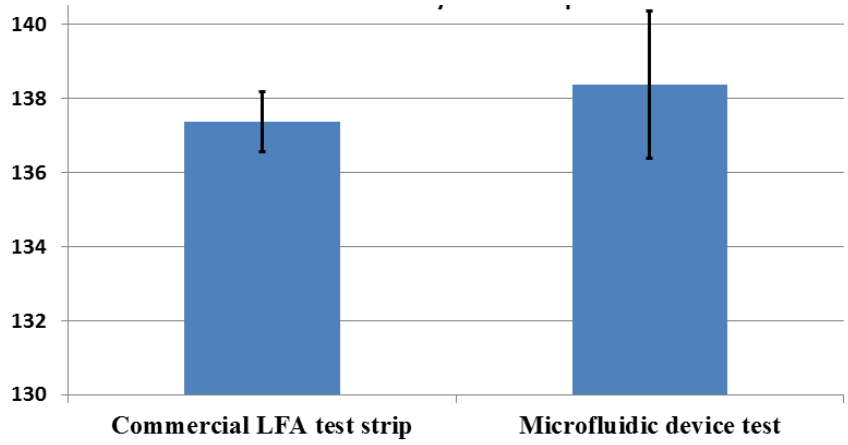

Color intensity blood test strip band	1	2	3	4	5	Mean	S.D
Commercial LFA strip test	136	138	137/4	138	137/5	137/4	0/82
Microfluidic device test	135/3	138/4	139	141	138	138/4	1/98

Figure 8 Color intensity of the results of the TSH test using the microfluidic chip and the LFA strip.

The results show that the color intensity of the commercial LFA test strip is changed from 136 to 138 while for microfluidic device is varied between 135 to 141, which means that the result of the performance of both devices are equivalent.

7.3.2.3. Image analysis for red blood cells hemolysis

In order to study of hemolysis in electroosmotic microdevice several parameters should be considered. Firstly, to decrease damage risk of RBCs, two smooth curves have been designed in the constrictions of the blood transport channel. Secondly, based on the literature [18, 19] to guaranty the purity of the extracted plasma, only 50 V are applied between inlet and outlet in a 22-mm-long channel. Furthermore, the numerical study confirms that the generated electric field inside the micodevice cannot lyse the RBCs, see Supplementray material 1. Finally, the test performances of TSH and MI blood panel, which hybrid to microfluidic chip, demonstrated the quantity and quality of separated plasma.

In addition, the ImageJ software has been to analyses the quality of plasma during the experiment. Variation of color intensity has been measured over a 160-µm line region after 20 seconds and 8 minutes from the beginning of the test inside MIMP filtration area and for the blood sample in the transport channel, see Figure 10.

The measurement shows that the variation of plasma color intensity is negligible (less than 1%) during the experiment (8 minutes) therefore the plasma is separated without hemolysis.

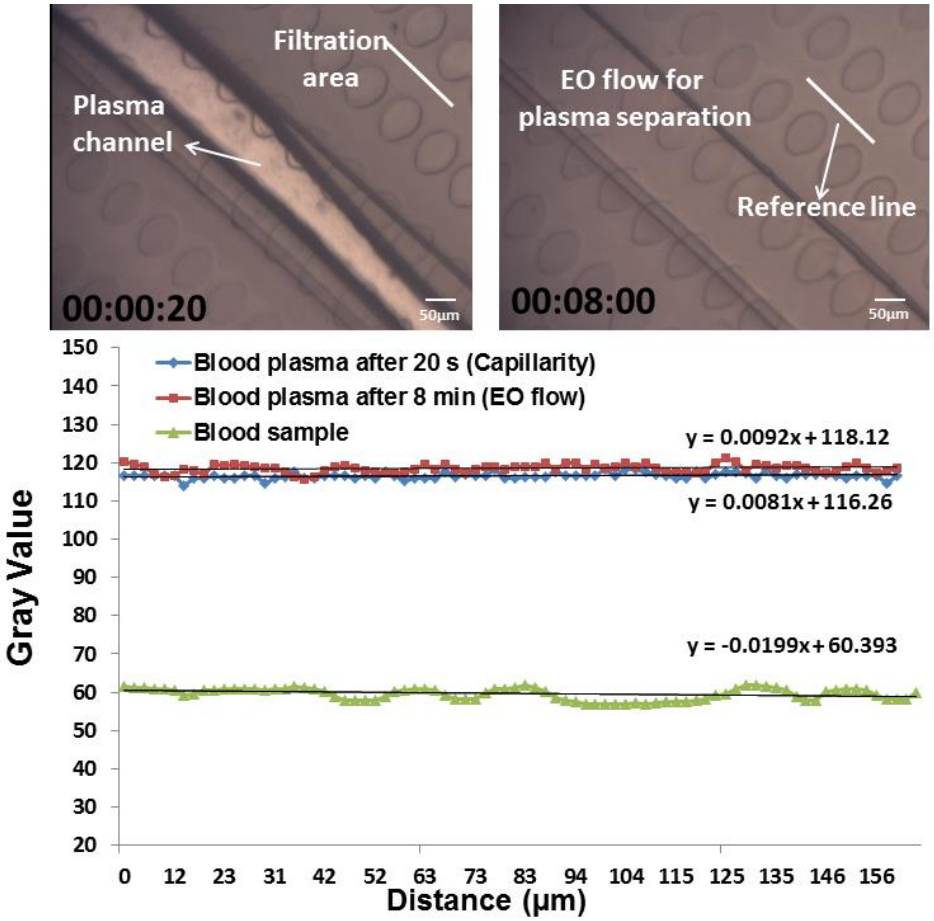

Figure 9 The micrographs of the change in color intensity during of blood plasma separation process (after 20 seconds and 8 minutes).

7.4. Conclusion

A novel microfluidic chip for blood plasma separation, which combines microfluidics with conventional lateral flow immune chromatography to extract enough plasma to perform a blood panel in a simple and portable device has been designed and fabricated in the present study. The microfluidic chip design is a combination of cross-flow filtration with a reversible electroosmotic flow that with only 50 V prevents clogging at the filter entrance and separates more than 1-µL of plasma of high purity (more than 99 %) in a reasonable time (5 to 8 minutes). The main advantage of this design is its portability and the small amount of sample required (a single droplet ~10µL). The potential as clinical tool has been proved combining with lateral flow immune chromatography technology to perform a qualitative detection of the TSH (thyroid-stimulating hormone) and a blood panel for measuring cardiac Troponin and Creatine Kinase MB. The results obtained from the microfluidic system are comparable to previous commercial lateral flow assays that required more sample for implementing less tests. According to the results, the combination of the new microfluidic chip with LFA

technology fulfils the requirements for a point-of-care (POC) device such as robustness, friendly use and simple handling, since the blood sample can be analyzed directly.

7.5. References

[1] M. Kersaudy-Kerhoas, E. Sollier, *Lab Chip*, 13, 17, 3323 (2013)

[2] S. J. Vella, P. Beattie, R. Cademartiri, A. Laromaine, A. W. Martinez, S. T. Phillips, K. a. Mirica, G. M. Whitesides, *Anal. Chem.* 84, 2883 (2012)

[3] X. Yang, O. Forouzan, T. P. Brown, S. S. Shevkoplyas, *Lab Chip*. 12, 274 (2012)

[4] T. Songjaroen, W. Dungchai, O. Chailapakul, C. S. Henry, W. Laiwattanapaisal, *Lab Chip*. 12, 3392 (2012)

[5] M. Amasia, M. Madou, *Bioanalysis*. 2, 1701 (2010)

[6] R. Gorkin, J. Park, J. Siegrist, M. Amasia, B. S. Lee, J. M. Park, J. Kim, H. Kim, M. Madou, Y.K. Cho, *Lab Chip*. 10, 1758 (2010)

[7] N. Pamme, *Lab Chip*. 7, 1644 (2007)

[8] Z. T. F. Yu, K. M. Aw Yong, J. Fu, *Small*. 10- 9, 1687 (2014)

[9] E. Sollier, H. Rostaing, P. Pouteau, Y. Fouillet, J. Achard, Sensors and Actuators B : Chemical. 141, 617–624 (2009)

[10] A. H. C. Ng, U. Uddayasankar, A. R. Wheeler, Analytical and Bioanalytical Chemistry. 397, -3, 991 (2010)

[11] H. Jiang, X. Weng, C. Hee Chon, X. Wu, D. Li, J. Micromech. Microeng. 21, 085019 (2011)

[12] Z. Wu, A. Q. Liu, and K. Hjort, *J. Micromechanics Microengineering*. 17, 1992 (2007)

[13] R. Johann, P. Renaud, *Electrophoresis*. 25, 3720 (2004)

[14] H. Madadi, J. Casals-Terré, R. Castilla-López, and M. Sureda-Anfres, *Microfluid. Nanofluidics*. 17,115 (2014)

[15] S. K. Srivastava, A. Artemiou, A. R. Minerick, *Electrophoresis*, 32- 18, 2530 (2011)

[16] S. Ozuna-Chacón, B. H. Lapizco-Encinas, M. Rito-Palomares, S. O. Martínez-Chapa, C. Reyes-Betanzo, *Electrophoresis*, 29, 3115 (2008)

[17] H. Madadi, J. Casals Terre, Microsyst Technol, 19, 143 (2013)

[18] J. Gao, X. Yin, Z. Fang, Lab Chip. 4, 47 (2004)

[19] R. B. Brown, J. Audet, J. R. Soc. Interface. 5, 131 (2008)

8. Conclusions

This thesis has described the design, test and validation of H-DC-iDEP and high throughput reciprocating electroosmotic microfluidic chip for the plasma separation from human blood. The research steps to make the electrokinetic based microdevice can be classified in three categories:

Optimization of iDEP geometry design and validation of the microdevice with numerical simulation which demonstrated there is a specific radius of posts (R) for each separation distance (K) which present maximum trapping also the relation between K and optimum R has been obtained. The effect of longitudinal distance has been studied which indicated the effect of increasing of longitudinal distances (L) on trapping is insignificant when K is smaller than 30 µm but trapping value has been enhanced when K is more than 30 µm. The result of DEP geometry optimization has been used in the design of hydrodynamic and DC-insulator based dielectrophoresis microdevice. A microfluidic channel with dead-end branches at each side which combines hydrodynamic and DC-iDEP methods for blood plasma separation was designed, fabricated and characterized. The new design allowed the extraction of 99% pure plasma from a single 2 µl blood sample without needs of any external pump. The microfluidic channel was modeled and designed using Finite Elements Models. In particular, two FEA models were used to model the microfluidic channel and to parametrically investigate the appropriate dimensions to achieve RBC trapping without lysis.

The proposed design has a small area (10 mm × 1 mm) and uses only two external electrodes to generate the required electric field with only 50 V. In this topology, 0.1 microliters of plasma from 2 microliters of blood in less than 7 minutes were separated.

None of previous studies combined the advantages of hydrodynamic separation with DC-iDEP to achieve higher purity in less time and less voltage requirements. A hydrodynamic effect enhanced DC-iDEP microfilter for blood plasma separation has been demonstrated in this work for the first time. It is an example of how DC-iDEP can speed particle separation in biological applications where time can be a constrain.

The H-DC-iDEP microfluidic device presented the role of electroosmotic force as driving force. In the last step a novel combination of cross-flow filtration with a reversible electroosmotic flow is used to maximize the amount of separated plasma. The main advantage of this design is its efficiency, since with small amount of sample (a single droplet ~10µL) a considerable amount of extracted plasma (more than 1µL) can be collected with high purity (more than 99%) and reasonable time (5 to 8 minutes). To demonstrate and validate the quality of the separated plasma, and to show its potential as clinical tool an immunological test for the qualitative detection of the TSH (thyroid-stimulating hormone) and

a Blood panel for measuring Cardiac Troponin and Creatine Kinase MB in plasma have been implemented by hybridizing the proposed microfluidic circuit with lateral flow immune chromatography technologies.

9. Future works

In this study, two high throughput microdevices for blood plasma separation are presented: 1- reciprocating electrostatic micropump, 2- Hydodynamic& DC-iDEP Microdevice. Both of them use photolithography and soft lithography microfabrication techniques. The experimental validation have shown that more than 1 µL of blood plasma from 10 µL blood sample can be extracted from the proposed designs, and through the hybridization with lateral flow technologies Point-of-care products could be developed. But this is not the only application of a blood plasma filter.

For instance, the presented microdevices could be applied for separation of microorganisms from blood. This is could be a therapeutic blood cleansing method for treating sepsis. Sepsis is a lethal disease caused by a systemic microbial infection that spreads via the bloodstream and compromise the body's immunological system.

Circulating tumor cells (CTCs) in the blood is an important intermediate step in cancer metastasis, which accounts for ~90% of all cancer related death. The presented microdevices can be also used to detect and separate different cancer cells from small amounts of blood in the exploratory stages of research.

In addition, clinical analysis of acute viral infection in blood requires the separation of viral particles from blood cells, since the aforementioned microfluidic device can use to continuously purify blood from viral particles like HIV particles. In general, the microfluidic systems can utilize for each blood test that is presented in Table 1.

Table 1. Different blood test and sign of diseases [1] http://www.nhlbi.nih.gov/health/health-topics/topics/bdt/types.

Blood test	**Sign of diseases**
Complete Blood Count (CBC)	Anemia, infections, clotting problems, blood cancers, and immune system disorders
Red Blood Cells	Anemia, dehydration (too little fluid in the body), bleeding, or another disorder.
White Blood Cells	Infection, blood cancer, or an immune system disorder
Platelets	Bleeding disorder (not enough clotting) or a thrombotic disorder (too much clotting).

Hematocrit level	Blood or bone marrow disorder.
Kidneys(creatinine levels)	Kidney disease or disorder
Electrolytes levels	Kidney disease, liver disease, heart failure, high blood pressure, or other disorders.
Calcium level	Kidney problems, bone disease, thyroid disease, cancer, malnutrition, or another disorder.
Blood Glucose	Diabetes.
Blood Clotting Tests	Risk of bleeding or developing clots in your blood vessels.
LDL and HDL cholesterol and triglyceride level	Signs of increased risk for coronary heart disease (CHD)

PART II: Publications

Journal Papers

1- Mahdi Mohammadi, Hojjat Madadi, Jasmina Casals, Jordi Sellarès “Multifunctional Blood Plasma Separator Microfluidics Chip for Point of Care Testing based on a Bilateral Electroosmotic Microfilter” Lab On a Chip Journal, under review, 2014

2- Hojjat Madadi, Jasmina Casals-Terré, Mahdi Mohammadi ” Self driven efficient blood plasma separator microfluidic chip for point of care testing “ Biofabrication Journal, Accepted, Feb 2015.

3- Mahdi Mohammadi, Hojjat Madadi, Jasmina Casals, Jordi Sellarès “Hydrodynamic and Direct-current insulator-based dielectrophoresis (H-DC-iDEP) microfluidic chip for blood plasma separation “Analytical and Bioanalytical chemistry Journal, under review, Nov 2014.

4- Hojjat Madadi, MahdiMohammadi, Jasmina Casals “A novel fabrication technique to minimize PDMS-microchannels deformation under high-pressure operation" Electrophoresis Journal, Vol 34, 3126–3132, 2013.

5- Mahdi Mohammadi, Hojjat Madadi, Jasmina Casals-Terré*, Jordi Sellarès, Mohammad Javad Zare” Numerical optimization of post-array geometries for enhanced direct-current insulator-based dielectrophoretic trapping” Electrophoresis Journal, under review, Oct 2014.

Conference Papers

1. Mahdi Mohammadi, Hojjat Madadi Jasmina Casals-Terré “High throughput reciprocating electroosmotic micropump for blood plasma separation using in the blood panel microfluidic device”, Biosensors & Bioelectronics Conference, Atlanta, USA Sep 28-30, 2015
2. Mahdi Mohammadi, Hojjat Madadi, Jasmina Casals “High throughput self-driven electroosmotic micropump for blood plasma separation” 13th Mediterranean Congress of Chemical Engineering (13MCCE), Barcelona, Spain, 3 October, 2014.

3. Mahdi Mohammadi, Hojjat Madadi, Jasmina Casals, Jordi Sellarès “Viable cell trapping via hydrodynamic and direct current insulator based dielectrophoresis (H-DC-iDEP) effects in a corrugated microfluidic channel” 4th European Conference on Microfluidics, Limerick, Ireland, 10th -12th December 2014.

4. Hojjat Madadi, Mahdi Mohammadi, Jasmina Casals" The Microfluidic Technology Meets the Lateral Flow ImmunochromatographicTechnology for Making a Point of Care Device" 4th European Conference on Microfluidics, Limerick, Ireland, 10th -12th December 2014.

5. Hojjat Madadi, MahdiMohammadi, Jasmina Casals "Self-powered Efficient Blood Plasma Separator Microfluidic Chip for Multi-functional Blood Analysis" 4th European Conference on Microfluidics, Limerick, Ireland, 10th -12th December 2014.

6. Mahdi Mohammadi, Hojjat Madadi, Jasmina Casals "UV-Bonding methodology for thiol-ENE resin based self-driven biomedical microchannels", 38th International conference on Micro and Nano Engineering, Toulouse, France 20 Sep, 2012.

7. Mahdi Mohammadi, Hojjat Madadi, Jasmina Casals" Design and optimization of a DC-iDEP microfluidic device to trap 5-micron sized alive cells" Conference on research and technological innovation, Terrassa, Barcelona, 13 June 2013.

8. Mahdi Mohammadi, Hojjat Madadi, Jasmina Casals "Design and optimization of a DC Insulator Based Dielectrophoresis microfluidic device to trap 5-micron sized alive cells. ", 3rd International Conference on Bio-Sensing Technology, Sitges (Barcelona), Spain, 12-15 May 2013.